Structural and functional characterization of *Campylobacter jejuni* Ferric uptake regulator (*Cj*Fur)

Sabina Sarvan

Thesis submitted to the
Faculty of Graduate and Postdoctoral Studies
in partial fulfillment of the requirements
for the Doctorate in Philosophy degree in Biochemistry

Ottawa Institute of Systems Biology
Department of Biochemistry, Microbiology and Immunology
Faculty of Medicine
University of Ottawa

In loving memory of my father, Izudin Sarvan (1959-2015)
I miss you dad!

ABSTRACT

Transition metals are crucial components of several metabolic pathways and are critical for DNA, RNA and protein synthesis. However, when found in excess, these metal ions are toxic. To maintain the physiological concentration of metal ions at non-toxic concentration, bacteria rely on members of the Ferric uptake regulator (Fur) family of metalloregulators. Intriguingly, despite being coined as "metalloregulator", specific members of the Fur family activate and repress gene expression in presence or absence of regulatory metals. Based on these observations, we hypothesized that the ability of these transcription factors to adopt different structural conformations underlies their ability to display different functions in presence and absence of metal ions. To address this important question, we solved the crystal structure of apo-Fur protein from *Campylobacter jejuni*. Structural analysis revealed that the protein adopts a V-shaped conformation harboring an evolutionary conserved cluster of positively charged residues on the surface. Using an extensive library of mutants and electrophoretic mobility shift analysis, we found that substituting residues forming the positively charged surface is detrimental for Fur interaction with DNA. Furthermore, our *in vivo* studies suggest that these positively charged residues are important for the regulation of *Cj*Fur target genes and that different mechanisms modulate the activity of Fur family of metalloregulators depending on the number of occupied metal binding sites. We showed that the disruption of metal binding sites of *Cj*Fur significantly reduces DNA binding *in vitro* and is deleterious for the repression of Fur target genes and gut colonization by *C. jejuni*. Finally, based on initial findings that adding a tag at the N-terminus of *Cj*Fur significantly reduces its ability to incorporate regulatory metal ions and bind DNA, we

developed a new protocol for the purification of a highly active untagged *Cj*Fur protein. Overall, our studies shed new lights on the mechanistic basis controlling Fur gene regulatory activity in *C. jejuni*.

ACKNOWLEDGMENTS

Firstly, I would like to express my sincere gratitude to my supervisor Dr. Jean-François Couture for giving me the opportunity to be a member of his lab. My work in the Couture lab began nine years ago as an undergraduate CO-OP student and a year later as an Honour's student. Dr. Couture's passion for research, his encouragement and continuous support have played an important role in my decision to pursue graduate studies in Biochemistry, under his supervision. I would like to thank Dr. Couture for his mentorship, motivation, invaluable advices and guidance during both the research and thesis writing phases of my PhD, as well as for his patience, understanding and support during some of the more challenging times I faced in the last seven years. I could not have imagined having a better mentor during my graduate studies.

In addition, I would like to thank my thesis advisory committee members Dr. Martin Pelchat and Dr. Alain Stintzi for their insightful feedback and encouragement over the last seven years.

Furthermore, I would like to thank the members of the Couture lab, both past and present for continual friendship, support and stimulating discussions during our coffee breaks, all of which made the journey in the Couture lab such an enjoyable experience. Special thanks go to Véronique Tremblay for her mentorship during my CO-OP work term, for her help and advices whenever needed over the past seven years. I am grateful for the friendship we built. I am appreciative of the work of my Honours students William, Karim, Allison and Evan whom greatly contributed to the development of our manuscripts and also allowed me to learn a lot about my own role as a mentor. I would

also like to thank our collaborators in particular Dr. Alain Stintzi, Dr. James Butcher, Dr. Momen Askoura and Dr. Joseph S. Brunzelle for their contribution.

I am thankful for the funding provided by Queen Elizabeth II graduate scholarships in science and technology, University of Ottawa Excellence and Admission scholarships and Fonds de Recherche du Québec-Santé to support my PhD research.

I will be forever grateful to Audrée, Camille, Dunja, Gianina, Ioana, Judith, Marija, Marika, Myriam, Pamela, Regina, Vanessa and Yasnee for being there when I needed a science break and for their support and encouragement that helped me get through the joys and the hardships both in life and during the course of my studies. Special thanks go to Ioana and Marija for listening, for keeping me sane and for always believing in me.

Finally, I wish to express my deepest appreciation to my family. My sisters, my brother and his girlfriend provided unwavering support and understanding. I could not have done this without you. I would like to thank my nephew Ali for his unconditional love and for bringing so much happiness to my life. A final thank you goes to my parents who made an untold number of sacrifices for our entire family, and provided unwavering emotional, moral and financial support before and throughout the course of my PhD. Thank you for your understanding, your patience, for always believing in me, standing by me and pushing me when I doubted myself. I hope I have made you all proud.

Finally, this thesis is dedicated to my late father who unfortunately did not live to see me complete this degree, but will stay in my heart forever.

TABLE OF CONTENTS

ABREVIATIONS

6XHis – hexahistidine

A

AhpC – Alkyl hydroperoxide reductase subunit C

Ala – Alanine
AmiE – Aliphatic aminase
Arg – Arginine
ArsR – Arsenical resistance operon repressor
Asp – Aspartic acid

B
BMe – β-mercaptoethanol
bp – base pair
*Bs*PerR - *Bacillus subtilis* Peroxide stress regulator
B. subtilis – Bacillus subtilis

C
C. coli – Campylobacter coli
C. jejuni – Campylobacter jejuni
Cd – Cadmium
cDNA – complementary deoxyribonucleic acid
cfrA – Ferric enterobactin receptor
CFU – Colony forming unit
Chip – Chromatin Immunoprecipitation
Chip-Chip – Chromatin immunoprecipitation combined with DNA microarray
Cj – Campylobacter jejuni
*Cj*Fur – *Campylobacter jejuni* Ferric uptake regulator
Co – Cobalt
CopY – Copper-inducible repressor
CsoR – Copper specific repressor
Cu – Copper
CV – column volumes
Cy5 – Cyanine 5
Cys – Cysteine

D
Da – Dalton

DBD – DNA binding domain
DD – Dimerization domain
DNA – Deoxyribonucleic acid
dsDNA – double stranded Deoxyribonucleic acid
DtxR – Diphtheria Toxin Repressor

E
E. coli – Escherichia coli
*Ec*Fur – *Escherichia coli* Ferric uptake regulator
ECL – Enhanced Chemiluminescence
*Ec*Zur – *Escherichia coli* Zinc uptake regulator
EDTA – Ethylenediamine tetraacetic acid
EMSA – Electrophoretic mobility shift assay
ESI-MS – Electrospray ionization mass spectrometry

F
Fe – Iron
Fe^{2+} – ferrous iron
Fe^{3+} – ferric iron
$FeSO_4$ – Ferrous sulfate
ftnA – bacterial non-heme ferritin
Fur – Ferric uptake regulator

G
GBS – Guillain-Barré Syndrome
Gln - Glutamine
Glu – Glutamic acid
gyrA- DNA gyrase subunit A

H
H-NS – histone-like nucleoid-structuring protein
H. pylori – Helicobacter pylori
H_2O_2 – Hydrogen peroxide
hddA - D-alpha-D-heptose-7-phosphate kinase
His – Histidine
*Hp*Fur – *Helicobacter pylori* Ferric uptake regulator
HRP – Horseradish peroxidase

I
ICP-MS – Inductively coupled plasma mass spectrometry
Ile - Isoleucine
IPTG – isopropyl β-D-1-thiogalactopyrnaoside
Irr – Heme-dependent iron responsive regulator

K

kat – catalase
KCl – Potassium chloride
kDa – kilodalton

L
L. monocytogenes – Listeria monocytogenes
LB – Luria-Bertani
Lys – Lysine

M
MEM – Minimum Essential Medium
MerR – Mercuric ion resistance regulator
*Mg*Fur - *Magnetospirillum gryphiswaldense* MSR-1
MH – Mueller Hinton
Mn – Manganese
$MnCl_2$ – Manganese chloride
MND – Menadione sodium bisulphite
$MnSO_4$ – Manganese sulfate
MntR – Manganese transport regulator
MPD – hexylene glycol
*Mt*Zur – *Mycobacterium tuberculosis* Zin uptake regulator
Mur – Manganese uptake regulator
MWCO - Molecular Weight Cut-Off

N
N. gonorrhoeae – Neisseria gonorrhoeae
N. meningitidis – Neisseria meningitidis
NaCl – Sodium Chloride
Ni – Nickel
NikR – Nickel-responsive regulator
norB – nitric oxide reductase
Nur – Nickel uptake regulator

P
P. aeruginosa – Pseudomonas aeruginosa
*Pa*Fur –*Pseudomonas aeruginosa* Ferric uptake regulator
PCR – Polymerase chain reaction
PBS – Phosphate buffered saline
PEG 3350 – Polyethylene glycol 3350
PerR – Peroxide stress regulator
pfr - ferritin
pH – potential of hydrogen
PMSF – Phenylmethylsulfonyl fluoride
Poly dI-dC – Poly deoxyinosinic-deoxycytidylic acid
pS – plasmid Strep
pSS – plasmid StrepSUMO

PVDF – Polyvinylidene difluoride

Q
Q Sepharose – Quaternary ammonium Sepharose

R
Rf – Retardation factor
RIPA buffer – Radioimmunoprecipitation assay buffer
RMSD – Root mean square deviation
RNA – Ribonucleic acid
ROS – Reactive oxygen species
ROX – Rhodamine X
RPM – Revolutions per minute
rrc – Desulforubrerythrin
rRNA – Ribosomal ribonucleic acid
RT-qPCR – Quantitative reverse transcription Polymerase chain reaction

S
S. aureus – Staphylococcus aureus
S. cerevisiae – Saccharomyces cerevisiae
S. enterica – Salmonella enterica
S. typhimurium – Salmonella typhimurium
s-*Cj*Fur – strep-*Cj*Fur
ss-*Cj*Fur – strepSUMO-*Cj*Fur
SAD - single-wavelength anomalous dispersion
*Sc*Nur – *Streptomyces coelicolor* Nickel uptake regulator
*Sc*Zur - *Streptomyces coelicolor* Zinc uptake regulator
SDS-PAGE – Sodium Dodecyl Sulfate Poly-Acrylamide Gel Electrophoresis
SEM - Standard Error of the Mean
slyD - FKBP-type peptidyl-prolyl cis-trans isomerase
Smt3 – Small ubiquitin-related modifier
sod – superoxide dismutase
SP Sepharose – Sulphopropyl Sepharose
spp. - species
*Sp*PerR – *Streptococcus pyogenes* Peroxide stress regulator
SUMO – Small Ubiquitin-like Modifier

T
TBS – Tris-Buffered Saline
TBST – Tris-Buffered Saline with Tween® 20
Tev – Tobacco Etch Virus
Thr – Threonine
tRNA – transfer RNA
trxB - thioredoxin reductase
Tyr – Tyrosine

U
ULP1 – Ubiquitin-like-specific protease 1
UV – Ultraviolet

V
V. cholerae – Vibrio cholerae
Val - Valine
*Vc*Fur – *Vibrio cholerae* Ferric uptake regulator

W
WT – wild type

Z
Zn - Zinc
Zur – Zinc uptake regulator

LIST OF FIGURES

LIST OF TABLES

CHAPTER 1. INTRODUCTION

1.1 *Campylobacter jejuni* and its pathogenesis

Campylobacteriosis is an infectious disease caused by members of the bacterial genus *Campylobacter* (Coker et al., 2002). Campylobacters are small, Gram-negative, curved or spiral rod-shaped bacteria that commensally colonize the gastrointestinal tract of an extensive number of animals (Percival and Williams, 2014; van Vliet and Ketley, 2001). *Campylobacter* species are microaerophilic bacteria and require an oxygen concentration and carbon dioxide concentration of 3-15% and 3-5%, respectively (van Vliet and Ketley, 2001). They possess a polar flagellum at one or both ends of the cell which confers high motility to the bacteria and constitutes an important factor for *Campylobacter* colonization and virulence (Dasti et al., 2010; van Vliet and Ketley, 2001).

All avians including domestic poultry namely chickens, turkeys, ducks and geese, as well as wild birds constitute a natural reservoir for *Campylobacter* species that include predominantly *Campylobacter jejuni* (*C. jejuni*) and *Campylobacter coli* (*C. coli*) strains (Gölz et al., 2014; Lee and Newell, 2006; Sahin et al., 2002, 2015; Shane, 1992). While considered as commensals in birds, *C. jejuni* and *C. coli* species are responsible for more than 90% of all human *Campylobacter* enteric infections (Dasti et al., 2010) and are the principal pathological organisms causing gastroenteritis worldwide (Kaakoush et al., 2015). In addition to human, other mammals are susceptible to *Campylobacter* infection. For example, contamination by *Campylobacter* was linked to epizootic abortion in cattle and sheep (Skirrow, 2006; Smith, 1918; Zilbauer et al., 2008). *C. jejuni* has a low

infective dose and consumption of as low as 500 to 800 organisms induces disease in humans (Black et al., 1988; Robinson, 1981). Asymptomatic carriage, mild diarrhea or severe gastroenteritis can follow infection with *C. jejuni*. In both developed and developing countries, young children are the most susceptible to infection (Dasti et al., 2010; van Vliet and Ketley, 2001; Zilbauer et al., 2008). *C. jejuni* infection is generally a self-limiting disease causing acute symptoms such as fever, vomiting and headaches which last between 1-3 days. These initial symptoms are typically followed by episodes of watery or bloody diarrhea as well as severe abdominal pain (Dasti et al., 2010; Kaakoush et al., 2015) which disappear 3-7 days after the beginning of the infection.

In addition to directly causing gastroenteritis, campylobacteriosis is considered an important risk factor for the development of a more serious and debilitating condition; the Guillain-Barré Syndrome (GBS) (Gibney et al., 2014; Godschalk et al., 2004; Mishu et al., 1993; Nachamkin et al., 1998; Platts-Mills and Kosek, 2014; Rees et al., 1995). GBS is a severe, life-threatening autoimmune condition that causes an ascending paralysis of the limbs and impairment of the peripheral nervous system (Dash et al., 2014; Nachamkin et al., 1998). Approximately 30% of all GBS cases are preceded by *C. jejuni* infection and these are more commonly diagnosed in men than in women (Nachamkin et al., 1998; Rees et al., 1995). Patients with preceding *C. jejuni* infection have a more severe form of GBS since the number of deaths, the necessity for mechanical ventilatory support and long-term neurological damage are higher in this group of patients (Nachamkin et al., 1998). Associations of *Campylobacter* enteritis with other chronic diseases have also been established. For instance, *C. jejuni* is implicated in the development or exacerbation of irritable bowel syndrome (Qin et al., 2011), reactive

arthritis (Pope et al., 2007) and the Miller-Fisher Syndrome (Salloway et al., 1996), among others.

Since *C. jejuni* infections are self-limiting, most humans recover without therapeutic treatment other than rehydration and replacement of fluids and electrolytes administered orally or intravenously (Bolton, 2015). However, in more severe cases or in immunocompromised patients, antimicrobial treatments are recommended. Macrolide antibiotics such as erythromycin are the first choice of treatment when it comes to *C. jejuni* infections. Ciprofloxacin, which belongs to the fluoroquinolone class of antibiotics, is also widely used for the treatment of gastroenteritis in humans (Kaakoush et al., 2015; Zilbauer et al., 2008). However, the resistance of *C. jejuni* to these groups of antibiotics has increased during the last two decades which compromises the efficacy of such treatments (Bolton, 2015; Engberg et al., 2001; Gibreel and Taylor, 2006; Kaakoush et al., 2015; Zilbauer et al., 2008). Macrolides bind to 23S rRNA and inhibit protein synthesis by blocking the translocation step and by inducing the premature dissociation of the peptidyl-tRNAs from the ribosome (Engberg et al., 2001; Gibreel and Taylor, 2006; Kaakoush et al., 2015). In *C. jejuni,* resistance to erythromycin is chromosomally mediated by target mutations of one of two adenines at the erythromycin binding-site in the 23S rRNA gene (Engberg et al., 2001; Kaakoush et al., 2015). In contrast to macrolides, the resistance to fluoroquinones is mediated through mutations of the genes encoding subunits of DNA gyrase (*gyrA*) and topoisomerase IV, two enzymes that are essential for DNA replication, transcription, recombination and DNA repair (Engberg et al., 2001; Jacoby, 2005; Kaakoush et al., 2015). The use of other antibiotics such as tetracycline, gentamycin or kanamycin has also been recommended for the treatment of

Campylobacter infections. However tetracycline-resistant as well as multidrug-resistant *Campylobacter* isolates, *i.e.* resistant to three or more antibiotics, have recently been reported (Kaakoush et al., 2015). The antibiotic resistance is mainly a consequence of the use of antimicrobials in animal production, urging the need for limiting and controlling the usage of such agents in agriculture (Engberg et al., 2001; Gibreel and Taylor, 2006; Kaakoush et al., 2015). The increase in antibiotic-resistant *Campylobacter* species is recognized as emerging public health problem (Engberg et al., 2001) since the infection with antibiotic-resistant *Campylobacter* species has been linked with longer duration of the illness and higher risk of deaths in immunocompromised patients (Engberg et al., 2001; Kaakoush et al., 2015). Therefore, the development of new therapeutic strategies towards the prevention and treatment of *Campylobacter* enteric infections is greatly needed.

1.2 Transition metals

To colonize, survive and replicate in the gastrointestinal tract, pathogenic bacteria such as *Campylobacter* must obtain several nutrients including transition metals from the human host. Transition metals are crucial components of several metabolic pathways and are critical for DNA, RNA and protein synthesis (Troxell and Hassan, 2013). They are omnipresent in all organisms as components of metalloproteins and important cofactors for many enzymes and are therefore essential for the survival of all living organisms. However, when their intracellular concentrations become too high, these metal ions display significant toxicity and can mediate the formation of reactive oxygen species (ROS) (Ball et al., 2000) which can potentially damage proteins, lipids and DNA (Imlay,

2003; Imlay et al., 1988). Interestingly, while an excess of some transitions metal ions such as zinc, can lead to cell death *in vitro* (Bozym et al., 2010), the molecular basis of such toxicity remains poorly defined. To prevent toxicity and control their intracellular availability, the concentration of metal ions is tightly controlled (Fillat, 2014; Giedroc and Arunkumar, 2007) by a large group of metal-sensing transcription factors in bacteria. These metalloregulators are important for the detection of the six biologically essential transition metals including, but not limited to, Mn^{2+}, Fe^{2+}, Co^{2+}, Ni^{2+}, Cu^{1+} and Zn^{2+} (Giedroc and Arunkumar, 2007). These proteins are divided in seven different families, which include the metal-releasable repressors ArsR, CsoR and CopY families, the metal-inducible repressors Fur, DtxR/MntR and NikR families and the single metal-responsive repressor-activator family MerR (Summers, 2009).

1.3 Iron homeostasis in *C. jejuni*

Like almost all forms of life, *C. jejuni* has an absolute requirement for iron. Iron is an essential constituent of various proteins such as heme-proteins and iron-sulfur cluster proteins and confers them the appropriate redox potential necessary for proper protein function (Andrews et al., 2003). The cellular processes in which iron is involved in bacteria are numerous and include energy metabolism, DNA biosynthesis, oxygen transport and redox reactions (Andrews et al., 2003; Braun, 2001; Fillat, 2014; Troxell and Hassan, 2013). Iron is important for host-pathogen interactions, as iron has been demonstrated to play a crucial role in the expression of important virulence factors affecting protein glycosylation, flagellar motility, chemotaxis and adhesion in *C. jejuni* (Palyada et al., 2004; Van Vliet et al., 2002).

The bioavailability of iron in the gastrointestinal tract is highly variable and correlates with the changes in pH, oxygen levels, and redox status of this complex environment (Wooldridge and Vliet, 2005). Under oxidizing conditions, iron exists mostly in the ferric form (Fe^{3+}) which is virtually insoluble and therefore not accessible to living organisms (Wooldridge and Vliet, 2005). Furthermore, hosts are known to restrict the concentrations of free iron in order to prevent the survival and proliferation of undesirable microorganisms (Butcher et al., 2010; Parrow et al., 2013).

To overcome the challenges associated with the low, but variable bioavailability of iron, multiple iron uptake systems rely on the chelation or reduction of insoluble ferric iron to increase its solubility in bacteria (Andrews et al., 2003). In particular, *C. jejuni* employs a variety of transmembrane transporters that allow the uptake of iron conjugated to a variety of exogenous siderophores; low molecular weight chelating agents that have the ability to bind and solubilize Fe^{3+} to facilitate its transport into the cell (Miller et al., 2009). More specifically, *C. jejuni* relies on siderophores produced by the intestinal microflora which include enterobactin and enantioenterobactin (Abergel et al., 2009) as well as lactoferrin and members of the transferrin family (Miller et al., 2008). *C. jejuni* also scavenges iron by internalizing heme-bound iron (Ridley et al., 2006).

Although iron is indispensable in *C. jejuni*, its intracellular concentrations must be tightly regulated in order to avoid iron toxicity. Similar to most Gram-positive and Gram-negative bacteria, the regulation of iron homeostasis is achieved by Fur protein in *C. jejuni*.

1.4 Fur family of metalloregulators

The Ferric Uptake Regulator (Fur) family of metalloregulators is involved in the

regulation of iron, manganese, zinc and nickel homeostasis through the activity of Fur, Mur (manganese uptake regulator), Zur (zinc uptake regulator) and Nur (nickel uptake regulator) proteins, respectively. In addition to these members, the Fur family of metalloregulators also includes the peroxide response regulator (PerR) and the heme-dependent iron response regulator (Irr) (Ahn et al., 2006; Bsat et al., 1998; Díaz-Mireles et al., 2004; Gaballa and Helmann, 1998; Hamza et al., 1998; Patzer and Hantke, 1998; Platero et al., 2007). Depending on the availability of metal cofactors, the Fur superfamily regulates the expression of proteins involved in metal acquisition, storage and consumption in order to maintain metal homeostasis and ensure that levels of free metals do not reach toxic levels. Moreover, members of Fur superfamily play a role in the expression of virulence factors in most pathogens and therefore are important factors contributing to bacterial pathogenicity. This is supported by previous study showing that deletion of *fur*, *perR* or *zur* diminishes or abolishes bacterial survival and/or virulence (Dowd et al., 2012; Dubbs and Mongkolsuk, 2012; Troxell and Hassan, 2013; Wen et al., 2011).

1.5 Ferric uptake regulator (Fur)

Fur is the founding member of the Fur family of metalloregulators. The strain defective in iron regulation, named *fur* mutant (for iron (Fe) uptake regulation), was first isolated in *Salmonella typhimurium* (*S. typhimurium*) in 1978 (Ernst et al., 1978). Three years later, the *fur* mutant, which constitutively expressed several high-affinity iron assimilation systems, was isolated in *Escherichia coli* (*E. coli*) (Hantke, 1981). The *fur* gene from *E. coli* was subsequently mapped (Bagg and Neilands, 1985; Hantke, 1984),

cloned (Hantke, 1984) and sequenced (Schäffer et al., 1985), and for the first time, the gene product referred to as Fur protein was shown to act as a repressor of the iron transport operon employing Fe^{2+} as a corepressor (Bagg and Neilands, 1987). Since then, homologues of the *E. coli fur* gene have been characterized in a wide-range of Gram-negative bacteria such as *Acinetobacter baumannii* (Daniel et al., 1999), *Bordetella* species (Brickman and Armstrong, 1995), *C. jejuni* (Vliet et al., 1998; Wooldridge et al., 1994), *Haemophilus ducreyi* (Carson et al., 1996), *Helicobacter pylori* (*H. pylori*) (Bereswill et al., 1998), *Legionella pneumoniae* (Hickey and Cianciotto, 1994), *Neisseria* species (Berish et al., 1993; Thomas and Sparling, 1994; Thomas et al., 1996), *Pseudomonas putida* (Venturi et al., 1995), *S. typhimurium* (Ernst et al., 1978), *Shigella dysenteriae*, *Vibrio cholerae* (*V. cholerae*) (Litwin et al., 1992), *Yersinia pestis* (Staggs and Perry, 1991). Fur proteins have also been described in Gram-positive bacteria such as *Bacillus subtilis* (*B. subtilis*) (Bsat et al., 1998) and *Staphylococcus epidermidis* (Heidrich et al., 1996) and in cyanobacteria e.g. *Anabaena* (Bes et al., 2001), *Synechocystis* (Kaneko et al., 1996) and *Synechococcus* (Ghassemian and Straus, 1996).

1.5.1 Fur: a master gene regulatory factor

Fur is considered a global transcriptional regulator of iron homeostasis. The transcription factor directly regulates the expression of genes important for iron uptake in environments scarce in iron as well as of the proteins important for iron storage and metabolism in iron rich conditions (Lee and Helmann, 2007). Fur also regulates the production of siderophores in *Pseudomonas aeruginosa* (*P. aeruginosa*) and several other iron acquisition systems including the ferrichrome uptake operon and siderophore

transport system in *Staphylococcus aureus* (*S. aureus*), heme and transferrin uptake systems in *Vibrio vulnificus* (*V. vulnificus*) and *Neisseria* species, hemoglobin binding protein in *Haemophilus ducreyi*, as well as ferritins in *Listeria monocytogenes* (*L. monocytogenes*) and *H. pylori* (Agarwal et al., 2005; Biegel Carson et al., 1996; Carpenter et al., 2009a; Delany et al., 2001; Fiorini et al., 2008; Horsburgh et al., 2001; Prince et al., 1993; Xiong et al., 2000). In addition to the regulation of intracellular iron concentration, Fur regulates the expression of proteins implicated in DNA synthesis, energy metabolism, acid and oxidative stress defense, tricarboxylic acid cycle, protein glycosylation, flagella biogenesis and biofilm development (Butcher et al., 2012; Seo et al., 2015). Collectively, these studies demonstrate that Fur is an important transcription factor and serves as a master regulator of gene expression. Unsurprisingly, Fur, through its ability to control the expression of virulence factors, is directly involved in the colonization and virulence of pathogenic bacteria such as *Vibrio* spp. (Kim et al., 2013; Mey et al., 2005), *P. aeruginosa* (Ochsner et al., 1995), *Legionella pneumophila* (Allard et al., 2006) and the toxigenic cyanobacterium *Microcystis aeruginosa* (Sevilla et al., 2008). Moreover, deletions of *fur* gene in *S. aureus* (Horsburgh et al., 2001), *L. monocytogenes* (Rea et al., 2004), *Edwardsiella tarda* (Wang et al., 2008) and *Pseudomonas syringae* (Cha et al., 2008) result in a decreased virulence in animal models. Similarly, deletion of the *fur* gene in *H. pylori* abolishes its ability to infect animal models (Bury-Moné et al., 2004; Gancz et al., 2006) and removal of the *fur* gene in *C. jejuni* significantly impacts the colonization of chicken's gastrointestinal tract (Palyada et al., 2004). In addition to its gene regulatory functions of virulence factors, *H. pylori* (Bijlsma et al., 2002; Gancz et al., 2006), *C. jejuni* (Askoura et al., 2016) and *S.*

typhimurium (Foster, 1991) Fur control the expression of genes involved in survival mechanisms to resist to acid stresses. Moreover, *Mycobacterium* species (Pym et al., 2001), *Yersinia pestis* (Gao et al., 2008), *Staphylococcus aureus* (Horsburgh et al., 2001), *P. aeruginosa* (Hassett et al., 1996) and *C. jejuni* (Butcher et al., 2012) rely on the gene regulatory functions of Fur to cope with oxidative stresses such as ROS. Mechanistically, Fur regulates the expression of genes such as catalase (*kat*) and superoxide dismutase (*sod*) to convert ROS species such as peroxide into water and oxygen (Carpenter et al., 2009a). Overall, these studies demonstrate that Fur is not only a simple repressor of iron uptake genes but is a global regulator integrating several biological cues and controlling several underlying pathways which contributes to the virulence of bacterial pathogens.

1.5.2 The paradigm of Fur

Several studies have shown that mutation of *fur* gene results in constitutive expression of iron uptake systems indicating that Fur protein acts as negative regulator of operons involved in iron transport (Bagg and Neilands, 1985; Ernst et al., 1978; Hantke, 1982). In addition, it has been shown that the level of aerobactin transcripts was directly regulated by the availability of iron (Bindereif and Neilands, 1985). Based on these findings, Bagg and Neilands have proposed a model for the regulation of iron transport where Fur acts as repressor and binds iron as corepressor (Bagg and Neilands, 1987). However, the mode of interaction of Fur with DNA has been subject to controversy. In *E. coli*, iron bound (holo) Fur binds a conserved palindromic 19-bp consensus sequence known as Fur box with the sequence 5'-GATAATGATAATCATTATC-3'. This Fur box overlaps the -35 and -10 sites at promoters of Fur-repressed genes (Andrews et al., 2003).

For several years, it was assumed that one Fur dimer would bind to each Fur box and generate 31 bp long footprints. However, this model was not in agreement with the tendency of Fur to oligomerize and DNA footprinting analysis showing that Fur binding does not generate protected fragments of only 31 bp (Lee and Helmann, 2007). The re-examination of the Fur-DNA interaction mode revealed that the Fur box is composed of a minimum of three repeats of the hexameric motif GATAAT rather than by a palindromic 19 bp target sequence (Escolar et al., 1998). However, it is not clear if each 6 bp motif represents the proposed binding site for one monomer or one dimer. In addition, Baichoo and Helmann revised the Fur-DNA interaction from *B. subtilis* wherein each 19 bp sequence is recognized by two Fur dimers, each interacting with one of two inverted overlapping 7-1-7 motifs (Baichoo and Helmann, 2002). Despite different models, one common characteristic of the proposed Fur boxes is the high percentage of A/T nucleotides. In some cases, like in *H. pylori*, there is no strong Fur box consensus sequence suggesting that Fur protein recognizes more than a specific DNA sequence and that the overall structural conformation of DNA in promoter region of target genes plays a role in DNA recognition.

1.5.3 Holo-Fur repression and activation

The classical model of Fur regulation specifies that under iron-replete conditions, iron binds to the iron-free (apo) Fur and induces a conformational change that promotes the binding of the holo-Fur to its target DNA to inhibit the expression of iron acquisition genes (Bagg and Neilands, 1987; Lavrrar et al., 2002). While Zn^{2+}, Mn^{2+} and Co^{2+} can also bind to Fur and activate its DNA binding activity *in vitro*, only Fe^{2+} is present at

levels sufficient to activate Fur under physiological conditions (Mills and Marletta, 2005). Mechanistically, binding of holo-Fur to DNA blocks the binding of RNA polymerase and thus prevents the transcription of Fur bound genes. However, in contrast to the first proposed model, the regulatory mechanism of Fur proteins is not limited to holo repression. Holistic approaches such as Chromatin Immunoprecipitation followed by annealing on a solid support (Chip) (Chip-Chip) and expression profiling revealed that a subset of genes bound by Fur are repressed rather than activated in Δ*fur* mutants, suggesting that Fur acts as a positive regulator of gene transcription (Butcher et al., 2012; Ernst et al., 2005; Miles et al., 2010) (**Figure 1.1**). Accordingly, Holo-Fur activation was also reported in *H. pylori* (Danielli et al., 2006), *V. cholera* (Craig et al., 2011), *S. typhimurium* (Teixidó et al., 2011), *Anabaena* sp. PCC 7199 (González et al., 2012), *Neisseria meningitidis* (*N. meningitidis*) (Delany et al., 2006), *Neisseria gonorrhoeae* (*N. gonorrhoeae*) (Yu and Genco, 2012) and *C. jejuni* (Butcher et al., 2012). Proteins that require Fur and iron for their expression include iron superoxide dismutase, succinate dehydrogenase and ferritin (Lee and Helmann, 2007).

Several models of gene activation by Fur protein are proposed but none are fully understood. The first model suggests that the positive regulation by Fur is indirect involving the holo-Fur repression of a small anti-sense regulatory RNA RyhB in *E.coli* (Massé and Gottesman, 2002), PrrF1 and PrrF2 in *P. aeruginosa* (Wilderman et al., 2004), NrrF in *Neisseria* spp (Ducey et al., 2009; Mellin et al., 2007; Metruccio et al., 2009), ArrF in *Azotobacter vinelandii* (Jung and Kwon, 2008) and FsrA in *B. subtilis* (Gaballa et al., 2008). In this model, the small RNAs repress target gene expression by forming mRNA-anti-sense RNA duplexes resulting in the degradation of the mRNAs. These

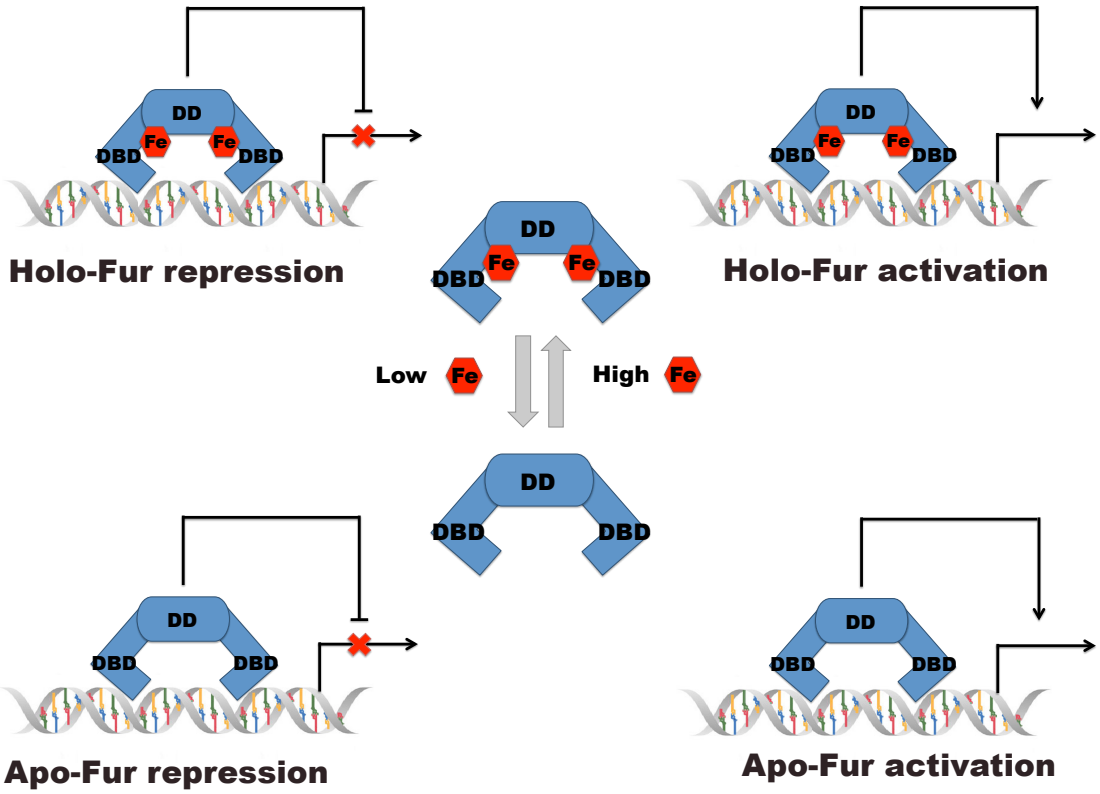
DD
Fe
Fe
DBD
DBD
Holo-Fur repression
Holo-Fur activation
Low
Fe
High
Fe
Apo-Fur repression
Apo-Fur activation

Figure 1.1. Regulatory mechanisms of Ferric uptake regulator (Fur)

Fur family of metalloregulators regulates gene expression by four general mechanisms. In most cases, it is the holo-form, or the iron bound that binds to DNA and represses or activates gene expression. In *Campylobacter jejuni*, *Helicobacter pylori* and *Neisseria gonorrhoeae* two additional regulatory mechanisms were observed and the apo-form or the iron free form of Fur also binds to DNA and acts as a repressor or activator of gene expression.

target genes include iron-containing enzymes and iron-storage proteins and thus by using this regulatory mechanism, also known as "iron-sparing response", bacteria decrease the translation of iron-containing proteins and use more efficiently the available iron during iron starvation (Fillat, 2014; Lee and Helmann, 2007; Troxell and Hassan, 2013). In the second model, holo-Fur indirectly activates gene expression by preventing the recruitment of repressors. For example, in *N. gonorrhoeae*, Fur binds to a region corresponding to the promoter region of *norB*. The Fur binding site overlaps with the putative binding site of a second repressor, the gonococcal ArsR homologue, and can therefore prevent its binding to DNA (Isabella et al., 2008). In the third model, holo-Fur physically displaces the histone-like protein H-NS from the promoter region of *E. coli ftnA* (Nandal et al., 2010). Considering that H-NS controls DNA conformation and negatively regulates gene transcription (Rimsky, 2004), its displacement by Fur enables the access of RNA polymerase to its promoter region and results in the positive regulation of genes (Nandal et al., 2010). Finally, the last and the most common model of holo-Fur activation consists in the direct activation of gene expression. In this model, holo-Fur binds a specific DNA sequence in the promoter region of a target gene enabling its expression. However, whether Fur recruits the RNA polymerase by directly interacting with its subunits remains an open question. This type of holo-Fur activation was observed in *P. aeruginosa* (Wilderman et al., 2004), *V. cholerae* (Craig et al., 2011), *S. typhimurium* (Foster and Hall, 1992), *S. enterica* (Teixidó et al., 2011), *Anabaena* sp. PCC 7199 (González et al., 2012), *N. meningitidis* (Delany et al., 2006; Grifantini et al., 2003) and *H. pylori* (Alamuri et al., 2006), suggesting that the positive regulation by Fur

is a widespread mechanism in prokaryotes. Collectively, these studies highlight the expanding repertoire of gene regulatory functions of Fur.

1.5.4 Apo-Fur regulation

In addition to Holo regulation, Fur can act as a transcription activator and repressor in absence of iron. DNase I footprinting analysis and electrophoretic mobility shift assays (EMSA) demonstrated that the apo form of *H. pylori* Fur binds to the promoter regions of two apo-Fur repressed genes *sodB* and *pfr* (Delany et al., 2001; Ernst et al., 2005). In both cases, the Fur binding site spans at least one of the promoter elements (the -10 or the -35 promoter element) and thus overlaps with RNA polymerase binding site. A similar mechanism was suggested for *Desulfovibrio vulgaris,* however whether apo-Fur directly interacts with its target genes awaits further investigation (Bender et al., 2007).

Activation of gene expression by apo-Fur has been proposed in *Vibrio vulnificus* (Lee et al., 2007), *S. typhimurium* (Hall and Foster, 1996) and *S. aureus* (Deng et al., 2012) among others (Fillat, 2014). Nevertheless, all four modes of regulation were observed only in *H. pylori* (Carpenter et al., 2013), *C. jejuni* (Butcher et al., 2012) and *N. gonorrhoeae* (Grifantini et al., 2003).

Since the Fur binding sites are located near the transcriptional start site, these studies suggest that the mechanism of apo-Fur and holo-Fur repression is similar and consists of blocking the binding of RNA polymerase to the promoter region of target genes, (Carpenter et al., 2009a; Fillat, 2014). Conversely, the mechanisms of apo-Fur and holo-Fur activation are still unclear. The Fur binding sites in both cases are far upstream

(100-200 bp) from the transcriptional start site, which likely does not obstruct the binding of RNA polymerase. One proposed model suggests that the binding of Fur to these regions triggers long range structural reorganization of DNA which alters promoter structure and facilitates the binding of RNA polymerase to activate transcription (Carpenter et al., 2009a).

1.6 The structure of the Fur family of metalloregulators

Owing to the critical role of Fur in bacterial pathogenicity, the crystal structures of several Fur proteins have been determined **(Table 1)**. Collectively, these structures show that Fur folds predominantly in two domains including a N-terminal DNA binding domain (DBD) and a C-terminal dimerization domain (DD) (**Figure 1.2**). The DBD is typically composed of a helix-wing-helix domain while the DD consists of three antiparallel β-strands and two α-helices. All these proteins possess two or three functional metal binding sites (**Figure 1.2**). The structural site (S1) is close to the C-terminus and is coordinated by four cysteine residues. The second structural site (S3) is also found within the DD domain and plays a role in stabilizing the dimeric form of the regulator. The third metal binding pocket is the regulatory site (S2) and is composed of residues located in a region, referred to as the hinge, linking the DBD and DD domains. Although the fold of these proteins is similar, there are several structural differences within the Fur family of proteins including additional secondary structure elements, such as loops and α-helices, found on the N- or C-termini of metalloregulators (Dian et al., 2011; Makthal et al., 2013) and different number, geometry and coordination of the metal binding sites

Table 1. List of available crystal structures of the members of the Fur family of metalloregulators

	Organism	PDB	Reference
***Pa*Fur**	*Pseudomonas aeruginosa*	1MZB	Pohl et al., 2003
***Vc*Fur**	*Vibrio cholerae*	2W57	Sheikh and Taylor, 2009
***Hp*Fur**	*Helicobacter pylori*	2XIG	Dian et al., 2011
***Mg*Fur**	*Magnetospirillum gryphiswaldense* MSR-1	4RAY, 4RAZ	Deng et al., 2015
***Mg*Fur+DNA**		4RB0, 4RB1, 4RB2, 4RB3	
DBD of *Ec*Fur	*Escherichia coli*	2FU4	Pecqueur et al., 2006
***Bs*PerR**	*Bacillus subtilis*	2FE3	Traoré *et al.*, 2006
		2RGV	Traoré et al., 2009
		3F8N	Jacquamet et al., 2009
***Sp*PerR (GASPerR)**	*Streptococcus pyogenes*	4I7H	Makthal et al., 2013
		4LMY	Lin et al., 2014
***Mt*Zur**	*Mycobacterium tuberculosis*	2O03	Lucarelli *et al.*, 2007
***Sc*Zur**	*Streptomyces coelicolor*	3MWM	Shin *et al.*, 2011
***Ec*Zur+DNA**	*Escherichia coli*	4MTD, 4MTE	Gilston *et al.*, 2014
***Sc*Nur**	*Streptomyces coelicolor*	3EYY	An *et al.*, 2009

A

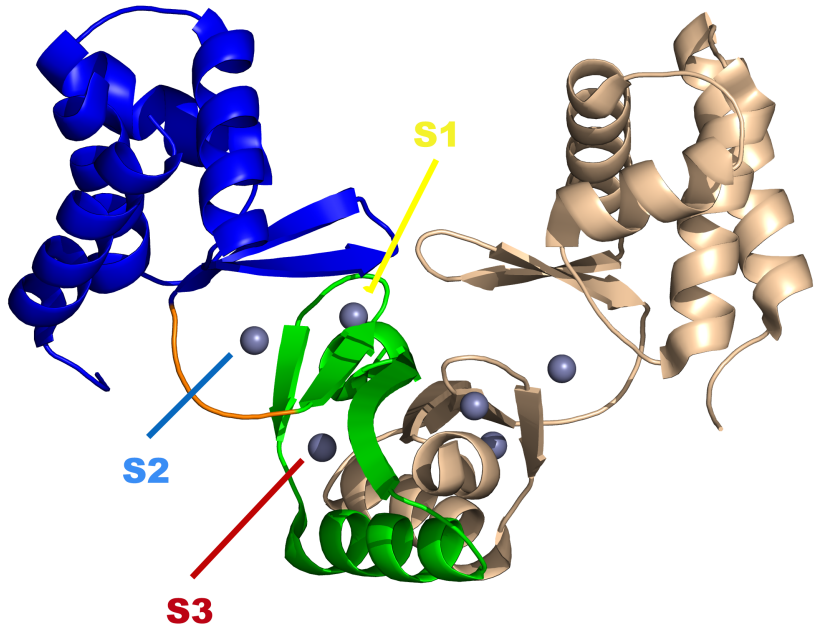

90°

B

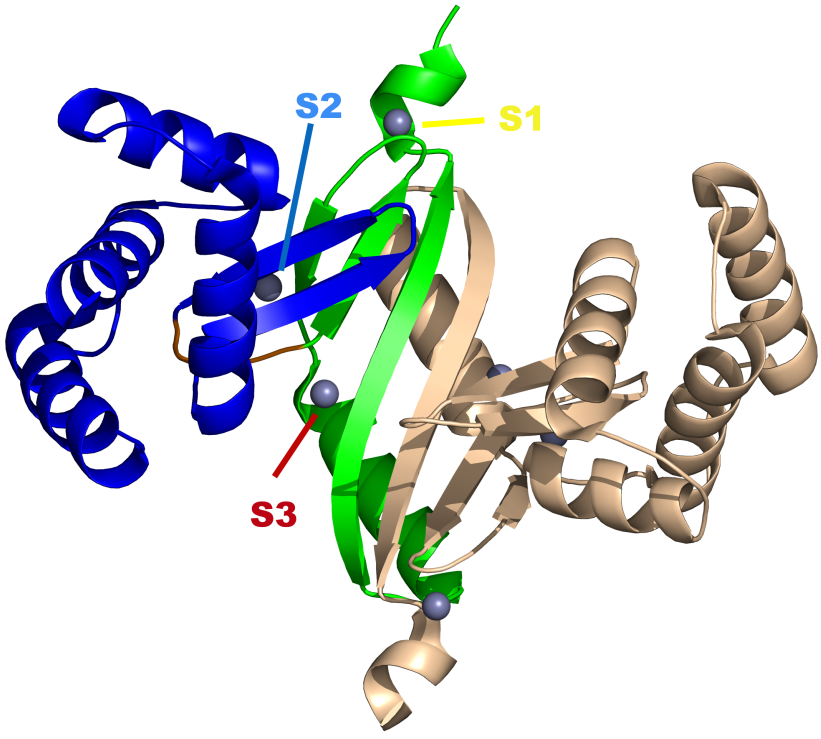

Figure 1.2. The overall structure of the dimeric form of the Fur family of metalloregulators

(A and **B)** Two views of the representative member of the Fur family of metalloregulators (*Hp*Fur, 2XIG) in ribbon representation. Protomer B is colored in wheat and protomer A is colored according to the domain boundaries: N-terminal DBD is shown in blue, the C-terminal DD in green and hinge region connecting these two domains in orange. Zn^{2+} ions are represented by grey spheres and different metal binding sites are identified (S1 in yellow, S2 in blue and S3 in red).

(Dian et al., 2011; Jacquamet et al., 2009; Pohl et al., 2003; Sheikh and Taylor, 2009; Traoré et al., 2006). These structural differences may explain different regulatory mechanisms observed between members of the Fur family of metalloregulators.

1.6.1 Secondary structure of metalloregulators

In the majority of Fur members, such as *Bs*PerR (Jacquamet et al., 2009; Traoré et al., 2006, 2009), *Sp*PerR (Lin et al., 2014; Makthal et al., 2013), *Hp*Fur (Dian et al., 2011), *Mg*Fur (Deng et al., 2015), *Pa*Fur (Pohl et al., 2003), and *Ec*Zur (Gilston et al., 2014), the DBD is composed of 4 α-helices followed by a two-stranded anti-parallel β-sheet. However, some variations are observed in the DBD of this family of transcription factors (**Figure 1.3**). For example, *Ec*Fur (Pecqueur et al., 2006), *Vc*Fur (Sheikh and Taylor, 2009) and *Sc*Nur (An et al., 2009) DBDs contain an additional short α-helix in the N-terminal domain between the two β-strands. The same domain in *Sc*Zur (Shin et al., 2011) and *Mt*Zur (Lucarelli et al., 2007) contains only three α-helices followed by a two-stranded anti-parallel β-sheet. Finally, the N-terminal α1 helix is elongated in *Bs*PerR (Jacquamet et al., 2009; Traoré et al., 2006, 2009), *Ec*Zur (Gilston et al., 2014), *Sp*PerR (Lin et al., 2014; Makthal et al., 2013) and *Hp*Fur (Dian et al., 2011) when compared to other Fur family members.

Similar to the DBD, the dimerization domain is well conserved within the Fur family of metalloregulators and consists of a α/β domain in which three antiparallel β-strands are covering one long α-helix (**Figure 1.4**). *Bs*PerR, *Hp*Fur, *Ec*Zur and *Sc*Zur structures contain an additional α-helix at their respective C-terminus which typically coincides with the presence of an extra structural Zn binding site coordinated by four

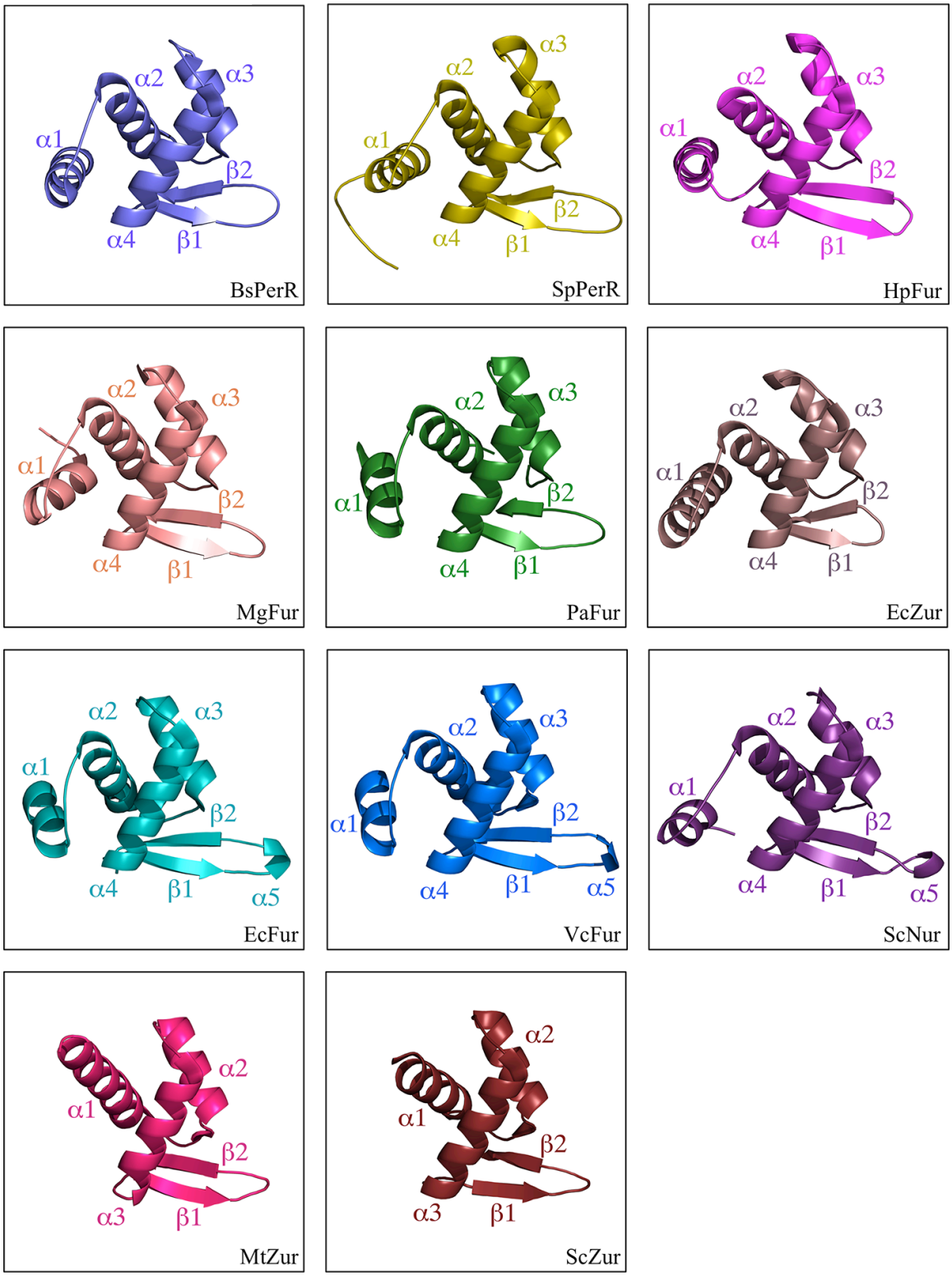
α1
α2
α3
β2
α4
β1
BsPerR
SpPerR
HpFur
MgFur
PaFur
EcZur
α5
EcFur
VcFur
ScNur
MtZur
ScZur

Figure 1.3 Variations observed in the DBD of the Fur family of metalloregulators

Cartoon representation of DBDs of *Bs*PerRZnMn (3F8N), *Sp*PerR (4I7H), *Hp*Fur (2XIG), Holo*Mg*Fur (4RAZ), *Pa*Fur (1MZB), *Ec*Zur (4MTD), *Ec*Fur (2FU4), *Vc*Fur (2W57), *Sc*Nur (3EYY), *Mt*Zur (2O03) and *Sc*Zur (3MWM) are represented. All structures were obtained from the RCSB PDB structure bank (http://www.rcsb.org/pdb/).

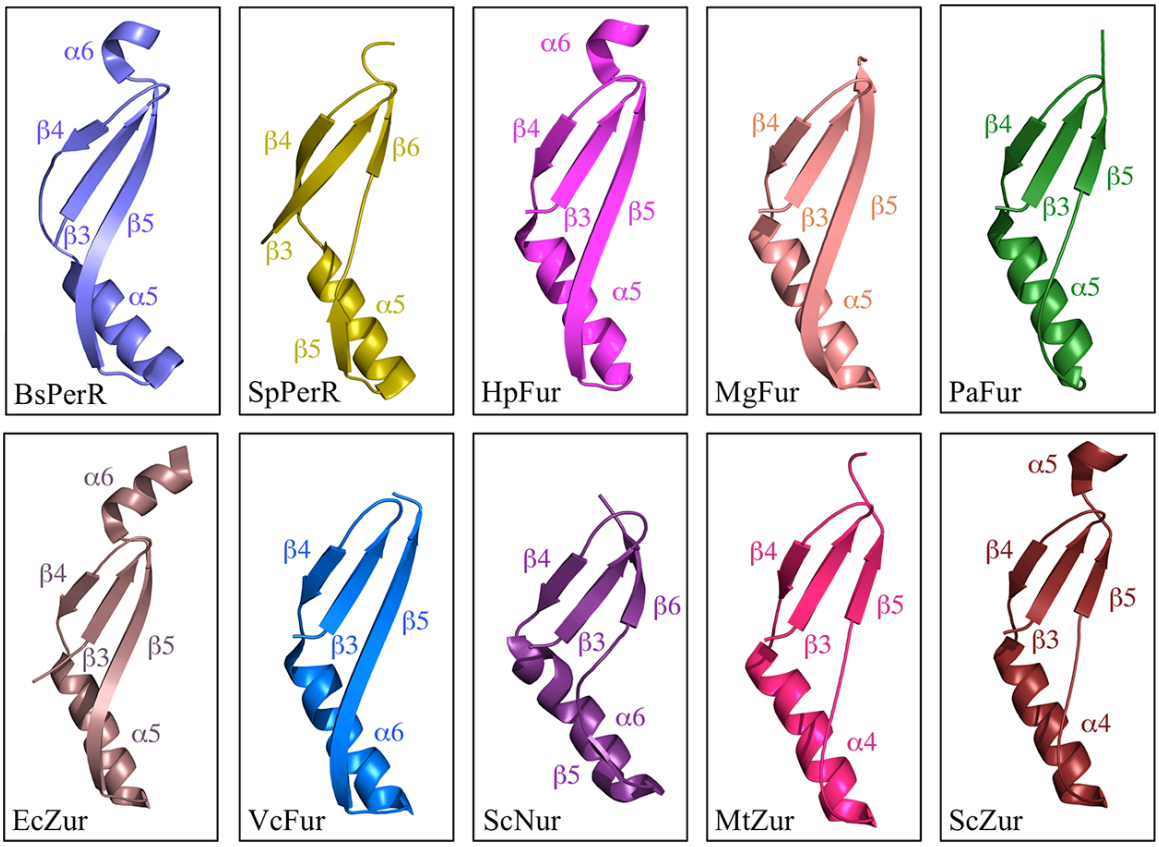
α6
β4
β3
β5
α5
BsPerR
β4
β6
β3
α5
β5
SpPerR
α6
β4
β3
β5
α5
HpFur
β4
β3
β5
α5
MgFur
β4
β5
β3
α5
PaFur
α6
β4
β3
β5
α5
EcZur
β4
β5
β3
α6
VcFur
β4
β6
β3
α6
β5
ScNur
β4
β5
β3
α4
MtZur
α5
β4
β5
β3
α4
ScZur

Figure 1.4 Variations observed in the DD of the Fur family of metalloregulators

Cartoon representation of DDs of *Bs*PerRZnMn (3F8N), *Sp*PerR (4I7H), *Hp*Fur (2XIG), Holo*Mg*Fur (4RAZ), *Pa*Fur (1MZB), *Ec*Zur (4MTD), *Vc*Fur (2W57), *Sc*Nur (3EYY), *Mt*Zur (2O03) and *Sc*Zur (3MWM) are represented. All structures were obtained from the RCSB PDB structure bank (http://www.rcsb.org/pdb/).

conserved cysteine residues found within the dimerization domains of corresponding proteins (Dian et al., 2011; Gilston et al., 2014; Jacquamet et al., 2009; Shin et al., 2011; Traoré et al., 2006). The dimerization domain of *Sc*Nur protein differs moderately from other Fur family members and these differences originate from the conformation of the β3-β4 sheet and the kinked form of α6 helix (**Figure 1.4**). Additionally, instead of having one long final β-strand covering the α-helix in the C-terminal domain, *Sc*Nur (An et al., 2009) contains two short β-strands similar to *Sp*PerR (Lin et al., 2014; Makthal et al., 2013) while *Pa*Fur (Pohl et al., 2003), *Mt*Zur (Lucarelli et al., 2007) and *Sc*Zur (Shin et al., 2011) contain only one short α-helix. In most Fur family members, the three-stranded β-sheets of DD from each protomer are combined into a six-stranded antiparallel β-sheet, which together with the pair of symmetry related α5 helices stabilize the dimeric form of the protein. In contrast, in *Sc*Nur dimer, two sheets from each protomer do not participate in the formation of the stable intermolecular sheet. These observations are most likely due to the binding of Ni ion to the unique metal site of *Sc*Nur (An et al., 2009).

1.6.2 Holo-structures

The majority of the crystal structures of the Fur family proteins for which the regulatory binding site (see below) is metallated adopt the canonical V-shaped conformation. Such arrangement of the domains is permissive for the interaction of the transcription factor with DNA wherein the DNA binding α-helices (helix α3 in *Mt*Zur and *Sc*Zur and helix α4 in all the other crystallized protein members of the Fur family of metalloregulators) are nearly perpendicular to each other. Such conformation can be

observed in the structures of *Hp*Fur, *Mg*Fur, *Pa*Fur and *Bs*PerRZnMn (Deng et al., 2015; Dian et al., 2011; Jacquamet et al., 2009; Pohl et al., 2003). Conversely, in *Vc*Fur, the orientation of the DBD relative to its dimerization domain is slightly different when compared to other Fur proteins (**Figure 1.5A**). The conformational change occurs within the hinge region of *Vc*Fur which results in a ~ 30° rotation bringing the DNA recognition helices closer to each other in space (Sheikh and Taylor, 2009). Similar to *Vc*Fur, a conformational change can also be observed in the hinge region of *Sc*Zur leading to a modest rotation of DBDs and a shorter distance between the DNA recognition helices (Shin et al., 2011). Furthermore, the structure of *Sc*Nur is very similar to *Hp*Fur, *Mg*Fur, *Pa*Fur and *Bs*PerRZnMn structures and aside the slight rotation of the DBD, the major difference consists in the conformation of the β1-β2 antiparallel β-sheet, which is fixed to the DD via the interaction with Ni ion and adopts horizontal conformation in *Sc*Nur, compared to a slant conformation of the flexible β-sheet in other Fur family members (An et al., 2009). Moreover, *Mt*Zur adopts a much wider conformation induced by the ~ 77° rotation of the DBDs positioning the DNA binding helices nearly parallel to each other, suggesting a divergent mode of DNA recognition for *Mt*Zur when compared to other members of the Fur family of metalloregulators (Lucarelli et al., 2007). Finally, the most divergent holo-structure is the structure of *Sp*PerR in which the DBDs are flipped to the opposite side of the dimerization domain. In this conformation, the protein adopts quasi-planar conformation that is not suitable for the interaction with DNA. Current model suggests that two adjacent *Sp*PerR dimers come together and form the DNA binding platform (Lin et al., 2014; Makthal et al., 2013). Notwithstanding the similar basic fold adopted by Fur family metalloregulators, there are important structural

A

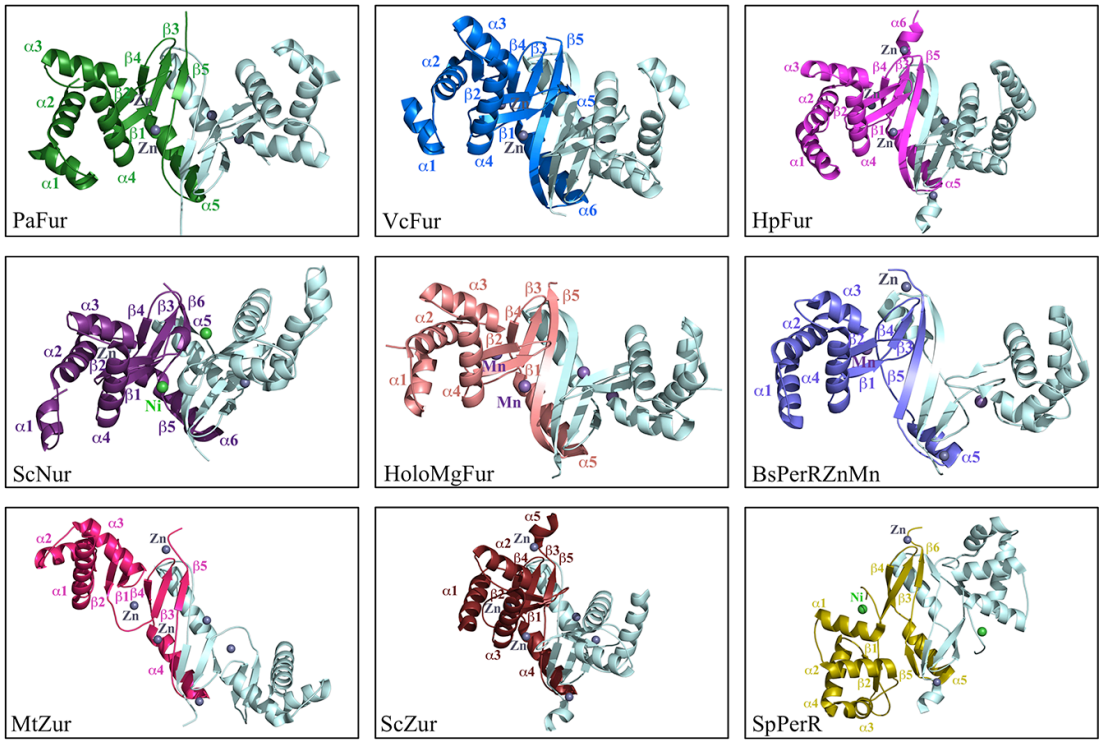
PaFur
VcFur
HpFur
ScNur
HoloMgFur
BsPerRZnMn
MtZur
ScZur
SpPerR

B

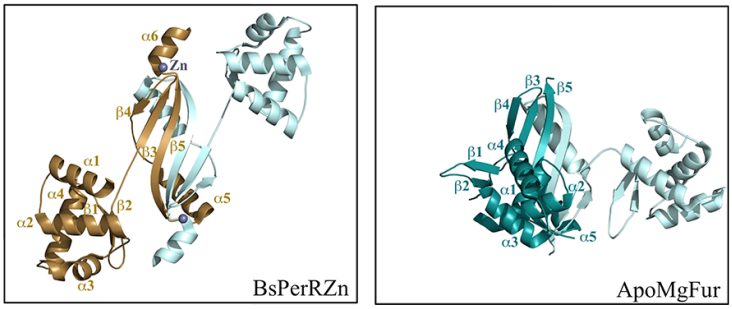
BsPerRZn
ApoMgFur

Figure 1.5 Overall structures of Fur family members are similar.

(A) Cartoon representation of Holo-structures of Fur family of regulators in which the protomer A is highlighted in green (*Pa*Fur; 1MZB), marine (*Vc*Fur; 2W57), magenta (*Hp*Fur; 2XIG), purple (*Sc*Nur; 3EYY), salmon (Holo*Mg*Fur; 4RAZ), blue (*Bs*PerRZnMn; 3F8N), pink (*Mt*Zur; 2O03), brown (*Sc*Zur; 3MWM), and yellow (*Sp*PerR; 4I7H).

(B) Cartoon representation of Apo-structures of Fur family of regulators in which the protomer A is highlighted in sand (*Bs*PerRZn; 2FE3) and dark teal (Apo*Mg*Fur; 4RAY).

β-sheets and α-helices of each protomer A are labeled accordingly. Zn, Mn and Ni ions are represented by grey, purple and green spheres, respectively. Dimerization domains are shown in the same orientation. All structures were obtained from the RCSB PDB structure bank (http://www.rcsb.org/pdb/).

differences, which may explain why some members are simple regulators of metal homeostasis, while others play a more important role as global regulators with multiple functions exhibiting a variety of regulatory mechanisms.

1.6.3 Apo-structures

Currently there are only two apo-structures of the Fur family of regulators available in the protein data bank namely apo-*Bs*PerRZn (Traoré et al., 2006) and apo-*Mg*Fur (Deng et al., 2015) (**Figure 1.5B**). These structures consist of an N-terminal DBD and a C-terminal dimerization domain connected by a short hinge region, however the positioning of the DBDs relative to DDs is different in each structure. In Apo-*Bs*PerRZn structure, the metalloregulator adopts a nearly flat structure with DBDs positioned beside the dimerization domain and the hinge region adopting an elongated conformation (Traoré et al., 2006). Conversely apo-*Mg*Fur adopts a V-shaped conformation with a slightly bent hinge region (Deng et al., 2015). Apo-*Mg*Fur structure is the first reported apo-Fur structure without transition metal ions. The superposition of the apo-*Mg*Fur protomers yielded an overall root mean square (rms) deviation of 4.6Å while the alignment of the each individual DBD and DD domains resulted in rmsd of, 0.4 Å and 0.9Å, respectively (Deng et al., 2015). These observations demonstrated that the hinge region is flexible and leads to different conformations of apo-*Mg*Fur protomers. Additional analysis of crystal packing showed that this conformation of apo-*Mg*Fur structure is stabilized by DBDs and DDs from symmetry related molecules. The conformation adopted by *Bs*PerRZn and *Mg*Fur in absence of regulatory metals is unsuitable for the interaction with DNA and the binding of the regulatory metal ions

induces large conformational changes and greatly stabilizes both structures (Deng et al., 2015; Jacquamet et al., 2009; Traoré et al., 2006).

1.6.4 Metal binding sites

The number of occupied metal binding sites varies from zero to three in reported structures of the Fur family of metalloregulators and their possible roles have been described. The first metal binding site, S1, is found within the dimerization domain of several Fur family regulators and is typically composed of four cysteine residues that tetracoordinate a Zn ion (**Figure 1.6**). The metallation of the dual CxxC motif plays a structural role by bringing together three β-strands of the DD in apo-*Bs*PerRZn, holo-*Bs*PerRZnMn, *Ec*Zur, *Sp*PerR, *Hp*Fur, *Mt*Zur and *Sc*Zur structures and likely play a role in the stabilization of the dimeric form of Fur regulators (Dian et al., 2011; Gilston et al., 2014; Jacquamet et al., 2009; Lin et al., 2014; Lucarelli et al., 2007; Makthal et al., 2013; Shin et al., 2011; Traoré et al., 2006). This metal binding site is absent in *Pa*Fur, *Vc*Fur and *Mg*Fur which can be explained by the lack of one or more cysteine residues (Deng et al., 2015; Pohl et al., 2003; Sheikh and Taylor, 2009). While *Pa*Fur contains only one cysteine residue in its dimerization domain, *Mg*Fur does not contain any; therefore these metalloregulators do not harbor a S1 site. Despite containing four cysteine residues in its dimerization domain, the structure of *Vc*Fur does not use these cysteines for binding a metal ion. Instead, two of these cysteine residues (Cys93 and Cys133) form a disulphide bond. Interestingly, oxidation of the four cysteine residues in *Ec*Fur stabilizes the monomeric form of the metalloregulator while reduction and metallation of this site with zinc promote protein dimerization (Pecqueur et al., 2006). However, in contrast to *Ec*Fur,

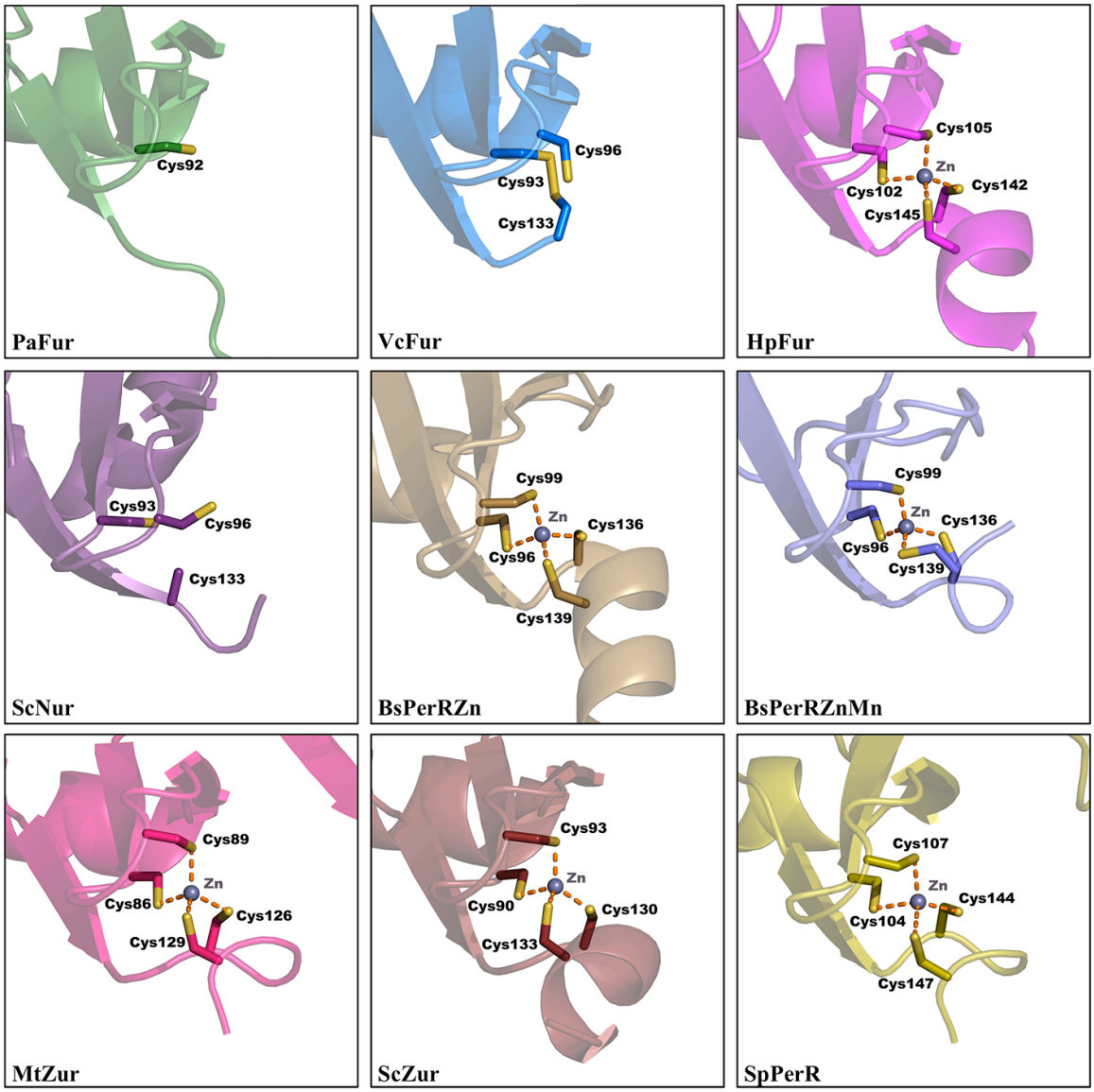
Cys92
PaFur
Cys96
Cys93
Cys133
VcFur
Cys105
Zn
Cys102
Cys142
Cys145
HpFur
Cys93
Cys96
Cys133
ScNur
Cys99
Zn
Cys136
Cys96
Cys139
BsPerRZn
Cys99
Zn
Cys136
Cys96
Cys139
BsPerRZnMn
Cys89
Zn
Cys86
Cys126
Cys129
MtZur
Cys93
Zn
Cys90
Cys130
Cys133
ScZur
Cys107
Zn
Cys144
Cys104
Cys147
SpPerR

Figure 1.6 Structural site S1 is composed of two CxxC motifs which bind Zn^{2+} ion

Zoomed view on S1 metal binding sites of *Pa*Fur (1MZB), *Vc*Fur (2W57), *Hp*Fur (2XIG), *Sc*Nur (3EYY), *Bs*PerRZn (2FE3), *Bs*PerRZnMn (3F8N), *Mt*Zur (2O03), *Sc*Zur (3MWM), and *Sp*PerR (4I7H). Zn ions and hydrogen bonds are depicted as grey spheres and orange dashed lines, respectively. All structures were obtained from the RCSB PDB structure bank (http://www.rcsb.org/pdb/).

the oxidation/reduction of cysteine residues in *Vc*Fur is not involved in monomer to dimer transition. This idea is supported by structural studies showing that the oxidized form of the metalloregulator still forms a dimer, suggesting that other factors are involved in the stabilization and formation of *Vc*Fur dimer. Finally, the presence of CxxC motifs does not always imply the binding of the zinc ion in Fur proteins. In *Sc*Nur (An et al., 2009), all four cysteine residues are conserved, nevertheless they do not coordinate zinc ion and the absence of the metal is not due to cysteine oxidation. It is however possible that the *Sc*Nur protein binds a zinc ion at this site *in vivo,* but that remains to be confirmed. In conclusion, while in some cases the S1 metal binding site is absent and is not required for the stability and activity of the transcription factor, its presence is, nevertheless, crucial for the formation of the dimeric form of several members of the Fur family of regulators (Gilston et al., 2014; Pecqueur et al., 2006; Shin et al., 2011; Traoré et al., 2006).

The second metal binding site, S2, is found at the interface between the DBD and the DD of Fur metalloregulators. Considering its position, this metal binding site is important for the activation of the transcription factors i.e. the binding of the metal ion at the S2 site induces conformational changes necessary for the formation of the V-shaped structure that is characteristic of active metalloregulators. Accordingly, the S2 site was coined as the regulatory metal binding site of several members of the Fur family of proteins (An et al., 2009; Deng et al., 2015; Dian et al., 2011; Gilston et al., 2014; Jacquamet et al., 2009; Sheikh and Taylor, 2009; Shin et al., 2011). The S2 site can be observed in the crystal structures of holo-*Bs*PerRZnMn, *Hp*Fur, holo-*Mg*Fur, *Mt*Zur, *Pa*Fur, *Sc*Nur, *Sc*Zur, *Sp*PerR and *Vc*Fur (**Figure 1.7**). The coordination of this metal

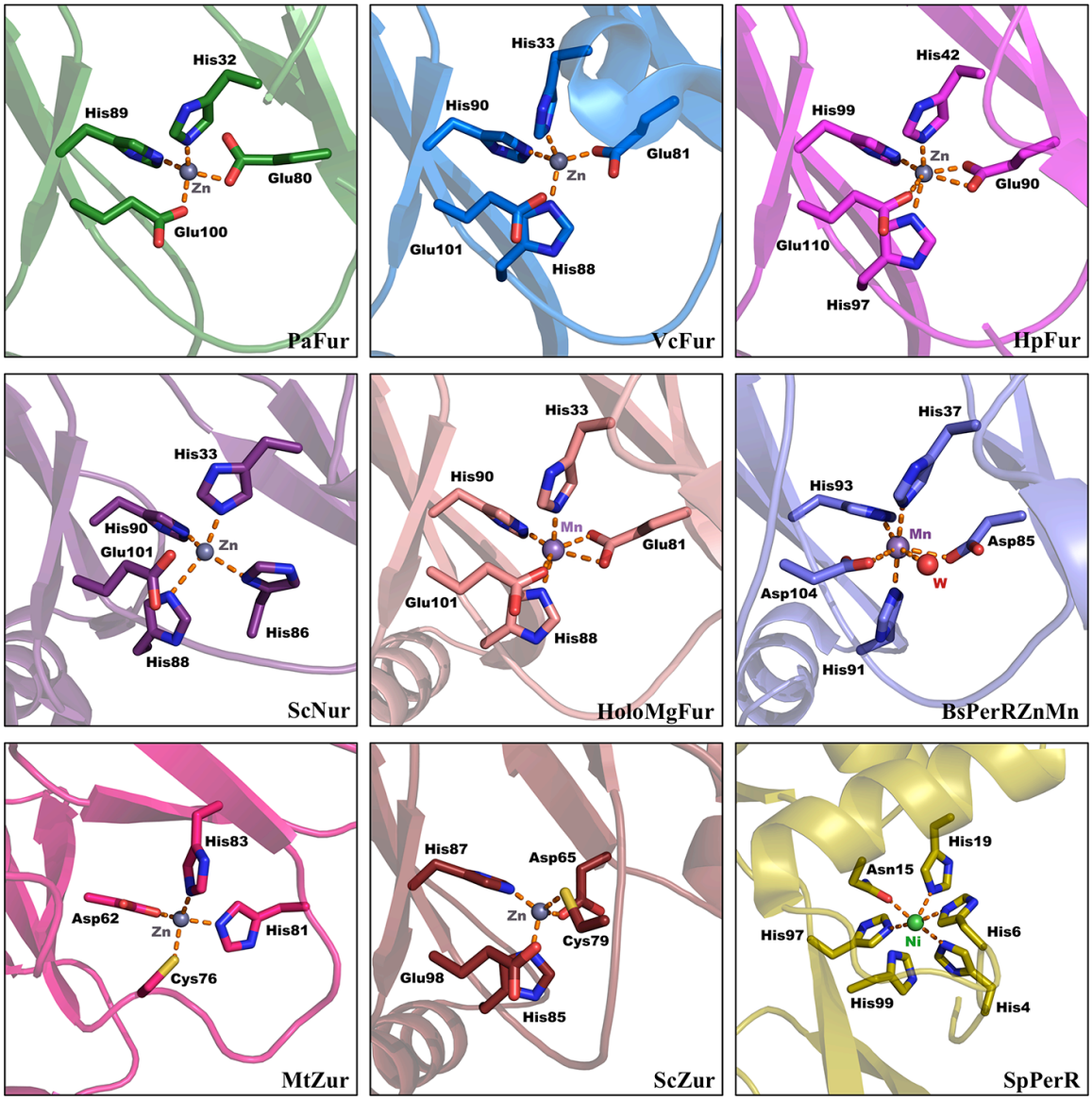
His32
His89
Zn
Glu80
Glu100
PaFur
His33
His90
Zn
Glu81
Glu101
His88
VcFur
His42
His99
Zn
Glu90
Glu110
His97
HpFur
His33
His90
Glu101
Zn
His86
His88
ScNur
His33
His90
Mn
Glu81
Glu101
His88
HoloMgFur
His37
His93
Mn
Asp85
W
Asp104
His91
BsPerRZnMn
His83
Asp62
Zn
His81
Cys76
MtZur
His87
Asp65
Zn
Cys79
Glu98
His85
ScZur
His19
Asn15
His97
Ni
His6
His99
His4
SpPerR

Figure 1.7 Coordination of the S2 metal binding site diverges within the Fur family of metalloregulators

Zoomed view on S2 metal binding sites of *Pa*Fur (1MZB), *Vc*Fur (2W57), *Hp*Fur (2XIG), *Sc*Nur (3EYY), Holo*Mg*Fur (4RAZ), *Bs*PerRZnMn (3F8N), *Mt*Zur (2O03), *Sc*Zur (3MWM), and *Sp*PerR (4I7H). Zn, Mn and Ni ions are represented by grey, purple and green spheres, respectively. Water molecules (W) and hydrogen bonds are depicted as red spheres and orange dashed lines, respectively. All structures were obtained from the RCSB PDB structure bank (http://www.rcsb.org/pdb/).

binding site shares similarities between metalloregulators such as all Fur, holo-*Bs*PerRZnMn and *Sc*Nur structures. In these proteins, this site is composed of three histidine residues, two from the DD and one from the DBD, and two negatively charged residues (two glutamate residues in Fur proteins and two aspartate residues in holo-*Bs*PerRZnMn). However, there are several important differences in the coordination of the metal ions in this site. The regulatory metal ions Zn^{2+} and Mn^{2+} in *Hp*Fur and holo-*Mg*Fur both have an octahedral geometry and are hexacoordinated by three histidines and two glutamates, where one of the glutamates binds in a bidentate manner. In regard to the S2 site, the coordination of Mn^{2+} ion in holo-*Bs*PerRZnMn share similarities with Holo-*Mg*Fur, however, in the latter one, the metal ion is coordinated by two aspartate residues both binding the metal in a monodentate manner with a water completing the sixth coordination. In contrast to the octahedral coordination observed in holo-*Bs*PerRZnMn, *Hp*Fur and holo-*Mg*Fur, the Zn ions in *Pa*Fur and *Vc*Fur S2 sites are tetrahedrally coordinated either by two histidine and two glutamate residues (2H/2E) or 3H/1E, respectively. However, all five residues involved in the coordination of the regulatory metal ions of *Bs*PerRZnMn, *Hp*Fur and holo-*Mg*Fur are conserved in these two proteins as well, suggesting that they could possibly be involved in the coordination of the regulatory Fe^{2+} ion. While these studies provided insights into the metallation mechanisms underlying the binding of metals in metalloregulator's S2 site, Zn substitutions in iron binding proteins can be misleading because Zn^{2+} and Fe^{2+} ions have different preferred geometries and the structures containing Zn ion in the regulatory metal site might not accurately represent the coordination observed in the cell. Thus determining the crystal structure of Fur proteins in complex with iron is needed to fully

understand the conformational changes induced by the binding of metal cofactor to the regulatory metal binding site. The Zn ion in *Sc*Nur is also tetracoordinated but all the four ligands are histidine residues with square-planar geometry, one of the preferred coordination geometries for nickel. The *Sp*PerR structure encompasses a Ni^{2+} ion in the S2 metal binding site, which is hexacoordinated in an octahedral geometry by five histidine residues (three from the DBD and two from the DD) and an asparagine residue from the DBD domain. Finally, all three Zur structures namely *Ec*Zur, *Mt*Zur and *Sc*Zur contain a Zn ion in their S2 site which is tetracoordinated by two histidine residues, one cysteine and one aspartate (MtZur and ScZur) or glutamate (EcZur). The presence of the cysteine residue in the regulatory metal binding site of Zur proteins explains the specificity of Zur orthologs for Zn^{2+} cofactor. Overall, in spite of their highly similar structural architecture these studies highlight the variability and the flexibility of the regulatory binding site to bind different metal ions, which may explain the specific roles of different members of the Fur family of metalloregulators.

The third metal binding site, S3, is found within the dimerization domain of Fur family members and is observed in nearly all Fur and Zur structures. Similar to the S2 site, variation in the coordination and the geometry of metals in the S3 site was reported (**Figure 1.8**). First, similar to the Mn^{2+}-bound *Mg*Fur, *Pa*Fur S3 site hexacoordinates a Zn^{2+} ion employing a distorted octahedral geometry. Metallation is mediated by two histidines, one aspartate binding in a bidentate manner, one glutamate and a water-mediated interaction with a glutamine residue. In contrast, Zn^{2+} ions in *Vc*Fur and *Hp*Fur S3 metal binding sites have tetrahedral geometry and are coordinated by two histidines and two negatively charged residues (one aspartate and one glutamate). Similar to *Vc*Fur

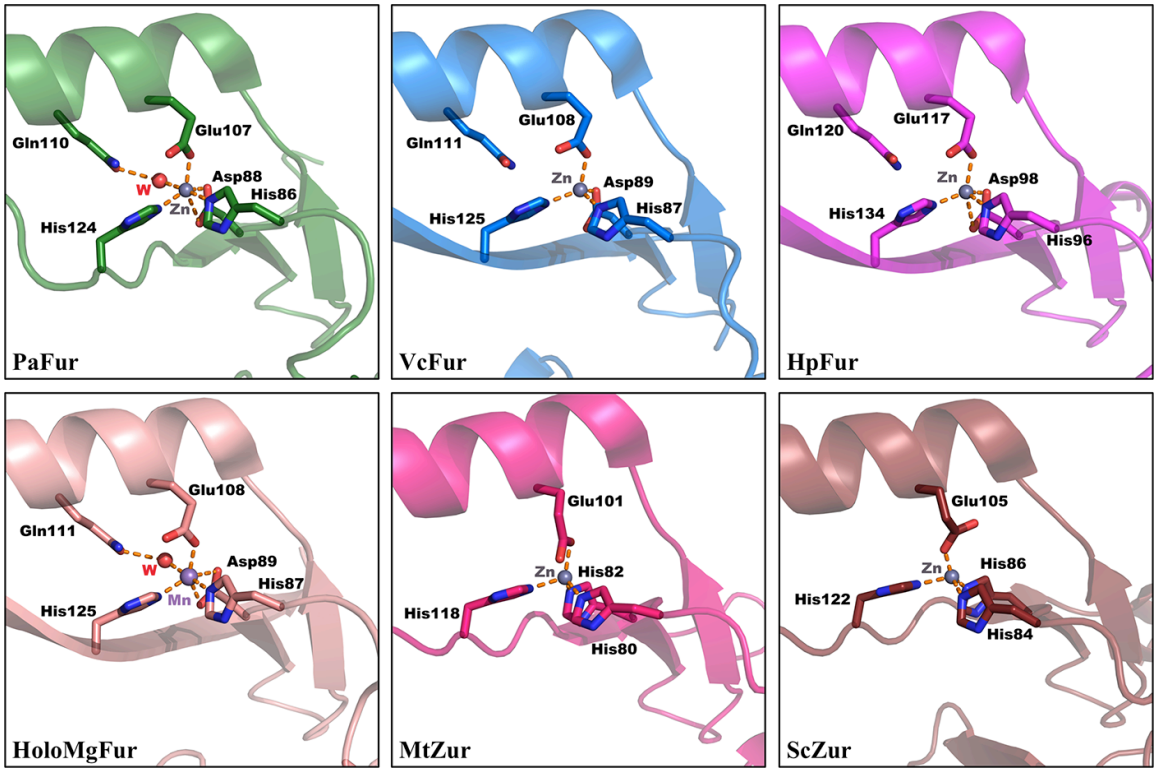
PaFur
Gln110
Glu107
W
Asp88
His86
Zn
His124
VcFur
Glu108
Gln111
Zn
Asp89
His87
His125
HpFur
Gln120
Glu117
Zn
Asp98
His134
His96
HoloMgFur
Glu108
Gln111
W
Asp89
His87
Mn
His125
MtZur
Glu101
Zn
His82
His118
His80
ScZur
Glu105
Zn
His86
His122
His84

Figure 1.8 Coordination of the S3 metal binding site diverges within the Fur family of metalloregulators

Zoomed view on S3 metal binding sites of *Pa*Fur (1MZB), *Vc*Fur (2W57), *Hp*Fur (2XIG), Holo*Mg*Fur (4RAZ), *Mt*Zur (2O03), and *Sc*Zur (3MWM). Zn, and Mn ions are represented by grey and purple spheres, respectively. Water molecules (W) and hydrogen bonds are depicted as red spheres and orange dashed lines, respectively. All structures were obtained from the RCSB PDB structure bank (http://www.rcsb.org/pdb/).

and *Hp*Fur, the S3 site in *Mt*Zur and *Sc*Zur has a tetrahedral geometry wherein three histidines and one glutamate participate in the coordination of a Zn^{2+} ion. While metal ion is frequently observed in the S3 site, the role of this metal binding site remains controversial. In contrast to S2 site, mutation of the S3 site in *Hp*Fur (Dian et al., 2011), *Sc*Zur (Shin et al., 2011) and *Mg*Fur (Deng et al., 2015) decreases but does not abolish DNA-binding activity of these proteins while in *Pa*Fur (Pohl et al., 2003), this site was identified as the regulatory site. Overall, these results show the versatility of the S3 site and suggest that its role may have diverged during evolution.

1.6.5 Structural characterization of protein-DNA complexes

Until recently, the structural basis underlying the binding of metalloregulators to DNA had remained vague at best with most models relying on computational approaches to characterize Fur DNA complexes (Dian et al., 2011; Pohl et al., 2003; Tiss et al., 2005). Recently, the structural determination of the *Ec*Zur in complex with DNA (PDB: 4MTD; 4MTE) provided the first insights into the intricate details of the interaction between a member of the Fur family and DNA (Gilston et al., 2014). The structure shows that *Ec*Zur DBD binds to the major and minor grooves of DNA and that the residues found in helix-turn-helix (HTH) motif of *Ec*Zur's DBD make over 100 contacts with DNA nitrogenous bases and phosphate backbone of the DNA molecule. Specifically, in each protomer, 8 direct interactions are observed between the side chain of Tyr45 and Arg65 and the N7 nitrogen of bases. The role of Arg65, which is highly conserved across evolution, is supported by previous mutational analysis showing that its substitution into a histidine blunts *Ec*Zur DNA binding activity (Patzer and Hantke, 2000). The same

crystal structure also shows that two *Ec*Zur dimers collaborate for binding to DNA and that cooperativity relies on a salt bridge between Arg52 and Asp49 that connects two adjacent independent dimers. Intriguingly, both residues are conserved in gram-negative Zur proteins but absent in Fur homologs suggesting that this interaction mode between two dimers is unique to Zur proteins. The crystal structure determination of the *Ec*Zur-DNA complex also enabled the identification of another *Ec*Zur regulated gene. In fact, *Ec*Zur was shown to bind the promoter region of the periplasmic lysozyme inhibitor *pliG* gene and to repress its expression. The characterization of *Ec*Zur interaction with the *pliG* operator revealed a single dimer-DNA intermediate suggesting that the metalloregulator can bind DNA using a single dimer. Collectively, the study by Gilson *et al*., demonstrated that *Ec*Zur uses two alternative modes of interactions with DNA wherein a dimer of dimer or a single dimer interact with DNA.

More recently, two crystal structures of the DNA bound form of *Magnetospirillum gryphiswaldense* MSR-1 Fur (*Mg*Fur) was reported (Deng et al., 2015). The authors solved the crystal structures of a single dimer of *Mg*Fur in complex with a 25 bp long oligonucleotide corresponding to the *feoAB1* operator as well as of a dimer of dimer of *Mg*Fur bound to *Pseudomonas aeruginosa* Fur box. These structures first demonstrated the ability of *Mg*Fur to bind DNA at different ratios. They also showed that binding to DNA induces moderate conformational changes in the DBDs that result in the shortening of the distance between the α4 helices of the two monomers allowing a better insertion of the DBD in consecutive major grooves. Akin to *Ec*Zur-DNA crystal structure, the majority of the interactions taking place at the interface between *Mg*Fur and DNA are hydrogen bonds and other electrostatic interactions involving the residue side

chains and the DNA phosphodiester backbone. More specifically, three key residues make several direct interactions with DNA and these contacts can be clustered in three different categories. First, the phenyl ring of Tyr56 makes van der Waals interactions with the methyl groups on T12' (' denotes the non-coding strand) and two consecutive thymine nucleotides T15' and T16' in the major groove of the *P. aeruginos*a Fur box and the *feoAB1* operator, respectively. These interactions are base specific as the loss of thymine residue impairs the binding of Fur to DNA. Second, Arg57 guanidium group forms bidentate hydrogen bonds with the O6 and N7 atoms of a conserved G7 in the *feoAB1* operator and the G10 of the *P. aeruginosa* Fur box. An additional hydrogen bond between Arg57 and T15' of the *P.aeruginosa* Fur box is also observed. Finally, the third category of interaction involves the shape readout of a minor groove with enhanced negative electrostatic potential by a lysine residue. Lys15 forms hydrogen bonds with A24' of the *feoAB1* operator and with T6 and T21' of the *P.aeruginosa* Fur box. Collectively, this study highlighted the role of Tyr56, Arg57 and Lys15 in binding DNA. Considering that these residues are conserved across evolution, this study also suggests that the DNA-interaction modes observed in this study are conserved.

In both DNA bound *Ec*Zur and *Mg*Fur structures, the DNA is slightly bent leading to the formation of larger major grooves and narrower minor grooves. However, DNA bending is not induced by Fur binding since the narrower minor grooves were previously reported in the absence of the Fur protein(Deng et al., 2015). Considering that Fur operators are A/T rich and that these sequences tend to form narrow minor grooves, the shape readout mechanism may be a peculiarity for the gene regulatory activity by the Fur family of metalloregulators.

1.7 *Campylobacter jejuni* ferric uptake regulator (*Cj*Fur)

C. jejuni Fur (*Cj*Fur) is an important transcription factor. Transcriptome profiling and chromatin immunoprecipitation combined with microarray analysis approaches (ChIP-chip) using wild type strain or *fur* deletion mutant in iron-rich or iron-limited growth conditions (Butcher et al., 2012; Holmes et al., 2005; Palyada et al., 2004) showed that holo-*Cj*Fur represses the transcription of all genes encoding iron-transport systems including enterobactin, heme and ferric-lactoferrin transporters, to name few. Moreover, the expression of several genes involved in oxidative stress defense such as *katA*, *ahpC*, thioredoxin reductase (*trxB*) and an ankyrin-repeat containing protein (*cj1386*) are also repressed by holo-*Cj*Fur (Holmes et al., 2005). In addition to repression, the same studies showed that the holo- form of the metalloregulator can also activate gene expression and more importantly, the protein maintain gene regulatory activities (positive and negative) in absence of regulatory metals. While the transcriptomic studies were unable to distinguish direct from indirect regulation (Holmes et al., 2005; Palyada et al., 2004), ChIP-chip analysis combined with qRT-PCR identified the genome wide distribution of *Cj*Fur-bound regions and confirmed all four modes of *Cj*Fur regulation, respectively (Butcher et al., 2012). These studies also identified *Cj*Fur as an important regulator of genes involved in flagella and membrane biogenesis, energy metabolism, non-iron ion transporters and numerous proteins with unknown function (Butcher et al., 2012; Holmes et al., 2005; Palyada et al., 2004). As previously mentioned, Fur proteins play an important role in colonization and bacterial virulence. Mutation of the *fur* gene significantly affects the ability of *C. jejuni* to colonize the gastrointestinal tract of chicks, demonstrating the importance of Fur regulation and iron homeostasis *in vivo* (Palyada et

al., 2004). Considering that *Cj*Fur regulates genes involved in other key cellular processes such as oxidative defense and flagellar biogenesis, which are important for cell survival and motility, it is believed that Fur may play a role in *C. jejuni* virulence.

Genome-wide profiling of *Cj*Fur binding sites was used in order to identify the consensus sequence recognized by *Cj*Fur (Butcher et al., 2012). While the study failed to define a universal consensus sequence for all *Cj*Fur binding sites, the authors identified consensus motifs for holo-*Cj*Fur-activated and holo-*Cj*Fur-repressed genes. The consensus sequence for holo-*Cj*Fur-repression (5'-TATTTTGATAATTATTATCA-3') is similar to the *Cj*Fur consensus sequence previously proposed (Palyada et al., 2004) and contains the palindromic 7-1-7 (underlined) sequence, feature found in classical Fur box. Conversely, the consensus sequence for holo-*Cj*Fur-activated genes (5'-TTTGGAACANTTTTTGCT-3') is non-palindromic and is significantly different from previously reported Fur boxes. Owing to a low number of apo-*Cj*Fur regulated genes, the consensus sequence for apo-*Cj*Fur regulation could not be determined. Therefore, this study suggests that *Cj*Fur recognizes multiple DNA-binding elements and the classical Fur box does not fully represent the target sequences recognized by Fur proteins.

1.8 Rationale and hypothesis

Considering that the Fur family of metalloregulators plays crucial roles in bacteria and that there are no Fur homologs in human, these proteins constitute excellent targets for the design of therapeutic molecules for the treatment of *Campylobacter* mediated infections. Since the apo-regulation was observed in only few pathogenic bacteria, the understanding of the mechanism controlling such activity could lead to a development of

therapeutic molecules targeting only the apo-Fur regulation and thus having a minimal effect on human microbiota.

Given that the Fur family of metalloregulators regulates gene expression by four general mechanisms, namely transcription activation/repression in apo-form and transcription activation/repression in holo-form, I hypothesized that the ability of Fur family of metalloregulators to adopt different structural conformations underlies these peculiar functional differences.

To address this hypothesis, I have used structural biology combined with biochemical approaches to characterize the structure of *Cj*Fur and to better understand the mechanistic basis underlying the binding of Fur family of metalloregulators to DNA in absence or presence of regulatory metal ions.

CHAPTER 2. MATERIAL AND METHODS

2.1 Strains and plasmid construction

E. coli DH5α was used as the host strain for DNA amplification and vector construction. **Table 1 in Appendix 1** lists the sequences of all the primers used for cloning in this study.

2.1.1 Construction of pStrepSUMO (pSS)-*Cj*Fur expression plasmid

The gene corresponding to *Campylobacter jejuni* Fur (**Figure 1 in Appendix 1**) was PCR-amplified from *Campylobacter jejuni* TGH9011 genomic DNA with primers pair 1 - 2 (**Table 1 in Appendix 1**) and cloned in a homemade vector referred to as pStrepSUMO (pSS). The *Cj* TGH9011 Fur contains a single amino acid substitution (Thr42Ile) as compared to *Cj* NCTC11168 Fur and this residue is not evolutionary conserved across Fur proteins (**Figure 3.3C**) and is therefore not expected to participate to its biological functions. The pSS vector is a derivative of the pHis parallel vector (pHis2) (Sheffield et al., 1999) and was constructed by replacing the hexahistidine Tag (6XHis) and the Spacer region of pHis2 by a DNA fragment corresponding to a Strep Tag placed in frame with the sequence encoding the Small Ubiquitin-like Modifier (SUMO) protein SMT3 from budding yeast (**Figure 2 in Appendix 1**). The cDNA of SMT3 was PCR amplified with the primers pair 3 - 4 and *S. cerevisiae* genomic DNA as template. The PCR product was subsequently cloned *Nde1-Nco1* in pHis2. Following amplification and purification of the vector, the *Cjfur* gene was cloned, in frame with the

open reading frame of the Strep-SUMO tag, using the *BamHI* and *XhoI* restriction sites. The insertion of *Cjfur* gene in pSS vector was confirmed by PCR reactions using the primers pair 1-2 and by sequencing at the Centre de Recherche du CHUL.

2.1.2 Construction of pStrep (pS)-*Cj*Fur expression plasmid

The gene corresponding to *Cj*Fur was amplified from pSS-*Cj*Fur plasmid with primers pair 5 – 6 (**Table 1 in Appendix 1**) and cloned in a homemade vector referred to as pStrep (pS). Similar to pSS vector, the pS vector is a derivative of pHis2 vector and was constructed by replacing the 6XHis Tag of pHis2 by a DNA fragment corresponding to a Strep Tag (**Figure 3 in Appendix 1**). The *Cjfur* gene was cloned in frame with the open reading frame of the Strep tag, using the *NcoI* and *XhoI* restriction sites. The insertion of *Cjfur* gene in pStrep vector was confirmed by PCR reactions using the primers pair 5 - 6 and by sequencing at the Centre de Recherche du CHUL.

2.1.3 Construction of pET-*Cj*Fur expression plasmid

The *Cjfur* gene was PCR amplified using pSS-*Cj*Fur plasmid as template and a pair of primers 7 - 8 (**Table 1 in Appendix 1**) specifically designed to include a *NdeI* and *XhoI* restriction sites on the 5' and 3' ends of the PCR product, respectively. The PCR product and the pET3d vector (Novagen) were digested with *NdeI* and *XhoI*, separated on an agarose gel and gel extracted according to the manufacturer's instructions (Qiagen). The digested PCR fragment was ligated to the digested pET3d vector using the T4 ligase (NEB). The insertion of the PCR product was confirmed by PCR reactions using the primers pair 7 - 8 and by sequencing at the Centre de Recherche du CHUL.

2.2 Protein expression

For the expression of ss-*Cj*Fur, s-*Cj*Fur and untagged *Cj*Fur proteins, the plasmids corresponding to pSS-*Cj*Fur, pS-*Cj*Fur and pET-*Cj*Fur were transformed into competent *E. coli* BL-21 Rosetta cells (Novagen) by incubating each DNA construct with bacteria during 30 minutes on ice and then heated to 42°C during one min. Following a two minute incubation on ice, Luria-Bertani (LB) broth was added to the cells which were then allowed to grow in an incubator-shaker (Excella E24, New Brunswick Scientific) during one hour at 37°C with constant shaking at 250 RPM. The cells were then plated onto LB agar supplemented with ampicillin (100 $\mu g \times mL^{-1}$) and chloramphenicol (50 $\mu g \times mL^{-1}$). The following day, the transformants were cultured in 500 mL of LB broth supplemented with the same antibiotics.

The expression of proteins was induced with 0.1 mM isopropyl β-D-1-thiogalactopyranoside (IPTG) (Sigma) at an OD_{600} of 0.4-0.5 during 3 hours at 37°C for ss-*Cj*Fur protein and 18 hours at 18°C for s-*Cj*Fur and untagged *Cj*Fur proteins. Following induction, *E. coli* cells were centrifuged at 3000 rpm during 30 minutes at 4°C (J6-MI Centrifuge, Beckman Coulter) and cells corresponding to 1 L cultures were resuspended in 25 mL of corresponding lysis buffer (**Table 2 in Appendix 1**). Cell pellets were stored at -80°C until protein purification.

2.3 Protein purification

Frozen pellets were thawed in cold water and 75 mL of lysis buffer was added to the cell suspension. Cells were lysed using three sonication cycles of one minute each (Misonix Sonicator 3000). The lysates were centrifuged at 31000×g during 30 minutes at 4°C (Beckman Avanti J-25 centrifuge, JA 25-50 rotor) and the supernatant was clarified by filtration using 0.45 μm filters.

2.3.1 Purification of ss-*Cj*Fur protein

Filtered cell lysate containing ss-CjFur was applied onto a Strep-TACTIN affinity chromatography column (Qiagen) pre-equilibrated by gravity with 10-column volumes (CV) of PBS buffer. Following the binding of ss-*Cj*Fur, Strep-TACTIN beads were washed with 15-CV of PBS buffer and the fusion protein was eluted from the resin in ~35 mL of PBS buffer supplemented with 2.5 mM D-desthiobiotin (Sigma). The StrepSUMO tag was removed using the SUMO specific protease, Ubiquitin-like-specific protease 1 (ULP1), during 16 hours at 4°C in a 10 kDa Molecular Weight Cut-Off (MWCO) dialysis bag (Thermo Scientific) in PBS buffer. *Cj*Fur was further purified by ion exchange chromatography using SP Sepharose Fast Flow Beads (GE Healthcare) equilibrated in 20 mM citrate pH 6.0 and 5 mM β-mercaptoethanol (BMe). Following the binding of the proteins, the SP sepharose column was washed with 5-CV of 20 mM Citrate pH 6.0 and 5 mM BMe buffer and the bound *Cj*Fur protein was eluted using a linear gradient that progressively increases the concentration of NaCl from 0 to 1 M. Fractions corresponding to *Cj*Fur were concentrated and further purified by size exclusion chromatography using a preparative grade Superdex S75 column (AKTA FPLC, GE Healthcare) equilibrated in

20 mM Tris pH 7.0, 250 mM NaCl, 5 mM BMe. *Cj*Fur eluted as a single peak at a molecular weight corresponding to a protein dimer. Fractions corresponding to *Cj*Fur dimer were pooled, concentrated to ~10 mg × mL^{-1} and *Cj*Fur concentration was measured by UV absorbance (NanoDrop ND-1000, Thermo Scientific). The extinction coefficient (ε) and the molecular weight (MW) of this construct, 13410 M^{-1} cm^{-1} and 18747.7 Da, respectively, were determined using the online ProtParam tool (https://web.expasy.org/protparam). We used the protein absorbance value for 0.1% ($Abs_{280nm}^{0.1\%}$) (=1 g/L) of 0.715 as unit of measure for protein concentration determination. This purification protocol leads to a *Cj*FurZn_2 protein used for the characterization of the apo-form of *Cj*Fur and purification from a 2 L culture would yield approximately 3-5 mg of purified protein. Purification yields of different Fur mutants were comparable to WT Fur protein.

2.3.2 Purification of s-*Cj*Fur

For the purification of s-*Cj*Fur, the cell lysate was applied onto Strep-TACTIN beads equilibrated with 10-CV of 50mM Tris pH 7.0, 100mM NaCl and 5mM BMe. Following the binding of s-*Cj*Fur, Strep-TACTIN beads were washed with 15-CV of 50mM Tris pH 7.0, 100mM NaCl and 5mM BMe buffer and the fusion protein was eluted according to manufacturer's instructions. The Strep tag of s-*Cj*Fur was removed using the Tobacco Etch Virus (TEV) protease during 16 hours at 4°C in 50mM Tris pH 7.0, 250 mM NaCl and 5mM BMe. Following TEV cleavage, s-*Cj*Fur was concentrated and further purified by size-exclusion chromatography using Superdex S75 pre-equilibrated in 20mM Tris pH 7.0, 250mM NaCl and 5mM Bme. Fractions

corresponding to protein dimer were concentrated and the concentration of the protein was quantified by UV absorbance. The extinction coefficient (ε) and the molecular weight (MW) of this construct, 11920 M^{-1} cm^{-1} and 18382.4 Da, respectively, were determined using the online ProtParam tool (https://web.expasy.org/protparam). We used the protein absorbance value for 0.1% ($Abs_{280nm}^{0.1\%}$) (=1 g/L) of 0.648 as unit of measure for protein concentration determination. This protocol was used for the purification of *Cj*Fur protein used for the characterization of holo-form of *Cj*Fur regulator and purification from a 2 L culture would yield approximately 10-13 mg of purified protein. Purification yields of different Fur mutants were comparable to WT Fur protein.

2.3.3 Purification of untagged *Cj*Fur

The supernatant of a cell extract resuspended in 50 mM Tris pH 7.0, 100 mM NaCl, 5 mM BMe was applied onto a 10 mL Q Sepharose Fast Flow Beads (GE Healthcare) pre-equilibrated in buffer A (20 mM citrate pH 6.0 and 5 mM BMe). The proteins were allowed to bind during one hour at 4°C and were centrifuged at 3000 RPM (Sorvall Legend RT Plus Centrifuge, Thermo Scientific) during 5 minutes at 4°C to recover the supernatant. The supernatant was then applied onto a 10 mL SP Sepharose Fast Flow Beads pre-equilibrated in buffer A. The proteins were allowed to bind for one hour at 4°C and the beads were centrifuged at 3000 RPM during 5 minutes at 4°C. The supernatant was discarded and the beads were washed during 10 minutes at 4°C with 10-CV of buffer A followed by the centrifugation of the beads at 3000 RPM. After repeating the washing step two more times, the beads were incubated at 4°C during 1 hour with 6-CV of buffer A supplemented with 500 mM NaCl. To remove residual beads, the eluted

proteins were filtered using 0.45 μm filters. The filtered proteins were dialyzed twice during 30 min at 4°C in a 10 kDa MWCO dialysis bag placed in 4 L of buffer A. The dialyzed proteins were subsequently loaded onto an Heparin column (GE Healthcare) pre-equilibrated with buffer A. Following the loading of the proteins, the heparin column was washed with 50 ml of buffer A and bound *Cj*Fur was eluted using a linear gradient that progressively increases the concentration of NaCl to 1 M in buffer A. Fractions corresponding to *Cj*Fur, which eluted at ~ 850 mM NaCl, were concentrated and applied to a preparative grade Superdex S75 equilibrated with 20 mM Tris pH 7.0, 250 mM NaCl, 5 mM BMe. Fractions corresponding to the *Cj*Fur dimer protein were pooled, concentrated to ~100 μL, and *Cj*Fur concentration was quantified by UV absorbance. The extinction coefficient (ε) and the molecular weight (MW) of this construct, 11920 M^{-1} cm^{-1} and 18066 Da, respectively, were determined using the online ProtParam tool (https://web.expasy.org/protparam). We used the protein absorbance value for 0.1% ($Abs_{280nm}^{0.1\%}$) (=1 g/L) of 0.660 as unit of measure for protein concentration determination. Purification from a 2 L culture would yield approximately 22-25 mg of purified protein.

2.4 Protein metallation for crystallization and electrophoretic mobility shift assays

Purified proteins were incubated with excess manganese chloride ($MnCl_2$) (3:1 metal to protein molar ratio was used for s-*Cj*Fur), which was gradually added to the protein with 5 minutes incubation on ice between each addition. Mn^{2+} was used as surrogate for Fe^{2+} because ferrous iron readily oxidizes to Fe^{3+}. Protein was then

incubated with metal ions during 16 hours at 4°C. In order to remove the excess of free metal ions, a second size exclusion chromatography was performed using Superdex S75 column and buffer mentioned above. After the second gel filtration, fractions corresponding to protein dimer were then concentrated and protein concentration was determined by UV absorbance. Purified protein was then used for crystallization assays or was flash-frozen in liquid nitrogen and stored at -80°C until the electrophoretic mobility shift assay.

2.5 Protein crystallization

Various crystallization screens such as the HT HR2-134 Index Screen, HT HR2-130 Crystal Screen, HT HR2-136 SaltRx Screen (Hampton Research), JCSG Core Suites Screens (Qiagen), MCSG Crystallization Suite Screens (Microlytic), Midas Screen (Molecular Dimensions), as well as several concentrations of purified recombinant *Cj*Fur protein were screened at 4°C and 21°C in order to obtain diffraction quality crystals. Vapor diffusion by the sitting drop method was used for initial 96-wells screens while the same approach or the hanging drop method were used for the optimization of lead conditions in 24-well plates.

2.5.1 ss-*Cj*Fur (*Cj*FurZn$_2$) crystallization

Plate-shaped crystals were grown for approximately two weeks at 4°C in 200 mM $MnSO_4$ and 10 – 20% PEG 3350 at 10 mg × mL^{-1} protein concentration. *Cj*FurZn$_2$ crystals were harvested and soaked in the mother liquor supplemented with increasing amount of ethylene glycol. Crystals were subsequently soaked in the crystallization

solution supplemented with 5%, 10%, 15% and 20% of ethylene glycol. Following the last soaking step, the crystal was harvested and flash-frozen in liquid nitrogen.

2.5.2 s-*Cj*Fur (*Cj*FurZn) crystallization

Following gel filtration and concentration, s-*Cj*Fur (7.5 mg × mL^{-1}) was immediately combined, in a 1:1 ratio, with a mother liquor composed of 0.1 M Bis-Tris pH 5.5, 0.25 M magnesium formate, 25% PEG 3350. *Cj*FurZn crystals were grown for approximately two weeks. Crystals were soaked and harvested in the mother liquor supplemented with 7.5% glycerol and flash-frozen in liquid nitrogen.

2.6 Data collection and crystal structure determination

Full datasets for ss-*Cj*Fur (*Cj*$FurZn_2$) and s-*Cj*Fur (*Cj*FurZn) were collected at the Life-Science Collaborative Access Team beamline at the Advance Photon Source, Chicago. Both crystal structures were determined using single-wavelength anomalous dispersion (SAD) at the zinc peak wavelength.

2.6.1 Crystal structure determination of ss-*Cj*Fur (*Cj*$FurZn_2$)

The reflections were processed and scaled using HKL2000 (Otwinowski and Minor, 1997) and four zinc atoms were identified and refined using the SHELX C/D programs (Sheldrick, 2010). Phases were calculated using SHELX-E and an initial model was built with ARP/wARP (Langer et al., 2008). This initial protein structure was used as a search model for molecular replacement using Phaser (McCoy et al., 2007). The

missing residues were modeled in the calculated phases using Coot (Emsley and Cowtan, 2004) and the structure was further refined using Refmac (Winn, 2003). The quality of the model was assessed using MolProbity (Chen et al., 2010; Davis et al., 2007) which indicates that 97.8% of non-glycine residues are found in the favoured regions of the Ramachandran plot.

2.6.2 Crystal structure determination of the s-*Cj*Fur (*Cj*FurZn)

Dataset collected on s-*Cj*Fur were indexed and scaled using xds (Kabsch, 2010a, 2010b) and AIMLESS (Evans and Murshudov, 2013) and the structure of s-*Cj*FurZn was solved by molecular replacement using ss-*Cj*Fur DBD and DD domains (PDB: 4ETS) as search models and the program Phaser (McCoy et al., 2007). The model was refined using BUSTER (Bricogne et al., 2011) and manual modifications to the model were done using Coot (Emsley and Cowtan, 2004). The quality of the model was assessed using MolProbity (Chen et al., 2010; Davis et al., 2007) with a score of 1.59. The final refined model has a Rwork of 18.4% and Rfree of 22.9%.

2.7 Comparative metal incorporation

To metallate the untagged *Cj*Fur, ss-*Cj*Fur and s-*Cj*Fur, protein samples were incubated with one molar equivalent of $MnCl_2$ for one hour on ice. $MnCl_2$ was added sequentially to prevent protein precipitation with 5 minutes incubation on ice between each addition. To remove the excess of $MnCl_2$, the proteins were applied onto Superdex S75 and the fractions corresponding to the dimer were pooled, concentrated and flash-frozen. The metal content for each protein sample was analyzed using ICP-MS analysis.

Each MS spectra were recorded in duplicate using a ThermoFisher X Series II ICP-MS on 1/100 dilution of metallated protein samples.

2.8 Inductively Coupled Plasma Mass Spectrometry Metal Analysis (ICP-MS)

The metal content of purified ss-*Cj*Fur, s-*Cj*Fur and untagged *Cj*Fur proteins was determined by the Inductively Coupled Plasma Mass Spectrometry (ICP-MS) at the Quantitative Bioelemental Imaging Center, Northwestern University, using a Thermo Fisher X Series II ICP-MS system. Using two serial dilutions (1/20 and 1/100) of purified proteins and recording 3 spectra per dilution, a total of six MS spectra per protein sample were recorded and used for metal content calculations.

2.9 Electrospray ionization mass spectrometry (ESI-MS)

Electrospray Ionization Mass Spectrometry (ESI-MS) analysis was performed at the SPARC BioCentre, The Hospital for Sick Children, Toronto. Prior analysis using a QSTAR Elite, 500 μM of purified untagged *Cj*Fur was first desalted and then applied to the mass spectrometer.

2.10 Electrophoretic Mobility Shift Assay (EMSA)

To perform EMSAs mirroring the holo-form of the transcription factor, forward (primer 1) and reverse (primer 2) (**Table 3 in Appendix 1**) Cy5-labeled primers (Eurofins MWG operon) corresponding to a 60 bp DNA fragment of the *katA* promoter region were annealed by incubation at 95°C for 15 minutes and slowly cooled down to

room temperature. For the gel shift assays, 2 nM of Cy5-labeled DNA fragment was incubated with increasing amounts (specified in Figure legends) of purified recombinant *Cj*Fur proteins, metallated with $MnCl_2$, during 1 hour on ice in binding buffer (20 mM Bis-Tris borate, pH 7.4, 50 mM KCl, 3 mM $MgCl_2$, 5% glycerol, 0.1% Triton X-100, and 50 μM $MnCl_2$). 5 ng/μL poly(dI-dC) was used as a non-specific binding competitor. Samples were separated on a native 6% polyacrylamide gel (19:1) during 1 hour at 100V at 4°C. Gels were freshly prepared with 100 mM Bis-Tris Borate, pH 7.4 and 100 μM $MnCl_2$ and pre-run for 25 minutes at 150V at 4°C.

To perform EMSAs in conditions mirroring the apo-form of *Cj*Fur, the promoter region upstream of the *Cj1345c* operon (200 bp) was PCR amplified using the *Campylobacter jejuni* NCTC11168 chromosomal DNA as a template and the primer pair 3-4 (**Table 3 in Appendix 1**) (Eurofins MWG Operon) with the forward primer (primer 3) labeled with Cy5. For the gel shift, approximately 2 nM of Cy5-labeled DNA fragment was incubated on ice with the increasing amounts (0-1000 nM) of purified recombinant ss-*Cj*Fur protein in binding buffer (20 mM Bis-Tris borate, pH 7.4, 50 mM KCl, 3 mM $MgCl_2$, 5% glycerol, 0.1% Triton X-100 and 0.1 μg poly dI-dC) during 45 minutes. Samples were then loaded on 5% non-denaturing polyacrylamide gel (19:1) and electrophoresed during 1 hour at 100V at 4°C. Gels were freshly prepared with 100 mM Bis-Tris borate, pH 7.4 and pre-run for 25 minutes at 150V at 4°C.

All steps were carried out in the dark to limit the exposure of the Cy5 fluorophore to light, which results in decreased fluorescence signals. Gels were visualized using a Typhoon Trio Variable Mode phosphoimager (GE Healthcare) and processed using ImageQuantTL software to adjust brightness and contrast of images and to quantify the

bands. Apparent dissociation constants (K_d^{app}) values were calculated using the one-site ligand-binding curve of GraphPad Prism. The experiment was performed with four technical replicates to allow for calculation of standard deviation values.

2.11 Site-directed mutagenesis

All the *Cj*Fur mutants were produced using the QuikChange II Site-Directed Mutagenesis Kit (Stratagene) and were purified as previously described for the respective wild type protein. Primers used in site-directed mutagenesis are listed in **Table 4 in Appendix 1**.

2.12 Construction of complemented mutant *Campylobacter jejuni* NCTC11168 strains

The *Campylobacter jejuni* NCTC11168 *Δfur* deletion mutant was prepared as previously described (Palyada et al., 2004). The *furWT*, *furR20E*, *furK25E*, *furK28E*, *furR30E*, *furY68A*, *furR69E*, *furΔS2* and *furΔS3* gene regions were PCR amplified from the corresponding pS-*Cj*Fur constructs using primers 9 and 10 (**Table 1 in Appendix 1**). Amplified PCR products were then cloned into the pRRK vector (Reid et al., 2008) using the In-Fusion HD Eco-Dry cloning kit (Clontech). All the mutants were then sequenced in order to confirm the absence of PCR-induced errors of the inserts. The *Campylobacter jejuni* NCTC11168 *Δfur* mutants were then transformed with these pRRK-*Cj*Fur WT or mutant constructs and positive colonies were selected on Mueller-Hinton (MH) agar plates supplemented with 20 $\mu g \times mL^{-1}$ chloramphenicol and 10 $\mu g \times mL^{-1}$ kanamycin. The

insertion of different mutant genes was confirmed by PCR and sequencing.

2.13 Western Blot Analysis

Cj NCTC11168, *Δfur* deletion mutant and complemented *furWT*, *furR20E*, *furK25E*, *furK28E*, *furR30E*, *furY68A*, *furR69E*, *furΔS2* and *furΔS3* strains were grown to midlog phase in biphasic MH cultures or in MEM-α medium supplemented with 10 mM sodium pyruvate under microaerophilic conditions (83% N_2, 4% H_2, 8% O_2 and 5% CO_2). In order to test the expression of different Fur mutant complements in iron-replete conditions, 40μM of $FeSO_4$ was added to the MEM-α medium supplemented with sodium pyruvate. The cells were pelleted by centrifugation at 4000 RPM (Sorvall Legend RT Plus Centrifuge, Thermo Scientific) for 10 minutes and resuspended in RIPA buffer (150 mM sodium chloride, 1% NP-40 or Triton X-100, 0.5% sodium deoxycholate, 0.1% SDS, 50 mM Tris pH8.0) supplemented with PMSF (MP Biomedicals) and protease inhibitor cocktail (Mini Complete, Roche). Cells were lysed on ice during 10 minutes and soluble cell content was quantified using Bradford protein assay. 4μg of each cell lysate was run at 200V for 45 minutes on a 15% acrylamide SDS-PAGE gel and subsequently transferred to a PVDF membrane at 100V for 1 hour. The membranes were blocked overnight in tris-buffered saline (TBS) + 0.1% Tween®20 and 5% fat-free milk powder. Membranes were subsequently incubated with the anti-Fur antibody at a 1:3000 dilution in the antibody solution (TBST buffer and 2% fat-free milk powder) during 1 hour at room temperature. Membranes were washed with TBST buffer, incubated with HRP-conjugated anti-rabbit secondary antibody at a 1:10000 dilution during 1 hour at room temperature in the antibody solution. Membranes were subsequently washed with TBST

buffer and incubated in ECL solution (Pierce™ ECL Western Blotting Substrate, Thermo Scientific) according to manufacturer's instructions. Western blots were analyzed using an Odyssey Fc Imaging system (LI-COR Biosciences).

2.14 RT-qPCR analysis

Cells were grown under microaerophilic conditions to midlog phase in MEM-α medium supplemented with 10 mM sodium pyruvate and with or without 40 μM $FeSO_4$. 10% of cold stop solution (10% buffer-saturated phenol in absolute ethanol) was added to cell cultures and the cells were harvested by centrifugation at 4000 RPM during 10 minutes. Cell pellets were resuspended in TE buffer (10 mM Tris-HCl, pH 8.0, 1 mM EDTA) and the RNA was extracted using the hot phenol-chloroform method (Tong et al., 1996). RNA precipitation was performed by an overnight incubation in absolute ethanol at -80ºC. RNA pellets were subsequently washed four times with 80% cold ethanol and were resuspended in RNase-free water. RNA was then treated with RNase-free DNase I (Invitrogen) to remove contaminating genomic DNA and was further purified using RNeasy Mini Kit (Qiagen). Absence of contaminating genomic DNA was confirmed by PCR and the quality of RNA was assessed on agarose gel. Reverse transcription was carried out using the QuantiTect Reverse Transcription Kit (Qiagen). RT-qPCR was performed with the MX3000P platform (Stratagene) using the Syber Green quantification method and ROX normalization. The relative expression levels of *katA* and *cfrA*, and *Cj1345c* and *Cj0948c*, holo-Fur-regulated and apo-Fur-regulated genes, respectively, were analyzed by RT-qPCR. The relative expression level of each gene was normalized to *slyD* (endogenous control) and to *fur*. The primers sets used for *katA*, *cfrA*, *Cj1345c*

and *Cj0948c* are listed in **Table 5 in Appendix 1**. The comparative C_T ($\Delta\Delta C_T$) method was used to determine the relative gene expression. All experiments were performed in triplicates and statistical significance was determined using the Student's t-test. *P* values <0.05 were considered significant.

2.15 Disc inhibition assay

Campylobacter jejuni NCTC11168, *Δfur* deletion mutant and complemented *furWT*, *furΔS2* and *furΔS3* strains were grown on MH agar plates supplemented with required antibiotics (chloramphenicol, kanamycin or both) for three days under microaerophilic conditions. Several colonies from each strain were cultured overnight in MH biphasic flasks. The overnight cell cultures were diluted in MH broth to an optical density at 600 nm of 1.0. For each strain, 4 mL of this diluted bacterial suspension was added to 90 mL of melted MH agar (cooled to approximately 50ºC) and the mixture was poured in equal volumes in three Petri dishes. After solidification, paper discs (6 mm diameter) were placed on the surface of the agar and 10 μL of 3% hydrogen peroxide (H_2O_2) was added to each paper disc. MH agar plates were subsequently incubated under microaerophilic conditions during 20 hours and the diameter of growth inhibition was measured in millimeters for each strain. All experiments were performed in triplicates and statistical significance was determined using the Student's t-test. *P* values <0.05 were considered significant.

2.16 Chick colonization assay

The chick colonization assay was performed as described previously (Palyada et al., 2004). Briefly, *Campylobacter jejuni* NCTC11168, complemented *furWT*, *furΔS2* and *furΔS3* strains were grown to mid-log phase in biphasic flasks under microaerophilic conditions at 37ºC. Bacterial suspensions were then diluted in fresh MH broth to an optical density at 600 nm of 0.13, which corresponds to approximately 10^8 CFU/mL. Water and food were withheld for 2 hours prior to inoculation. Three days old chicks were inoculated orally with 300 μL of the diluted bacterial suspension. Each bacterial suspension was serially diluted and plated on MH-agar plates to confirm that all the chicks received approximately the same number of viable *C. jejuni*. The chicks were euthanized seven days post inoculation and their ceca were collected and weighed. The cecal contents were extracted and homogenized in MH broth. The cecal contents were then serially diluted and plated onto selective Karmali agar (Oxoid) supplemented with chloramphenicol and kanamycin for the complemented strains. The Karmali plates were incubated under microaerophilic conditions during 48 hours at 42ºC and the resulting colonies were counted and expressed as CFU per gram of ceca. The data were statistically analyzed with a nonparametric Mann-Whitney rank sum test. *P* values below 0.05 were considered statistically significant.

CHAPTER 3. STRUCTURAL CHARACTERIZATION OF CAMPYLOBACTER JEJUNI FERRIC UPTAKE REGULATOR (CJFUR)

3.1 Rationale

Previous studies revealed that *Cj*Fur protein displays a variety of regulatory mechanisms. Similar to several characterized Fur family members, the iron bound protein can act as a repressor (Holmes et al., 2005; Palyada et al., 2004) or akin to *N. meningitidis* (Delany et al., 2006; Grifantini et al., 2003), *N. gonorrhoeae* (Jackson et al., 2010) and *H. pylori* (Carpenter et al., 2009b) Fur proteins, *Cj*Fur can also act as iron-dependent transcription activator (Butcher et al., 2012; Palyada et al., 2004). Moreover, *Cj*Fur can regulate gene expression and may bind to DNA in absence of metal bound to its regulatory site (Butcher et al., 2012). Taking into account the structural diversity of the Fur family of proteins, we sought to determine the crystal structure of *Cj*Fur in order to gain new insights into structural features that may explain different regulatory mechanisms observed for the Fur family of metalloregulators.

3.2 Results

3.2.1 Crystal structure of *Cj*FurZn$_2$

In order to solve its crystal structure, *Cj*Fur protein was overexpressed in Rosetta cells as a Strep-SUMO fusion protein (ss-*Cj*Fur) and was purified by a series of affinity, ion exchange and size exclusion chromatography steps (**Figure 3.1**). ss-*Cj*Fur fusion protein was first purified from other proteins in the crude cell extract by affinity

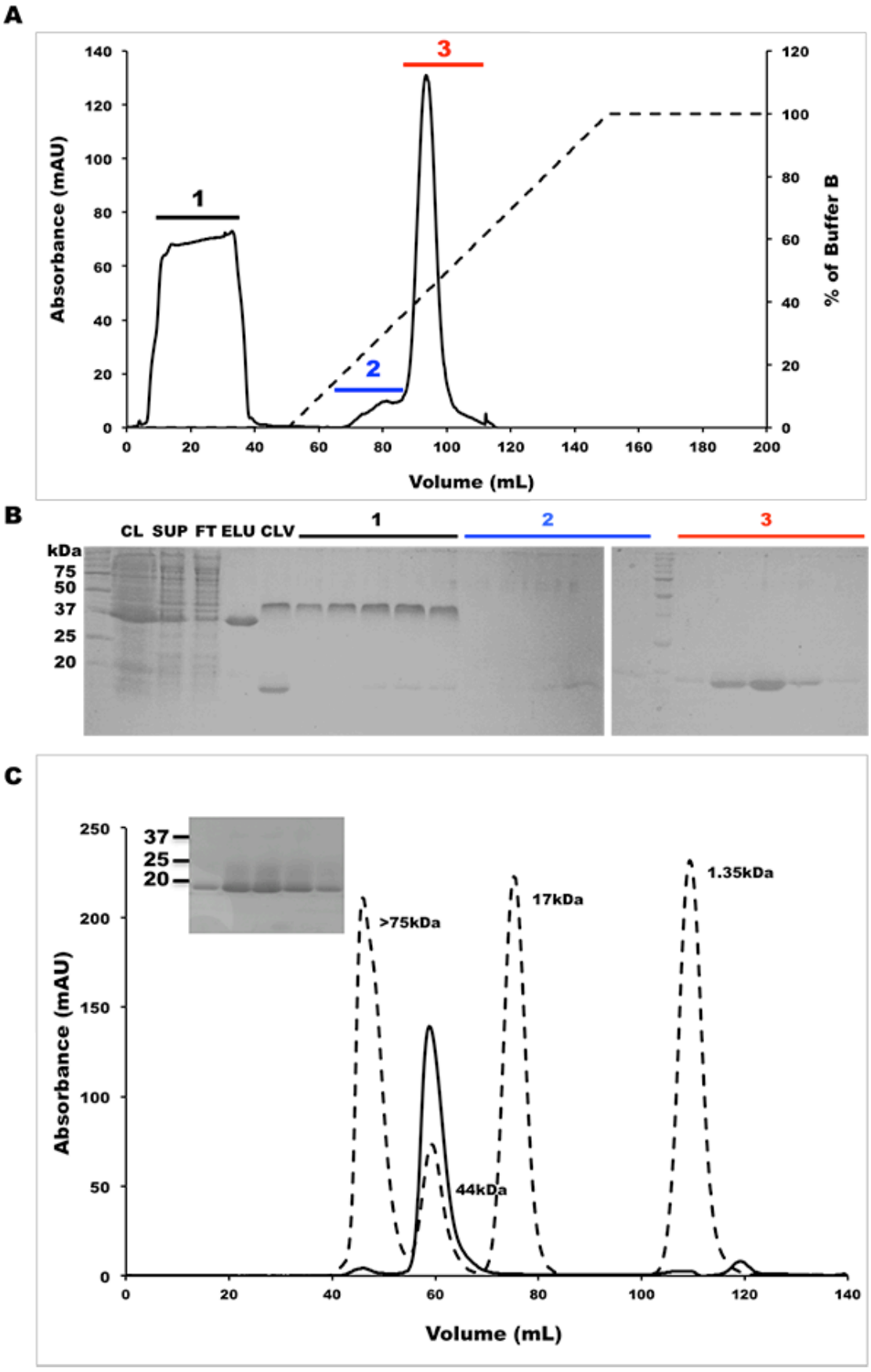
A
Absorbance (mAU)
% of Buffer B
Volume (mL)
1
2
3
B
CL SUP FT ELU CLV
kDa
75
50
37
25
20
C
Absorbance (mAU)
Volume (mL)
37
25
20
>75kDa
17kDa
1.35kDa
44kDa

Figure 3.1. Purification of ss-*Cj*Fur

(A) Ion exchange chromatography of ss-*Cj*Fur. Dashed and solid lines represent the percentage of Buffer B and the UV absorbance over the volume loaded on the SP sepharose, respectively. Three different peaks are identified and fractions corresponding to these peaks were analyzed on SDS-PAGE gel

(B) Coomassie stained SDS PAGE gel of the fractions highlighted in panel A. Different steps of *Cj*Fur purification steps were analyzed on SDS-PAGE gel. CL: cell lysate, SUP: supernatant, FT: flow through of the Strep-TACTIN column, ELU: eluted sample, CLV: fraction after cleavage with ULP1. 1, 2 and 3 represent three different peaks obtained during the ion exchange chromatography. Cleaved *Cj*Fur elutes between 30% and 55% of Buffer B, corresponding to peak 3 and to a concentration of NaCl of 300 mM to 550 mM.

(C) Size-exclusion chromatography of ss-*Cj*Fur. Solid and dashed lines represent the UV absorbance of *Cj*Fur protein sample and the different molecular weight standards, respectively. *Cj*Fur protein elutes between 50 ml and 70 mL. The SDS-PAGE of the fractions corresponding to the main peak is presented as the inset in the chromatogram.

Figure adapted from Sarvan S., Couture JF. (2017) "Method for the Successful Crystallization of the Ferric Uptake Regulator from *Campylobacter jejuni*." In: Butcher J., Stintzi A. (eds) Campylobacter jejuni. Methods in Molecular Biology, vol 1512. Humana Press, New York, NY

chromatography using the Strep-TACTIN column, which has a high affinity and specificity for the Strep Tag. The Strep-SUMO tag was then removed using SUMO specific protease, ULP1, and the *Cj*Fur protein was further purified and successfully separated from the tag using the ion exchange chromatography. *Cj*Fur protein was finally purified by size exclusion chromatography and as shown in **Figure 3.1C**, eluted as a single peak corresponding to protein dimer. Separation of the fractions corresponding to the main peak on a coomassie-stained SDS-Page gel showed that the *Cj*Fur is nearly 100% pure and amenable to use in crystallization studies.

Using the vapor diffusion technique, *Cj*Fur protein was crystallized in a solution containing 200 mM $MnSO_4$ and 10 – 20% PEG 3350 and the structure of *Cj*FurZn_2 was determined using single-wavelength anomalous dispersion technique. The structure is composed of two protomers (A and B) that form the asymmetric unit and the functional dimer (**Figure 3.2**). Protomer A consists of residues 4–83 and 90–149, whereas protomer B comprises residues 2–16 and 26–154. Similar to other Fur proteins, each *Cj*Fur protomer folds in two domains including the N-terminal DNA binding domain (DBD), which is composed of 5 consecutive α-helices (α1, α2, α3, α3-2 and α4) followed by a two-stranded antiparallel β-sheet (β1-β2), and the C-terminal dimerization domain (DD) composed of 3 β-sheets (β3-β4-β5) intersected between β4 and β5 by an α-helix (α5). The structure ends by a short α-helix (α6) that coordinates one zinc atom.

3.2.2 Comparison of *Cj*FurZn_2 to other Fur and Fur-like structures

We then sought to inspect structural differences between *Cj*FurZn_2 and other structurally characterized Fur and Fur-like homologs. Using the PyMol software (The

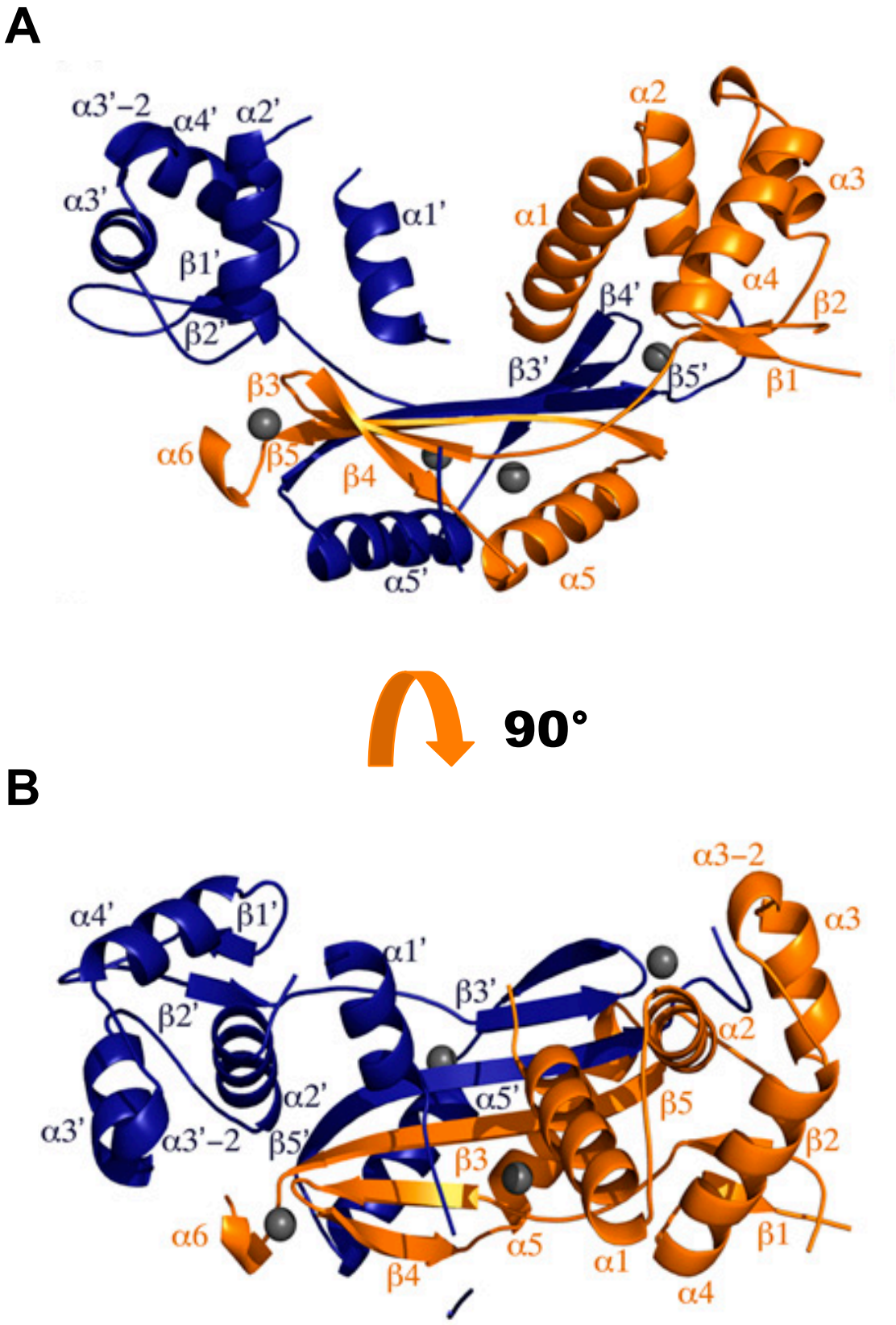
A
α3'–2
α4'
α2'
α3'
α1'
β1'
β2'
α2
α3
α1
α4
β2
β4'
β3'
β5'
β1
β3
α6
β5
β4
α5'
α5
90°
B
α3–2
α3
α4'
β1'
α1'
β3'
β2'
α2
α2'
α5'
β5
α3'
α3'–2
β5'
β2
β3
α6
α5
α1
β1
β4
α4

Figure 3.2 Crystal structure of *Cj*FurZn$_2$

(A and **B)** Two orthogonal views of the *Cj*FurZn$_2$ crystal structure in which protomer A and B are rendered in orange and blue, respectively. Secondary structures are labeled accordingly and zinc atoms are represented by grey spheres.

Figure adapted from Butcher J*, Sarvan S*, Brunzelle J, Couture JF, Stintzi A. (2012) "The structure and regulon of *Campylobacter jejuni* ferric uptake regulator Fur define apo-Fur regulation" PNAS 109(25):10047-52 PMID:22665794

PyMOL Molecular Graphics System, Version 1.8 Schrödinger, LLC.), we aligned the structures of *Cj*FurZn$_2$, *Hp*Fur, *Vc*Fur, *Pa*Fur and *Bs*PerRZnMn and calculated the root mean square deviations (RMSD) between superimposed atoms. While the structures of *Hp*Fur, *Vc*Fur, *Pa*Fur and *Bs*PerRZnMn superpose considerably well with a RMSD of 1.2-2.2Å, the structure of *Cj*FurZn$_2$ differs greatly with a RMSD of ~14Å. In spite of the structural homologies resulting in a similar basic fold between *Cj*Fur and other structurally characterized Fur proteins, the superposition of their DDs leads to a different orientation of *Cj*Fur's DBD when compared to other Fur and Fur-like proteins. *Cj*FurZn$_2$ adopts an atypical conformation resulting from a rotation of approximately 180° of its DBD which positions the α1 helix within the V-shaped dimer while the β1-β2 antiparallel β-sheet and the DNA-binding helix α4 are found on the exterior of the structure (**Figure 3.3A**). In contrast, the structures of *Hp*Fur, *Vc*Fur, *Pa*Fur and *Bs*PerRZnMn bring their DNA-binding helix α4 and the β1-β2 antiparallel β-sheet within the V-shaped dimer. Close inspection of the superposition of *Cj*FurZn$_2$ protein with its closest homolog, *Hp*Fur, revealed that the rotation of the DBD originates from the conformation of the hinge region, which in *Cj*FurZn$_2$ is elongated whereas in *Hp*Fur and similar to other structurally characterized Fur proteins, it adopts a loose turn conformation (**Figure 3.3B**).

3.2.3 Metal binding sites of *Cj*FurZn$_2$

*Cj*Fur structure contains two occupied Zn^{2+} binding sites per protomer, hence its name, *Cj*FurZn$_2$ (**Figure 3.3A**). The metal binding site S1 contains Zn^{2+} ion that is

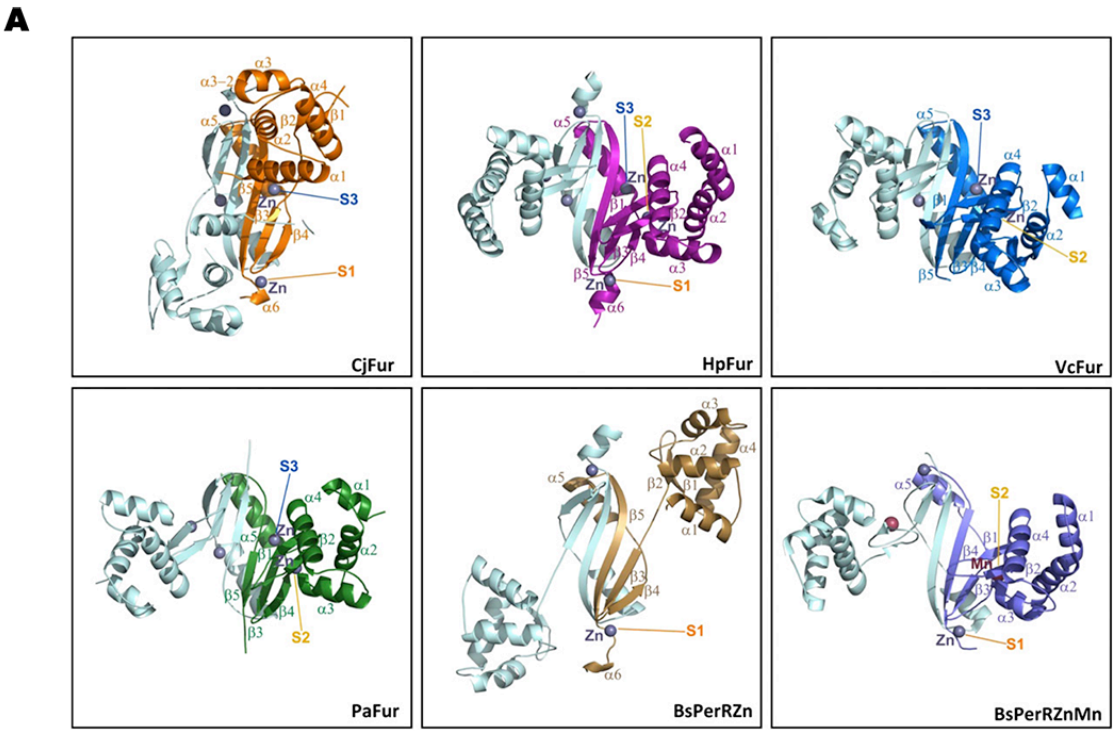
A
CjFur
HpFur
VcFur
PaFur
BsPerRZn
BsPerRZnMn
B
C
α1
α2
α3
α3-2
α4
β1
β2
β3
β4
α5
β5
α6
CjFur MLIENVEYDVLIERFKKILRQGGLKYTKQREVLIKTLYHSD-THYTPESLYMEIKQAEPDLNVGHATVYRTLNLLEEAEMVT 81
HpFur -MKRLETLESIIERLRMSIKKNGLKNSKQREEVVSVLYRSG-THLSPEEITHSIRQ--KDKNTSTSSVYRILNFLEKENFIC 78
VcFur ----------VSDNNQALKDAGLKVTLPRLKILEVLQQPECQHISAEELYKKLID--LGEEIGLATVYRVLNQFDDAGIVT 69
PaFur ----------VVENS-ELRKAGLKVTLPRVKILQMLDSAEQRHMSAEDVYKALME--AGEDVGLATVYRVLTQFEAAGLVV 68
EcFur ----------VTDNNTALKKAGLKVALPRLKILEVLQEPDNHEVSAEDLYKRLID--MGEEIGLATVYRVLNQFDDAGIVT 69
MtZur ---------MASAAGVRSTRQR-----AAISTLLETLR--DDFR--SAQELHDELRR--RGENIGLTTVYRTLQSMASSGLVD 62
ScNur ---------MVSTDWKSDLRQRGYRLTPQRQLVLEAVR--DTLEHATPDDILGEVRK--TASGINLSTVYRTLELLEELGLVS 69
BsPerR ------MAAHEIKEALETLKETGVRITPQRHAILEYLVN-SMAHPTADDIYKALEG--KFPNMSVATVYNNLRVFRESGLVK 73
CjFur SISFGSAGKKYEIANKPHHDHVICKNCGKIIEFENPIIERQQALIAKEHGFKLTGHLMQLYGVCGDCNNQKAKVKI------ 157
HpFur VLETSKSGRRYEIAAKEHHDHIICLHCGKIIEFADPELENRQNEVVKKYQAKLISHDMKMFVWCKECQESEC---------- 150
VcFur RHHFEGGKSVFEISTQHHHDHLVCLDCGEVIEFSDDVIEQRQKELAAKYNVQLTNHSLYLYGKCGSEGSCKDNPNAHKPKK- 150
PaFur RHNFDGGHAVFEIADSGHHDHMVCVDTGEVIEFMDAELEKRQKEIVRERGFELVDHNLVLY-------------VRKKK-- 134
EcFur RHNFEGGKSVFEITQQHHHDHLICLDCGKVIEFSDDSIEARQREIAAKHGIRLTNHSLYLYGHC-AEGDCREDEHAHEGK-- 148
MtZur TLHTDTGESVYRRCSEHHHHHDVCRSCGSTIEVGDHEVEAWAAEVATKHGFSDVSHTLEIFGTCSDCRS------------- 131
ScNur HAHLGHGAPTYHIADRHIHHVCRDCTNVIEADLSVAADFTAKLREQFGFDTDMKHFAIFGRCESCSLKGSTTDS------ 145
BsPerR ELTYGDASSRFDFVTS-DHYHAICENCGKIVDGHYPGIDEVEQLAAHVTGFKVSHRLEIYGVCQECSKKENH--------- 145

Figure 3.3 *Cj*Fur adopts an atypical conformation when compared to other Fur and Fur like proteins

(A) *Cj*Fur DBD adopts an atypical conformation. Overall structure of Fur and Fur-like proteins in which protomer A is highlighted in orange (*Cj*Fur), purple (*Hp*Fur; 2XIG), blue (*Vc*Fur; 2W57), green (*Pa*Fur; 1MZB), brown (*Bs*PerRZn; 2FE3), and violet (*Bs*PerRZnMn; 3F8N). β-Sheets, α-helices, and metal binding sites of each protomer A are labeled accordingly. To facilitate the analysis, the dimerization domains are shown in the same orientation. All structures were obtained from the RCSB PDB structure bank (http://www.rcsb.org/pdb/).

(B) Superimposition of protomers A of *Cj*Fur (orange) and *Hp*Fur (purple). Secondary structures are labelled. Zoomed view on the hinge region connecting the DBD and DD.

(C) Sequence alignment of Fur and Fur-like proteins. Sequence alignment of Fur proteins *C. jejuni* (*Cj*), *H. pylori* (*Hp*), *V. cholera* (*Vc*), *P. aeruginosa* (*Pa*), *E. coli* (*Ec*) and of the Fur-like Zur from *M. tuberculosis* (*Mt*Zur), Nur from *S. coelicolor* (*Sc*Nur), and PerR from *B. subtilis* (*Bs*PerR). Sequences were aligned using the ClustalW option in MEGA5 (Tamura et al., 2011). *Cj*Fur secondary-structure elements are shown above the alignment. Asterisks indicate the residues involved in the predicted *Cj*Fur S2 site. S1 residues are shaded in orange, predicted S2 residues are in yellow, and S3 residues are in blue. Positions with 100% amino acid conservation are indicated by dark gray, 100–80% by medium gray, and 80–60% by light gray.

Figure adapted from Butcher J*, Sarvan S*, Brunzelle J, Couture JF, Stintzi A. (2012) "The structure and regulon of *Campylobacter jejuni* ferric uptake regulator Fur define apo-Fur regulation" PNAS 109(25):10047-52 PMID:22665794

tetracoordinated by two pairs of cysteine residues namely Cys105/Cys108 and Cys145/Cys148 and is found within the DD of *Cj*FurZn$_2$. This zinc-binding site is required for the stabilization of the β3-β4-β5 structure and the formation of Fur dimer (Dian et al., 2011). Metal binding site S3 is found near the dimerization domain of *Cj*FurZn$_2$ and contains a Zn^{2+} ion hexacoordinated by residues Asp101, Glu120, His137 and two water molecules. The third metal binding site, S2, which connects DBD and DD, is unoccupied in *Cj*FurZn$_2$ structure. The absence of metal ion in S2 can be explained by the rotation of *Cj*Fur DBD, which positions residues involved in the coordination of Fe^{2+} in a non-permissive orientation for the coordination of metal ion. Considering that this site is known to be the iron sensing regulatory site in *Cj*Fur closest homolog, *Hp*Fur, and essential for its DNA binding activity (Dian et al., 2011), we reasoned that *Cj*FurZn$_2$ represents a snap-shot view of the apo-form of the transcription factor and that we solved the first crystal structure of a Fur protein in its apo conformation.

To confirm these results, purified ss-*Cj*Fur sample was analyzed by inductively coupled plasma mass spectrometry (ICP-MS), which shows that the purified protein used for crystallization assays is free of iron and manganese and contains approximately two Zn atoms per protomer (**Table 2**).

3.2.4 DNA-binding activity of apo-*Cj*Fur

Given that the structure of *Cj*Fur differs greatly from the previously characterized Fur proteins but still adopts a caliper-like conformation suitable for the interaction with DNA, we sought to characterize the DNA-binding activity of apo-*Cj*Fur protein.

Table 2: Inductively Coupled Plasma Mass Spectrometry (ICP-MS) metal analysis of recombinant *Cj*Fur protein

Metal	Metal content (%)*
Mn^{2+}	< 0.2
Fe^{2+}	< 0.2
Co^{2+}	< 0.1
Ni^{2+}	< 0.1
Cu^{2+}	1.55
Zn^{2+}	260.45

*The percent metal content is shown as a molar ratio of metal/*Cj*Fur concentration as determined by ICPMS.

Table adapted from Butcher J*, Sarvan S*, Brunzelle J, Couture JF, Stintzi A. (2012) "The structure and regulon of *Campylobacter jejuni* ferric uptake regulator Fur define apo-Fur regulation" PNAS 109(25):10047-52 PMID:22665794

Electrophoretic mobility shift assays (EMSA) were performed in order to examine the interaction of purified recombinant *Cj*FurZn$_2$ with DNA fragments derived from the upstream regions of the apo-regulated genes *Cj1345c*, *rrc*, *Cj0415* and *hddA*. Consistent with the crystal structure, incubation of *Cj*FurZn$_2$ with DNA in absence of regulatory metals yields protein-DNA complexes that could be separated from the free probes. These results indicate that *Cj*FurZn$_2$ can bind DNA in absence of regulatory metal *in vitro* (Figure 3.4).

3.2.5 Mapping the residues involved in apo-*Cj*Fur regulation

In order to identify apo-*Cj*Fur residues binding DNA, we generated the electrostatic potential map of apo-*Cj*Fur using *Cj*FurZn$_2$ structure. The electrostatic potential surface shows a positively charged area (depicted in blue) containing several evolutionary conserved basic residues including Arg14, Lys17, Lys25, Lys28, Arg30, and Arg69 (**Figure 3.5**). In order to determine the role of this region in apo-*Cj*Fur interaction with DNA, we substituted these residues with glutamic acid. In addition, Tyr68, an evolutionary conserved residue previously shown to be important for the DNA binding activity of Fur protein (Tiss et al., 2005) was mutated to alanine. Each mutant was tested using EMSA in absence of regulatory metal ion using the 200 bp fragment derived from the upstream region of the *Cj1345*c gene as DNA binding element. Our results show that the substitution of Arg20, Lys25, Lys28 and Arg69 by glutamic acid residues abolish the apo-*Cj*Fur binding to *Cj1345c* promoter region (**Figure 3.5D**). Moreover, identical substitutions of residues Lys17 and Arg30 and replacement of Tyr68 to alanine significantly reduce apo-*Cj*Fur binding to DNA. While found in the positively

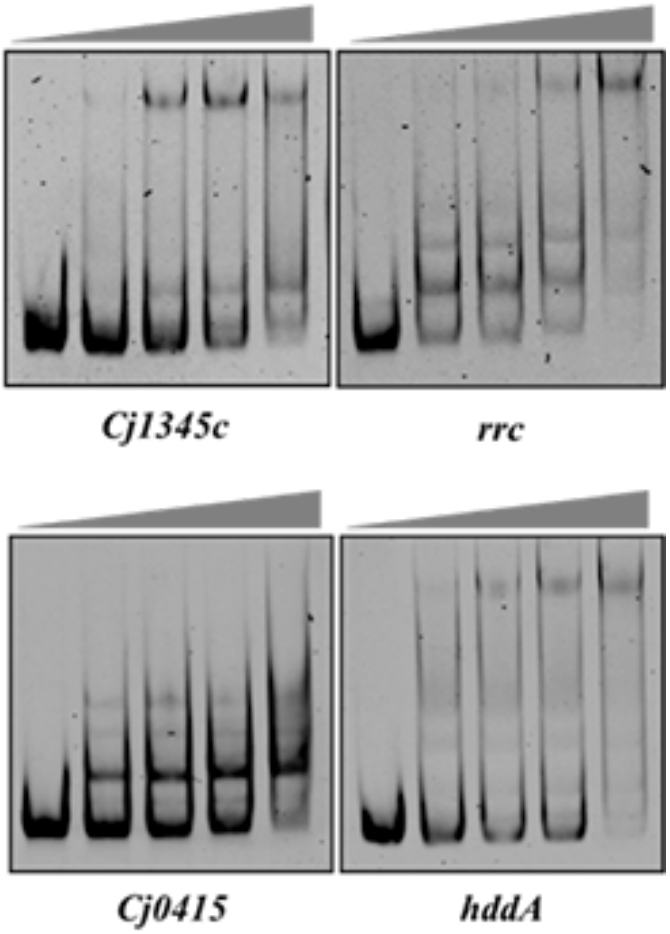
Cj1345c
rrc
Cj0415
hddA

Figure 3.4. Electrophoretic mobility shift assays of *Cj1345c*, *rrc, Cj0415* and *hddA* promoter regions bound by *Cj*FurZn$_2$

*Cj*FurZn$_2$ directly binds to *Cj1345c, rrc, Cj0415* and *hddA* promoter regions. EMSAs were performed with 2.5nM of Cy5-labelled PCR amplified DNA fragments (-200 to -1 bp upstream of the transcriptional start site) of *Cj1345c, rrc, Cj0415* or *hddA* promoter regions and increasing concentrations (0, 50, 100, 200 and 1000nM) of purified *Cj*FurZn$_2$. Binding buffer, gel as well as the running buffer used in these four EMSA studies did not contain $MnCl_2$.

Figure adapted from Butcher J*, Sarvan S*, Brunzelle J, Couture JF, Stintzi A. (2012) "The structure and regulon of *Campylobacter jejuni* ferric uptake regulator Fur define apo-Fur regulation" PNAS 109(25):10047-52 PMID:22665794

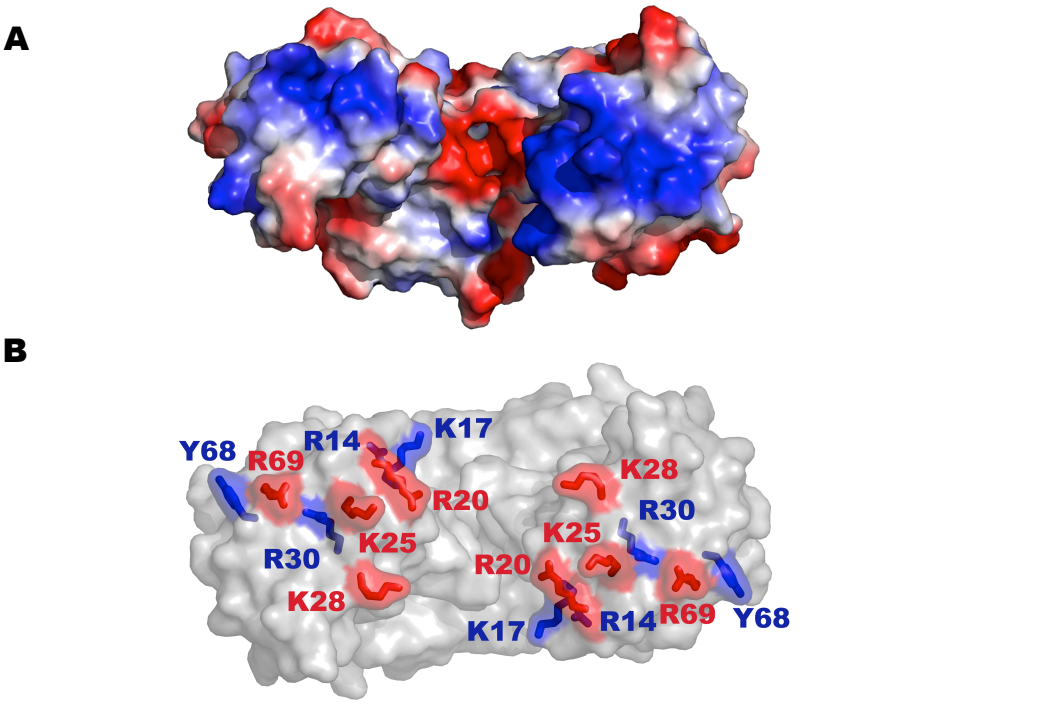
A
B
Y68
R69
R14
K17
R20
K25
R30
K28
K28
R30
K25
R20
K17
R14
R69
Y68
C
WT
R20E
R30E
R14E
K25E
Y68A
K17E
K28E
R69E
D
Log2 (Fold Change)
2
1.5
1
0.5
0
-0.5
-1
-1.5
-2
-2.5
Cj1345c
Cj0948c
C. jejuni Δfur
C. jejuni Δfur + furWT
C. jejuni Δfur + furR20E
C. jejuni Δfur + furK25E
C. jejuni Δfur + furR30E
C. jejuni Δfur + furY68A
C. jejuni Δfur + furR69E

Figure 3.5. Apo-*Cj*Fur structure and regulation

(A) Electrostatic potential surface of apo-*Cj*Fur (*Cj*FurZn2) crystal structure. Positively charged surfaces are represented in blue ($+81k_bTe^{-1}$) and negatively charged surfaces in red ($-81\ k_bTe^{-1}$) (k_b = Bolzmann's constant, T = temperature in Kelvin and e = charge of an electron).

(B) Residues forming the positively charged surface were mutated to glutamic acid or alanine. Residues impairing the DNA binding activity of apo-CjFur are rendered in red and mutated residues that still bind to DNA are represented in blue.

(C) Electrophoretic mobility shift assay of *Cj1345c* promoter region (2nM) with increasing amount (0-1000 nM) of *Cj*FurWT, *Cj*FurR14, *Cj*FurK17E, *Cj*FurR20E, *Cj*FurK25E, *Cj*FurR30E, *Cj*FurY68A and *Cj*Fur R69E. Lane 1: 0nM, lane 2: 10 nM, lane 3: 25 nM, lane 4: 50 nM, lane 5: 75 nM, lane 6: 100 nM, lane 7: 200 nM, lane 8: 300 nM, lane 9: 400 nM, lane 10: 500 nM, lane 11: 600 nM, lane 12: 700 nM, lane 13: 800 nM, lane 14: 900 nM and lane 15: 1000 nM.

(D) Average value of triplicate RT-qPCR analysis of the expression of the Fur regulated *Cj1345c* and *Cj0948c* genes in *C. jejuni* Δfur, Δfur+furWT, Δfur+furR20E, Δfur+furK25E, fur+furR30E, Δfur+furY68A, Δfur+furR69E in iron-limited conditions. All values are relative to *C.jejuni* Δfur+furWT and normalized to *slyD* and *fur*. Error bars represent the standard error of the mean (SEM) and * denotes statistical significance ($P < 0.05$) using unpaired 2-tail student t-test. Each experiment was done with three independent RNA samples.

charged region and amenable to make electrostatic interactions with DNA, the Arg14Glu mutation increases the apparent affinity to DNA of apo-*Cj*Fur. Overall, these results suggest that residues Arg20, Lys25, Lys28 and Arg69 are crucial for apo-*Cj*Fur binding to DNA.

After determining the impact of these residues on the ability of *Cj*Fur to bind DNA in absence of regulatory metal *in vitro*, we sought to evaluate the changes in the transcriptional activity of these mutants in *Campylobacter jejuni*. We constructed complemented *Campylobacter jejuni* NCTC11168 strains expressing either wild type Fur or the mutants tested above. After confirming that the complemented mutants were expressed at a level similar to the complemented wild type *fur* (**Figure 1 in Appendix 2**), we evaluated, by RT-qPCR (**Figure 3.5E**), the expression of *Cj*1345c and *Cj*0948c, two genes known to be activated and repressed by *Cj*Fur in iron-limited conditions, respectively. Consistent with our *in vitro* DNA binding assays, most mutants failed to activate the expression of *Cj1345c*. Similarly, the same mutants were unable to repress *Cj0948c* expression in iron-limited conditions. Overall, these results suggest that Arg20, Lys25, Lys28 and Arg69 are important for the gene regulatory activity of *Cj*Fur. Moreover, our results suggest that a similar set of residues is involved in the activation and repression of gene expression in iron-limited conditions.

3.2.6 Mapping the apo-*Cj*Fur binding site on *Cj*1345c promoter region

After demonstrating that the promoter region of *Cj*1345c was bound by apo-*Cj*Fur, we sought to identify *Cj*Fur binding site within this 200 bp DNA element. Binding assays

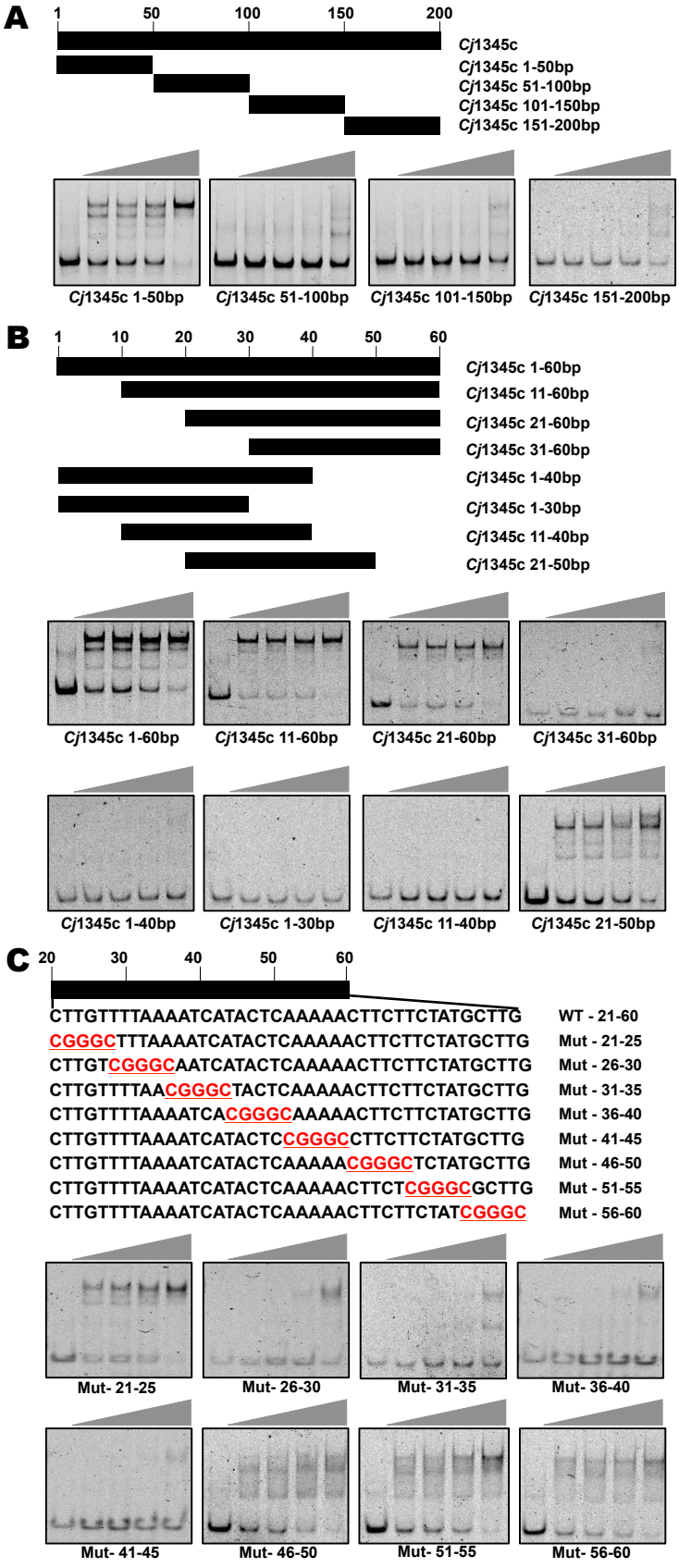
A
1
50
100
150
200
Cj1345c
Cj1345c 1-50bp
Cj1345c 51-100bp
Cj1345c 101-150bp
Cj1345c 151-200bp
Cj1345c 1-50bp
Cj1345c 51-100bp
Cj1345c 101-150bp
Cj1345c 151-200bp
B
1
10
20
30
40
50
60
Cj1345c 1-60bp
Cj1345c 11-60bp
Cj1345c 21-60bp
Cj1345c 31-60bp
Cj1345c 1-40bp
Cj1345c 1-30bp
Cj1345c 11-40bp
Cj1345c 21-50bp
Cj1345c 1-60bp
Cj1345c 11-60bp
Cj1345c 21-60bp
Cj1345c 31-60bp
Cj1345c 1-40bp
Cj1345c 1-30bp
Cj1345c 11-40bp
Cj1345c 21-50bp
C
20
30
40
50
60
CTTGTTTTAAAATCATACTCAAAAACTTCTTCTATGCTTG WT - 21-60
CGGGCTTTAAAATCATACTCAAAAACTTCTTCTATGCTTG Mut - 21-25
CTTGTCGGGCAATCATACTCAAAAACTTCTTCTATGCTTG Mut - 26-30
CTTGTTTTAACGGGCTACTCAAAAACTTCTTCTATGCTTG Mut - 31-35
CTTGTTTTAAAATCACGGGCAAAAACTTCTTCTATGCTTG Mut - 36-40
CTTGTTTTAAAATCATACTCCGGGCCTTCTTCTATGCTTG Mut - 41-45
CTTGTTTTAAAATCATACTCAAAAACGGGCTCTATGCTTG Mut - 46-50
CTTGTTTTAAAATCATACTCAAAAACTTCTCGGGCGCTTG Mut - 51-55
CTTGTTTTAAAATCATACTCAAAAACTTCTTCTATCGGGC Mut - 56-60
Mut- 21-25
Mut- 26-30
Mut- 31-35
Mut- 36-40
Mut- 41-45
Mut- 46-50
Mut- 51-55
Mut- 56-60

Figure 3.6 Mapping of the apo-*Cj*Fur binding site on *Cj*1345c promoter region

(A) Electrophoretic mobility shift assay of apo-*Cj*Fur (0, 50, 100, 250 and 500 nM) with four 50 bp long DNA fragments spanning the 200 bp *Cj1345c* promoter region. 2 nM of Cy5 labeled DNAs were used.

(B) Electrophoretic mobility shift assay of apo-*Cj*Fur (0, 50, 100, 250 and 500 nM) with eight oligonucleotides of different lengths spanning the first 60bp (-200 bp to -140 bp upstream of the *Cj1345c* gene) of the *Cj1345c* promoter region. 2 nM of Cy5 labeled DNAs were used.

(C) Electrophoretic mobility shift assay of apo-*Cj*Fur (0, 50, 100, 250 and 500 nM) with eight different *Cj1345c* promoter region mutants spanning the 20-60 bp region (-180 bp to -140 bp upstream of the *Cj1345c* gene). 2 nM of Cy5 labeled DNAs were used.

performed with fragments corresponding to nucleotides 1-50, 51-100, 101-150 and 150-200 revealed that only the fragment corresponding to the first 50 bp (**Figure 3.6A**) was bound by apo-*Cj*Fur suggesting that despite the AT-richness of *C. jejuni* genome, apo-*Cj*Fur specifically recognizes a binding motif in the promoter region of *Cj*1345c. In order to further delimit the *Cj*Fur binding site, we conducted EMSAs with overlapping fragments covering the first 60 base pairs of the 200 bp DNA element. As shown in **Figure 3.6B**, any binding reactions performed with DNA elements containing nucleotides 21-50 were bound by apo-*Cj*Fur. To further delineate the binding motif, we performed binding reaction with 40 bp long DNA probes corresponding to the 21-60 bp region in which groups of five nucleotides were mutated. As shown in **Figure 3.6C**, we failed to detect binding when the central region of the 40 bp fragment, corresponding to nucleotides 26-45 was mutated with guanines and cytosines. The fragment corresponding to nucleotides 26-45 is located between -175 and -155 bp upstream of the *Cj1345c* gene. Altogether, these results suggest that we identified the minimal DNA fragment required for the binding of apo-*Cj*Fur and the close inspection of the sequence revealed a presence of a palindromic sequence (underlined) TTTAAA-TCATACT-AAAAA suggesting a possible emerging consensus motif for the apo-Fur regulation.

Chapter 4. Characterization of holo-*Cj*Fur-DNA interaction

4.1 RATIONALE

At the beginning of my graduate studies, the structural basis underlying the interaction between *Cj*Fur and DNA was unknown. The determination of *Cj*Fur-DNA structure is necessary in order to fully understand the structural basis of DNA recognition by *Cj*Fur, which will lead to a better understanding of *Cj*Fur regulatory mechanisms. While performing several crystallization assays of *Cj*Fur-DNA complexes, which have proven to be unsuccessful, we combined homology modeling and several biochemical approaches to characterize the mode of action of the holo-*Cj*Fur.

4.2 RESULTS

4.2.1 Residues involved in holo-*Cj*Fur regulation

After characterizing the *Cj*Fur-DNA interaction in absence of the regulatory metal ion, we sought to identify potential regions involved in the interaction between holo-*Cj*Fur and a DNA element corresponding to a fragment of the *katA* promoter region. Since we were unable to crystallize and determine the crystal structure of holo-*Cj*Fur, we built a model of holo-*Cj*Fur structure using SWISS_MODEL (Arnold et al., 2006; Guex and Peitsch, 1997; Schwede et al., 2003) software and the structure (2XIG) of *Helicobacter pylori* Fur (sequence identity of 38.5% with *Cj*Fur) as a template. **Figure 4.1A** represents modeled holo-*Cj*Fur dimer, which positions its DNA-binding helix α4

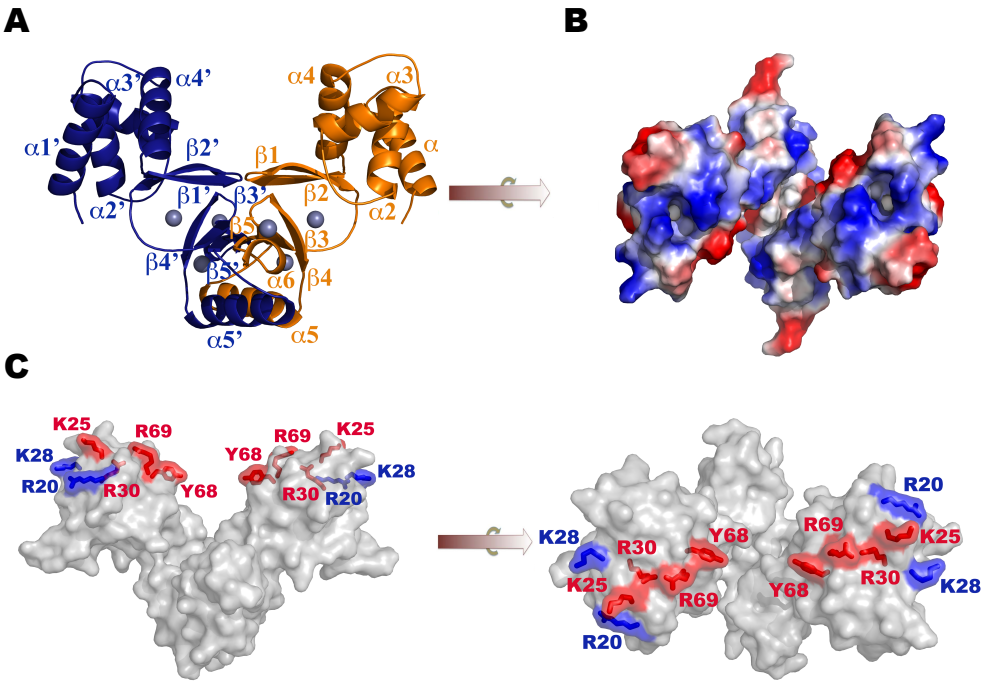
A
α3'
α4'
α4
α3
α1'
β2'
β1
α
β1'
β3'
β2
α2'
α2
β5'
β3
β4'
β5''
α6
β4
α5'
α5
B
C
K25
R69
K28
Y68
R69
K25
R20
R30
Y68
R30
R20
K28
K28
R30
Y68
R20
R69
K25
K25
R69
Y68
R30
K28
R20

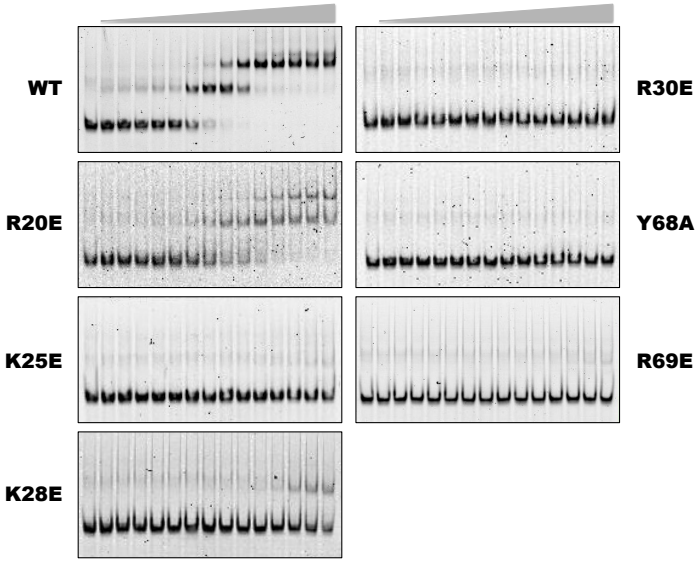
D
WT
R30E
R20E
Y68A
K25E
R69E
K28E

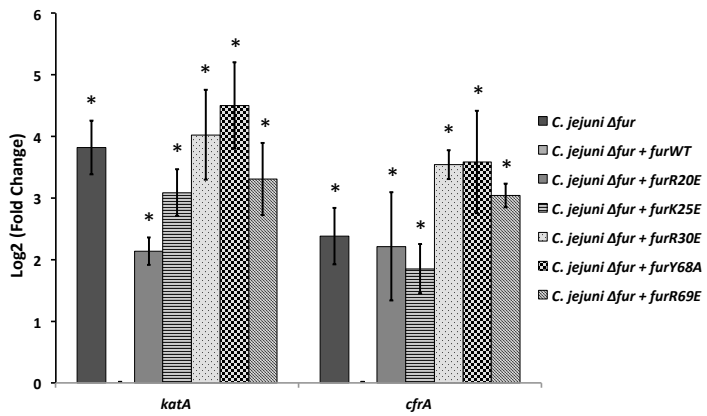
E
Log2 (Fold Change)
0
1
2
3
4
5
6
katA
cfrA
C. jejuni Δfur
C. jejuni Δfur + furWT
C. jejuni Δfur + furR20E
C. jejuni Δfur + furK25E
C. jejuni Δfur + furR30E
C. jejuni Δfur + furY68A
C. jejuni Δfur + furR69E

Figure 4.1. Holo-*Cj*Fur structure and regulation

(A) Modeled holo-*Cj*Fur structure using SWISS_MODEL software and *Hp*Fur crystal structure (2XIG) as template. Protomer A and protomer B are rendered in orange and blue, respectively and the zinc atoms are represented by grey spheres. Secondary structures are labelled.

(B) Electrostatic potential surface of holo-*Cj*Fur is represented. Positively charged surfaces are represented in blue ($+73 k_b Te^{-1}$) and negatively charged surfaces in red ($-73 k_b Te^{-1}$) (k_b = Bolzmann's constant, T = temperature in Kelvin and e = charge of an electron).

(C) Residues forming the positively charged surface were mutated to glutamic acid or alanine. Residues impairing the DNA binding activity of holo-*Cj*Fur are rendered in red and mutated residues that still bind to DNA are represented in blue.

(D) Electrophoretic mobility shift assay of *katA* promoter region (2 nM) with increasing amount (0-100 nM) of *Cj*FurWT, *Cj*FurR20E, *Cj*FurK25E, *Cj*FurR30E, *Cj*FurY68A and *Cj*FurR69E. Lane 1: 0nM, lane 2: 0.1 nM, lane 3: 0.25 nM, lane 4: 0.5 nM, lane 5: 0.75 nM, lane 6: 1 nM, lane 7: 2 nM, lane 8: 4 nM, lane 9: 8 nM, lane 10: 10 nM, lane 11: 20 nM, lane 12: 30 nM, lane 13: 50 nM, lane 14: 80 nM and lane 15: 100 nM.

(E) Average value of triplicate RT-qPCR analysis of the expression of the Fur regulated *katA* and *cfrA* genes in *C. jejuni* Δfur, Δfur+furWT, Δfur+furR20E, Δfur+furK25E, Δfur+furR30E, Δfur+furY68A, Δfur+furR69E in iron-replete conditions. All values are relative to *C. jejuni* Δfur+furWT and normalized to *slyD* and *fur*. Error bars represent the standard error of the mean (SEM) and * denotes statistical significance ($P < 0.05$) using unpaired 2-tail student t-test. Each experiment was done with three independent RNA samples.

and the β1-β2 antiparallel β-sheet within the V-shaped dimer similar to other holo-Fur homologs.

4.2.2 Residues involved in holo-*Cj*Fur regulation

Following the modeling of holo-*Cj*Fur, we calculated the surface electrostatic potential. Akin to the patches of positively charged residues observed in apo-*Cj*Fur, we noted a positively charged region on the surface of the *Cj*Fur's DBD (**Figure 4.1B**). In order to determine whether these residues interact with DNA in presence of regulatory metals, each residue was substituted with a glutamic acid (Arg20, Lys25, Lys28, Arg30 and Arg69) or an alanine (Tyr68). Owing to its potential for oxidation, iron was replaced by Mn^{2+} in our *in vitro* studies. EMSAs show that the substitution of Arg20 and Lys28 reduces the binding of holo-*Cj*Fur to *katA* promoter region, whereas mutations of residues Lys25, Arg30, Tyr68 and Arg69 are detrimental for this interaction (**Figure 4.1D)**. The effect of these mutations on the transcriptional activity of Fur in presence of the regulatory metal ion (Fe^{2+}) was examined by measuring the expression levels of known holo-*Cj*Fur targets, namely *katA* and *cfrA*, using the RT-qPCR approach. As shown in **Figure 4.1E,** all mutants failed to repress the *katA* and *cfrA* gene expression. Overall, our results suggest that the *Cj*Fur protein employs the same evolutionary conserved region to regulate all four regulatory mechanisms unrelatedly to the conformational changes observed between the apo and holo forms of the protein.

Chapter 5. Characterization of *Cj*Fur S2 and S3 metal binding sites

5.1 RATIONALE

Our initial structural studies demonstrated that *Cj*FurZn_2 adopts a unique three-dimensional structure in which its DBD is rotated of approximately 180° when compared to other metalloregulators. In adopting this peculiar conformation, the S3 and the S1 metal binding sites are occupied by zinc atoms but the residues forming the S2 site are in a conformation non conducive for binding metals. Based on these observations, it was proposed that the structure represented the conformation of an apo-*Cj*Fur. The structure also raised the possibility that the S2 site in *Cj*Fur is not important for the activity of the metalloregulator. To test this hypothesis, residues forming the S2 and S3 metal binding sites were mutated and several biochemical approaches were used in order to assess the role of the S2 and S3 metal binding sites in the binding of the regulatory metal ion and controlling the activity of *Cj*Fur.

5.2 RESULTS

5.2.1 Role of *Cj*Fur S2 and S3 metal binding sites in the binding of the regulatory metal ion

To better understand the role of *Cj*Fur metal binding sites, we generated point mutation at these sites using *Cj*Fur amino acid sequence as template. His43 and His102, two residues predicted to form the S2 binding site, were substituted to alanine residues. The mutant protein, also referred to as *Cj*FurΔS2, was homogeneously purified and its

ability to bind metals was assessed using ICP-MS. As shown in **Figure 5.1A** and consistent with the *Cj*FurZn_2 structure, we detected nearly two molar equivalents of zinc atoms per *Cj*Fur protomer and manganese in approximately 1:1 stoichiometry with the wild type protein. In contrast, *Cj*FurΔS2 failed to bind manganese. Surprisingly, despite an intact S3 site, analysis of the zinc content revealed that *Cj*FurΔS2 could only metallate one zinc atom per protomer suggesting that the S2 site is important for the function of the S3 site. To evaluate whether the S3 is also important for the metallation of S2, we repeated a similar experiment with a *Cj*Fur mutant (also referred to as *Cj*FurΔS3) in which His99 and His137 were substituted with alanine residues. Similar to *Cj*FurΔS2, *Cj*FurΔS3 failed to bind manganese and incorporate a second zinc atom, suggesting that both the S2 and S3 sites are important for binding manganese and are interdependent.

5.2.2 Role of *Cj*Fur S2 and S3 metal binding sites in DNA-binding activity

The binding of metals in the regulatory site of Fur proteins is important for the DNA binding activity. Given that the S2 and S3 sites are important for the binding of manganese, we posited that both sites are important for DNA binding activity. To test this hypothesis, we performed binding reactions with increasing concentrations of wild type *Cj*Fur, *Cj*FurΔS2 or *Cj*FurΔS3 and a DNA probe corresponding to the promoter region upstream of the *Cj1345c* operon, a region known to be regulated by *Cj*Fur in apo-conditions. As shown in **Figure 5.1B**, in binding conditions devoid of metals, wild type *Cj*Fur binds to DNA with high affinity while *Cj*FurΔS2 generate several distinguishable

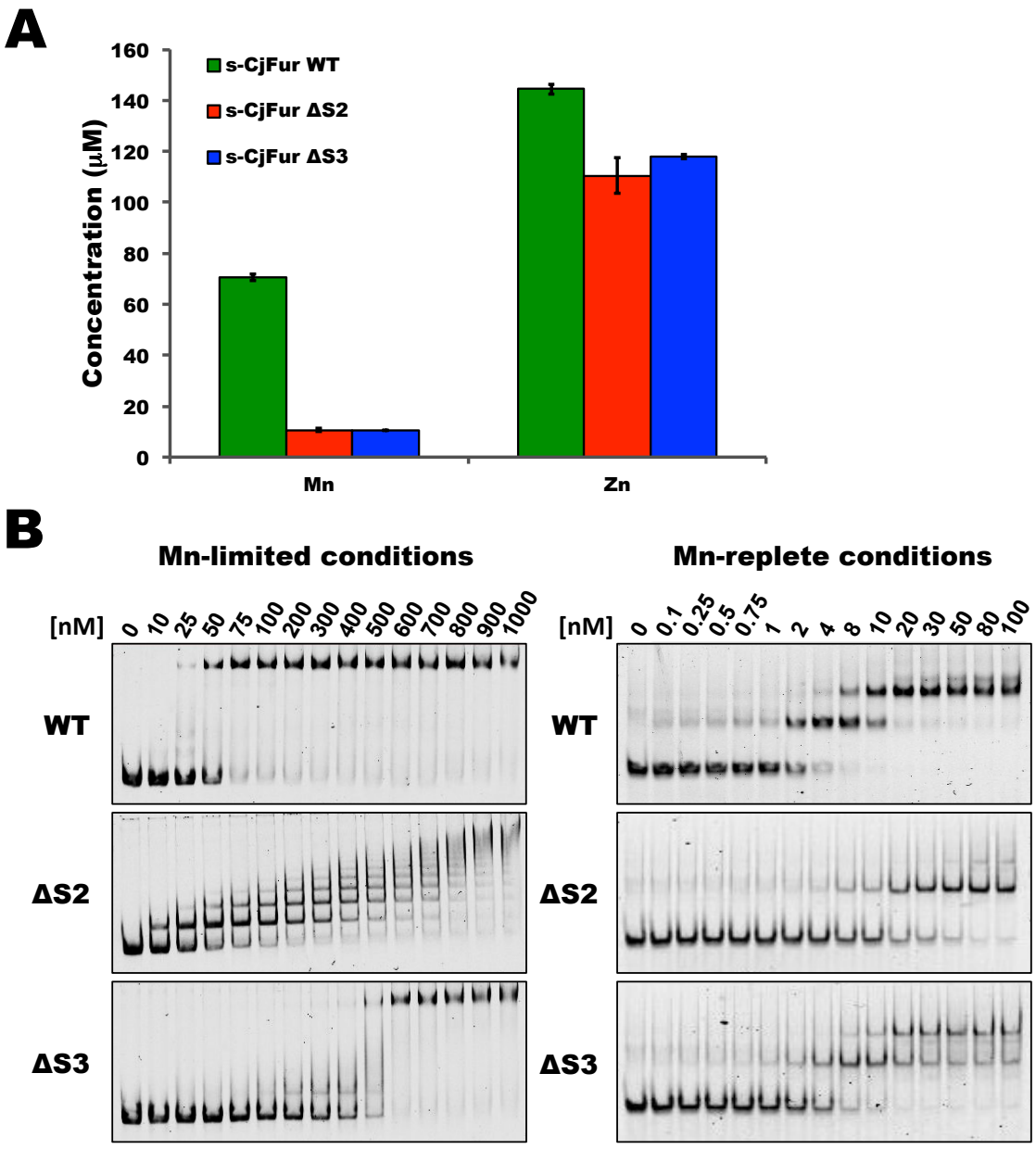
A
160
140
120
100
80
60
40
20
0
Concentration (μM)
s-CjFur WT
s-CjFur ΔS2
s-CjFur ΔS3
Mn
Zn
B
Mn-limited conditions
Mn-replete conditions
[nM]
0 10 25 50 75 100 200 300 400 500 600 700 800 900 1000
[nM]
0 0.1 0.25 0.5 0.75 1 2 4 8 10 20 30 50 80 100
WT
ΔS2
ΔS3
WT
ΔS2
ΔS3

Figure 5.1. Role of *Cj*Fur metal binding sites

(A) ICP-MS metal analysis of 100 μM purified recombinant *Cj*FurWT, *Cj*FurΔS2 and *Cj*FurΔS3.

(B) Electrophoretic mobility shift assay of
Left panel: *Cj1345c* promoter region (2 nM) in Mn-limited conditions with increasing amount (0-1000 nM) of *Cj*FurWT, *Cj*FurΔS2 and *Cj*FurΔS3
Right panel: *katA* promoter region (2 nM) in Mn-replete conditions with increasing amount (0-100 nM) of *Cj*FurWT, *Cj*FurΔS2 and *Cj*FurΔS3.

DNA bound *Cj*FurΔS2 complexes and mutation of the S3 metal binding site negatively affects *Cj*Fur DNA binding activity. To measure the differences in the impact of impairing the S2 or S3 metal binding sites between apo and holo conditions, we repeated the binding assays in presence of an excess of metals and a DNA fragment corresponding to the promoter region of *katA*, a holo-regulated gene. Comparative analysis between the binding assays performed in the holo and apo conditions with the wild type proteins reveals that in contrast to the apo-conditions, wild type *Cj*Fur forms two distinguishable binding species. In contrast, in the range of concentration tested, *Cj*FurΔS2 fails to generate two different DNA bound *Cj*Fur complexes and shows weaker binding to *katA* promoter region. Similarly, *Cj*FurΔS3 binds more weakly to DNA; however, the impact of its mutation is less deleterious in the holo-conditions when compared to the binding reactions performed in the apo-conditions. These observations suggest that both, the S2 and S3, sites are important for *Cj*Fur-DNA binding activity in manganese-limited and manganese-replete conditions.

5.2.3 Role of *Cj*Fur S2 and S3 metal binding sites in the regulation of *Cj*Fur target genes

To assess the potential role of *Cj*Fur S2 and S3 metal binding sites *in vivo*, complemented strains were constructed by introducing wild type *Cj*Fur, *Cj*FurΔS2 or *Cj*FurΔS3 genes in *C. jejuni Δfur* isogenic deletion mutant. Given that previous studies demonstrated that Fur is important for resistance to reactive oxygen species (ROS) (Troxell and Hassan, 2013), we tested for the sensitivity of different *Cj*Fur strains to the oxidant hydrogen peroxide (H_2O_2). As shown in **Figure 5.2A**, the *C. jejuni Δfur* strain

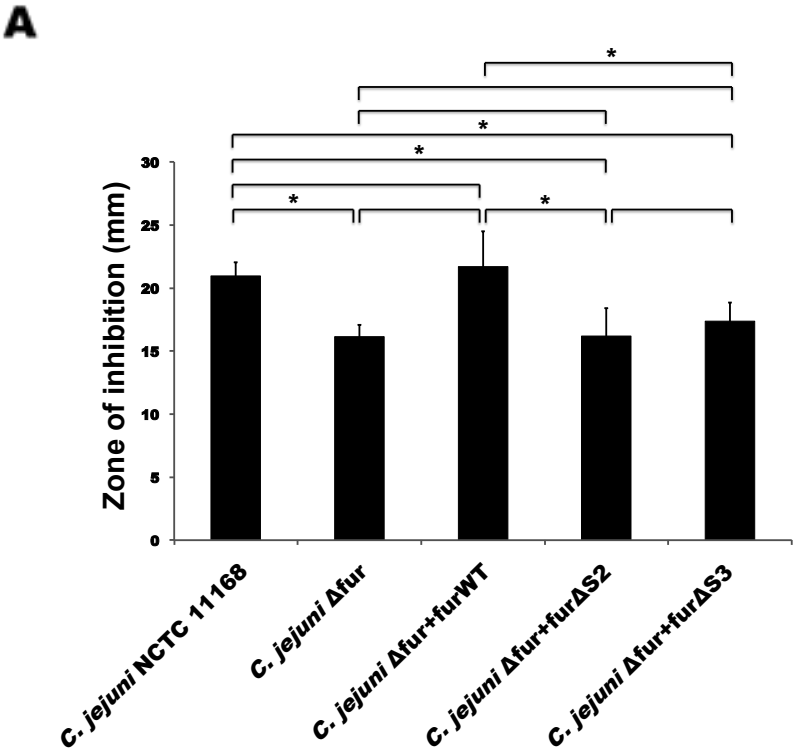
A
Zone of inhibition (mm)
0
5
10
15
20
25
30
*
*
*
*
*
*
C. jejuni NCTC 11168
C. jejuni Δfur
C. jejuni Δfur+furWT
C. jejuni Δfur+furΔS2
C. jejuni Δfur+furΔS3

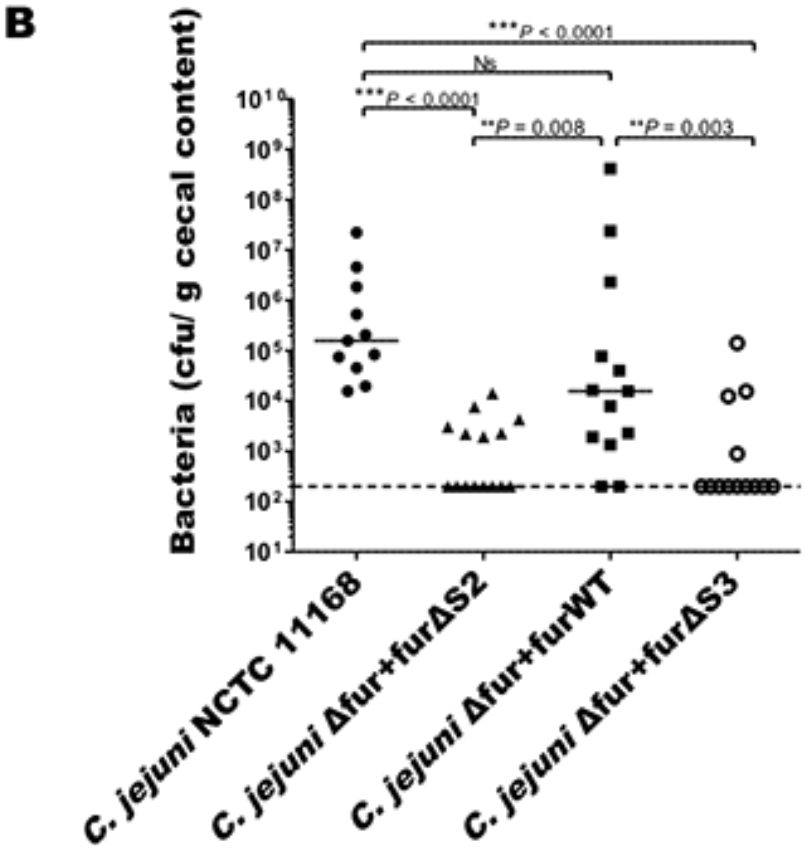
B
Bacteria (cfu/ g cecal content)
***P < 0.0001
Ns
***P < 0.0001
**P = 0.008
**P = 0.003
C. jejuni NCTC 11168
C. jejuni Δfur+furΔS2
C. jejuni Δfur+furWT
C. jejuni Δfur+furΔS3

Figure 5.2. *Cj*Fur S2 and S3 sites are important for the regulations of genes and colonization of the chick ceca

(A) Growth inhibition assay. 10 μL of 3% H_2O_2 was used and the results were taken after 28 hours of exposure to H_2O_2. Error bars represent the standard deviation and * denotes statistical significance ($P < 0.05$) using unpaired 2-tail student t-test. Three replicates were performed.

(B) *Campylobacter jejuni* wild type, complemented WT, ΔS2 and ΔS3 colonization levels in the chick cecum. Each data point represents the cfu per gram of cecal content recovered for each strain tested. Bars represent the median colonization of each strain and the dashed line indicates the detection limit of the assay. * denotes statistical significance ($P < 0.05$) using a nonparametric Mann-Whitney rank sum test.

mutant exhibited increased resistance toward 3% H_2O_2 relative to the NCTC strain or the strain complemented with wild type *Cj*Fur. Consistent with their inability to bind DNA, the *C. jejuni Δfur* strain complemented with *Cj*FurΔS2 and *Cj*FurΔS3 show an increased H_2O_2 resistance suggesting that both *Cj*Fur S2 and S3 sites are important for the regulation of genes involved in resistance to hydrogen peroxide in *C. jejuni*.

To determine whether *Cj*Fur S2 and S3 regulator sites are important in the colonization of chick ceca, 3-day-old chicks were inoculated with either wild type *C. jejuni* NCTC11168 or *Cj*FurΔS2 or *Cj*FurΔS3 strains. Chicks were also inoculated with a strain complemented with wild type *Cj*Fur. As shown in **Figure 5.2B**, both *C. jejuni* NCTC11168 and the complemented wild type Fur colonized the ceca at a level of approximately 10^4-10^5 cfu/g. The *Cj*FurΔS2 or *Cj*FurΔS3 mutant strains were significantly affected in their ability to colonize the ceca relative to the wild type and the NCTC11168 strains showing an average colonization of 10^2 cfu/g. Overall, these results indicate that metallation of both sites, S2 and S3, is important for the colonization of chick ceca by *Campylobacter jejuni*.

5.2.4 Crystal structure of *Cj*FurZn

To further understand the role of the S3 regulatory site on the activity of *Cj*Fur, we carried out crystallization trials to obtain crystals of wild type *Cj*Fur devoid of metal in its S3 site. After screenings several crystals obtained in various conditions, we obtained a unique crystal form that yielded the first crystal structure of *Cj*Fur with only the structural zinc-binding site occupied. The crystal structure of the new apo-*Cj*Fur

(referred to as *Cj*FurZn) protein construct was built and refined to a final R_{work}/R_{free} ratio of 18.4/22.9 at 1.81 Å resolution. The bond lengths in the model have a RMSD value of 0.01 Å and the angles in the new apo-*Cj*Fur model fall within favoured and allowed regions (98.9% favored, 0.8% allowed) of the Ramachandran plot. Only Lys97 in one of the protomers was modeled with bond angles in the un-allowed region of the Ramachandran plot.

The structure shows that the protein assembles into a biological dimer (**Figure 5.3**) in which each protomer folds in two domains, the DBD and the DD, that are structurally similar to the *Cj*FurZn$_2$. The asymmetric unit contains two protomers, A and B, which consist of residues 3–59, 61-86 and 89–149, and residues 1–84 and 90–154, respectively. Close inspection of the DBD reveals that the α1-helix faces the inner surface of the V-cleft in a conformation that is similar to *Cj*FurZn$_2$. Consistently, the electrostatic surface potential contour map shows that the DBD has a large positively charged surface facing the outside of the caliper-like structure the bottom of the V-cleft has an overall negative charge.

One of the two metal atoms characterized in the previous apo-*Cj*Fur structure could be detected in the new apo-*Cj*Fur protomers. This metal, which is most likely zinc, corresponds to the structural zinc tetra-coordinated by Cys105, Cys108, Cys145 and Cys148 in the S1 metal binding site (**Figure 5.3B**).

In comparison to *Cj*FurZn$_2$, *Cj*FurZn DBDs undergo slightly different structural reorganization (**Figure 5.4**). The DBD of *Cj*FurZn protomer A undergoes a clockwise rotation of approximately ~5º shifting the C-terminus of its α1-helix by ~5Å inwardly.

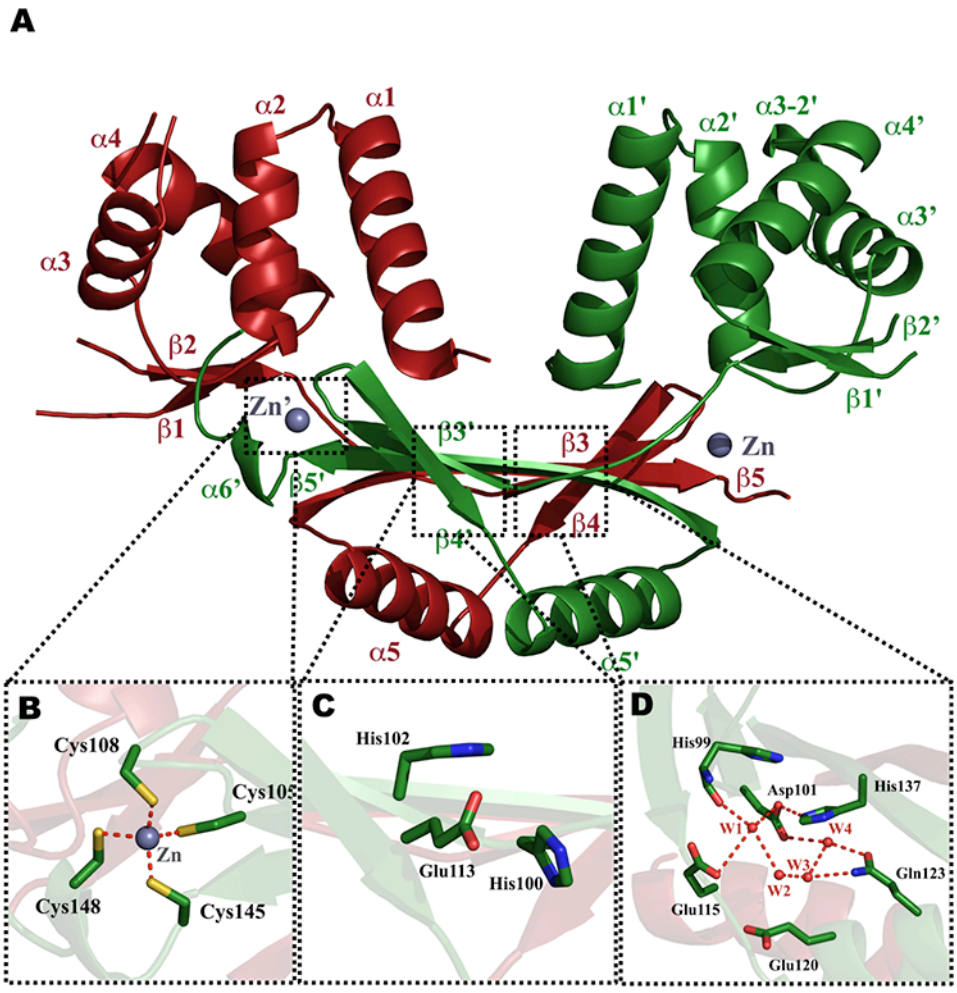
A
α4
α2
α1
α3
β2
β1
Zn'
α6'
β5'
β3'
β4'
α5
α1'
α2'
α3-2'
α4'
α3'
β2'
β1'
β3
Zn
β5
β4
α5'
B
Cys108
Cys105
Zn
Cys148
Cys145
C
His102
Glu113
His100
D
His99
Asp101
His137
W1
W4
W3
W2
Gln123
Glu115
Glu120

E

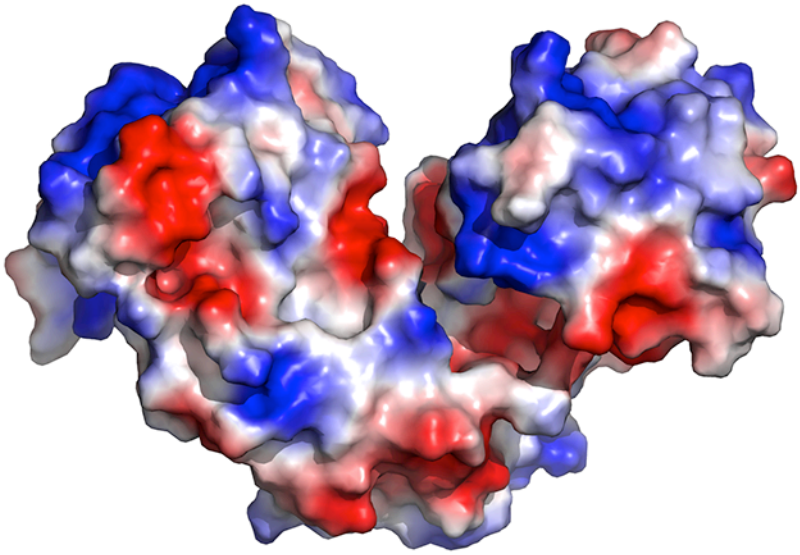

Figure 5.3 Crystal structure of *Cj*FurZn

(A) Crystal structure of *Cj*FurZn. Protomer A and Protomer B are rendered in green and red, respectively. Zn ions are represented by grey spheres. Secondary structures are labeled.

*Cj*FurZn metal binding sites S1 **(B)**, S2 **(C)** and S3 **(D)** are represented. Zinc ion is highlighted in grey. Water molecules and hydrogen bonds are represented by red spheres and orange dash lines, respectively.

(E) Electrostatic surface potential of *Cj*FurZn is represented. Positively charged surfaces are represented in blue ($+81k_bTe^{-1}$) and negatively charged surfaces in red ($-81\ k_bTe^{-1}$) (k_b = Bolzmann's constant, T = temperature in Kelvin and e = charge of an electron).

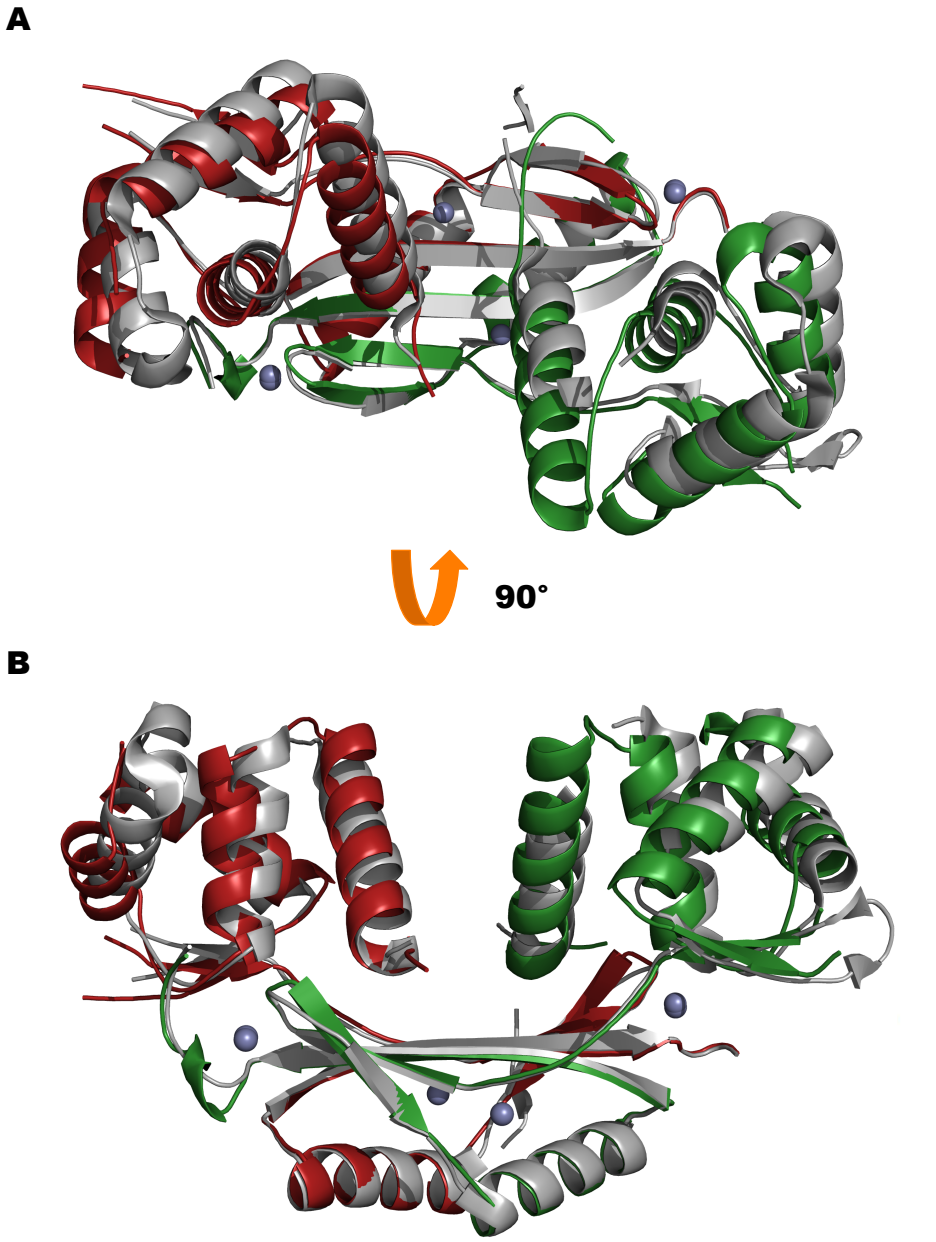
A
90°
B
C
His99
His137
Asp101
W1
W2
Zn
Gln123
Glu115
Glu120
D
His99
Asp101
His137
W1
W4
W3
Gln123
W2
Glu115
Glu120

Figure 5.4 Structural comparisons between *Cj*FurZn and *Cj*FurZn$_2$

(A and **B)** Two orthogonal views of the superimposition of *Cj*FurZn (grey) and *Cj*FurZn$_2$ (Protomer A and Protomer B rendered in red and green, respectively) crystal structures. Zinc ions are represented by grey spheres.

Zoomed view on *Cj*FurZn$_2$ **(C)** and CjFurZn **(D)** S3 metal binding sites. The zinc ions and water molecules are represented by grey and red spheres, respectively. Hydrogen bonds are highlighted as orange dashed lines.

The rotation also displaces the α4-helix C-terminus by an equivalent distance and moves the N-terminus of α3-helix by ~3Å outward of the V-shaped cleft. The DBD of *Cj*FurZn protomer B does not undergo a rotation but instead its α3 and α4 helices are displaced toward the inner portion of the V-shaped cleft. Altogether, these observations suggest that the DBD can undergo asymmetric reorganization when the S3 site is not metallated.

After observing notable structural reorganization of *Cj*FurZn DBD, we posited that the orientation of residues forming the S3 site would differ between *Cj*FurZn and *Cj*FurZn$_2$. In *Cj*FurZn$_2$, the Zn^{2+} ion is hexacoordinated by residues Asp101, Glu120, His137 and two water molecules (**Figure 5.4C**). Zoomed view on the S3 site reveals that in contrast to *Cj*FurZn$_2$, *Cj*FurZn has two additional water molecules in its S3 site (**Figure 5.4D**). In the *Cj*FurZn$_2$ structure, one water molecule makes a short hydrogen bond with the backbone carbonyl of His99 and an electrostatic interaction with the zinc atom. The other water molecule bridges an interaction between the side chain's amide of Gln123 and the zinc atom. In *Cj*FurZn, two additional water molecules occupy the S3 site, which presumably buffer the loss of the metal ion. One of these water molecule makes a water mediated hydrogen bond with Glu115 carboxylate while the other water molecule makes a direct electrostatic interaction with Gln128 side chain. Comparative analysis of *Cj*FurZn and *Cj*FurZn$_2$ S3 site shows that the rotation Glu120 side chain places its carboxylate group away from the S3 site enabling the binding of the two additional water molecules. The side chain of Glu115 also rotates around its C_β to optimize the hydrogen bonding with one of the water molecule. Altogether, these results show that while the loss of metal binding in the S3 site can be compensated by water molecules, it causes a distortion in the DBD that negatively affects the DNA binding activity of *Cj*Fur.

Chapter 6. Purification and characterization of the untagged *Cj*Fur protein

6.1 RATIONALE

Close inspection of *Cj*FurZn and *Cj*FurZn$_2$ structures described above revealed that in both structures the N-terminal end of the protein is oriented towards the inside of the V-cleft and interacts with the dimerization domain of *Cj*Fur. We noticed that the same pocket located on the dimerization domain stabilized a remnant of the cloning in both structures (**Figure 6.1**). Although the tag remnant in *Cj*FurZn is shorter than in *Cj*FurZn$_2$ structure, both crystal structures suggest that any remnant left on the N-terminus of the protein may prevent the crystallization of the holo-form of *Cj*Fur structure. In order to address this problem, we decided to redesign a novel construct in which *Cj*Fur is overexpressed without affinity tags.

6.2 RESULTS

6.2.1 Purification of the untagged *Cj*Fur

In order to express *Cj*Fur in absence of tags, the cDNA of the transcription factor was cloned in the pET3d vector. Following large-scale overexpression of *Cj*Fur, the cells were lysed in a low ionic strength buffer. Surprisingly, preliminary binding studies showed that following centrifugation, untagged *Cj*Fur could not bind to SP Sepharose, a strong cation exchange resin (data not shown). The absence of interaction between *Cj*Fur,

A

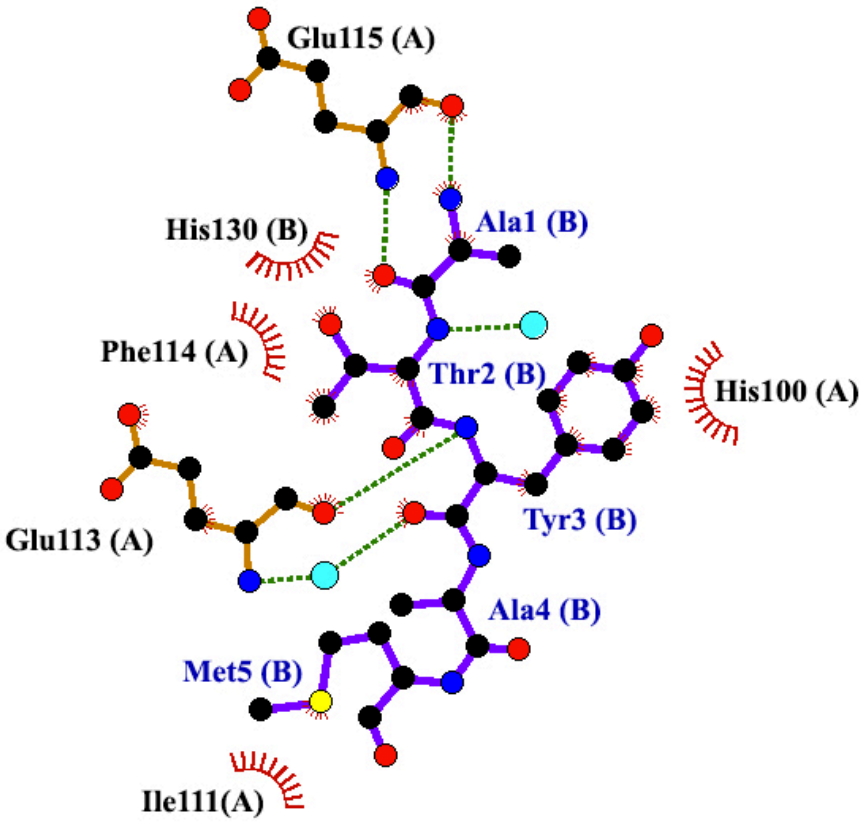
Glu115 (A)
His130 (B)
Ala1 (B)
Phe114 (A)
Thr2 (B)
His100 (A)
Glu113 (A)
Tyr3 (B)
Ala4 (B)
Met5 (B)
Ile111(A)

B

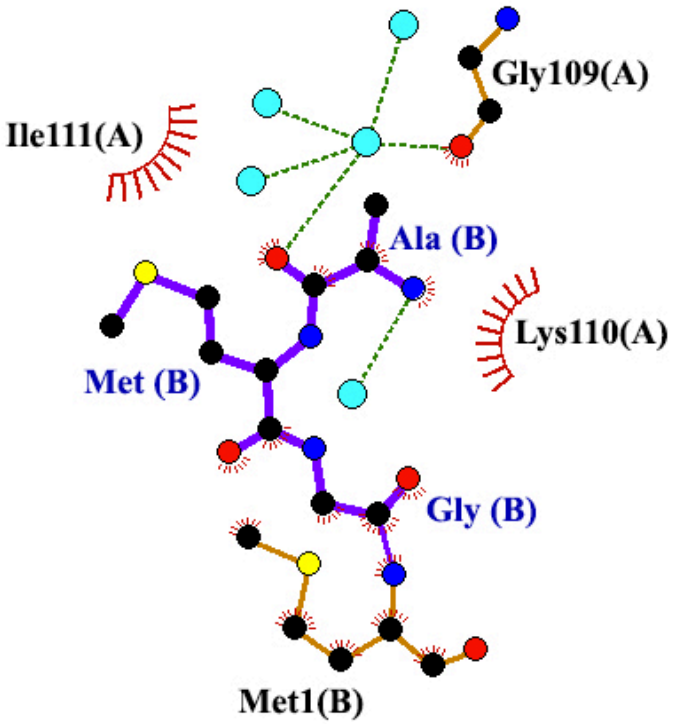
Gly109(A)
Ile111(A)
Ala (B)
Lys110(A)
Met (B)
Gly (B)
Met1(B)

Figure 6.1 Interaction of the remnant of the cloning with *Cj*Fur DD

Schematic representation of the interaction between

(A) the *Cj*FurZn$_2$ (ss-*Cj*Fur) DD (orange) and the tag remnant (purple).

(B) the *Cj*FurZn (s-*Cj*Fur) DD (orange) and the tag remnant (purple).

Carbon, nitrogen, oxygen and sulfur atoms are rendered in black, blue, red and yellow, respectively. Water molecules are represented by turquoise spheres. Hydrogen bonds and hydrophobic contacts are highlighted as green dashed lines and red half-ovals, respectively. The letter in brackets represents *Cj*Fur protomer.

a DNA binding protein containing positively charged patches on the surface of its DBD, and the cation exchange resin raised the possibility that contaminating proteins mask the positively charged regions of the metalloregulator. To address this problem, the *Cj*Fur containing cell lysate was first applied to Q Sepharose, a strong anion exchange resin. As anticipated, *Cj*Fur failed to interact with the resin. However, the negative selection resulted in the removal of several contaminating proteins (**Figure 6.2**). The flow-through was then applied onto the SP Sepharose. Consistent with our hypothesis, *Cj*Fur was retained by the anionic beads (**Figure 6.2**) and elution of the metalloregulator with 500 mM NaCl yielded a significant improvement in the purity of *Cj*Fur **(Figure 6.2)**. However, as shown in **Figure 6.2**, several contaminants co-eluted with *Cj*Fur. Considering that apo-*Cj*Fur showed an enrichment of positively charged residues on its surface, we sought to use heparin affinity chromatography to improve the purity of *Cj*Fur. Similar to SP Sepharose, Heparin molecules are high capacity cation exchangers due to their anionic sulfate groups. Consistent with our hypothesis, binding and elution of *Cj*Fur from the Heparin sepharose, resulted in an increase in the purity of the metalloregulator. The protein sample eluted from Heparin sepharose was concentrated and further purified using size exclusion chromatography. As shown in **Figure 6.2**, purified untagged *Cj*Fur eluted as a single peak at approximately 58 mL. Despite several optimization strategies, approximately 5 lowly abundant protein contaminants co-eluted with *Cj*Fur. We then sought to evaluate the purity of *Cj*Fur using ESI-MS. Following removal of the salt, the mass spectra was collected on an Orbitrap Classic (Thermo Fisher) mass spectrometer. As shown in **Figure 6.3**, we observed a single peak corresponding to a

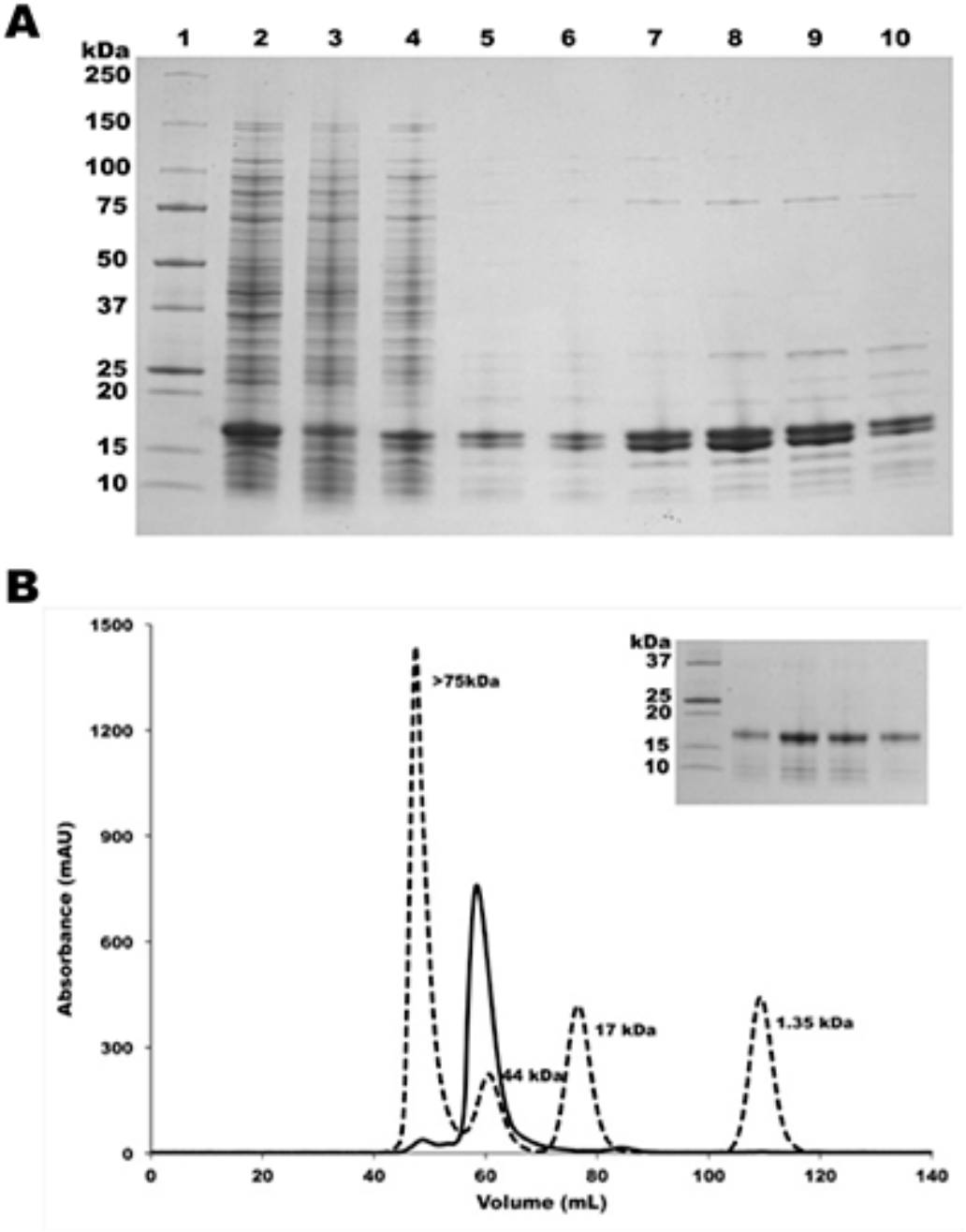
A
kDa
1
2
3
4
5
6
7
8
9
10
250
150
100
75
50
37
25
20
15
10
B
Absorbance (mAU)
1500
1200
900
600
300
0
0
20
40
60
80
100
120
140
Volume (mL)
>75kDa
44 kDa
17 kDa
1.35 kDa
kDa
37
25
20
15
10

Figure 6.2. Purification of untagged *Cj*Fur using a combination of three ion affinity chromatography steps

(A) Fractions of the protein sample at different steps of the purification scheme were separated on 4-20% SDS-PAGE gradient gels to assess protein purity. 1: molecular weight marker, 2: cell lysate, 3: supernatant, 4: flow through of the Q Sepharose column, 5: sample eluted from SP Sepharose column, 6: sample after dialysis (sample loaded on Heparin column), 7-10: fractions of sample eluted from Heparin column at a concentration of NaCl of 775 mM to 875 mM.

(B) Size-exclusion chromatography of *Cj*Fur on Superdex 75. Solid and dashed lines represent the UV absorbance of *Cj*Fur protein sample and the different molecular weight standards, respectively. Fractions of the eluted protein were run on 4-20% SDS-PAGE gradient gel to assess protein purity and yield, which is presented as the inset in the chromatogram.

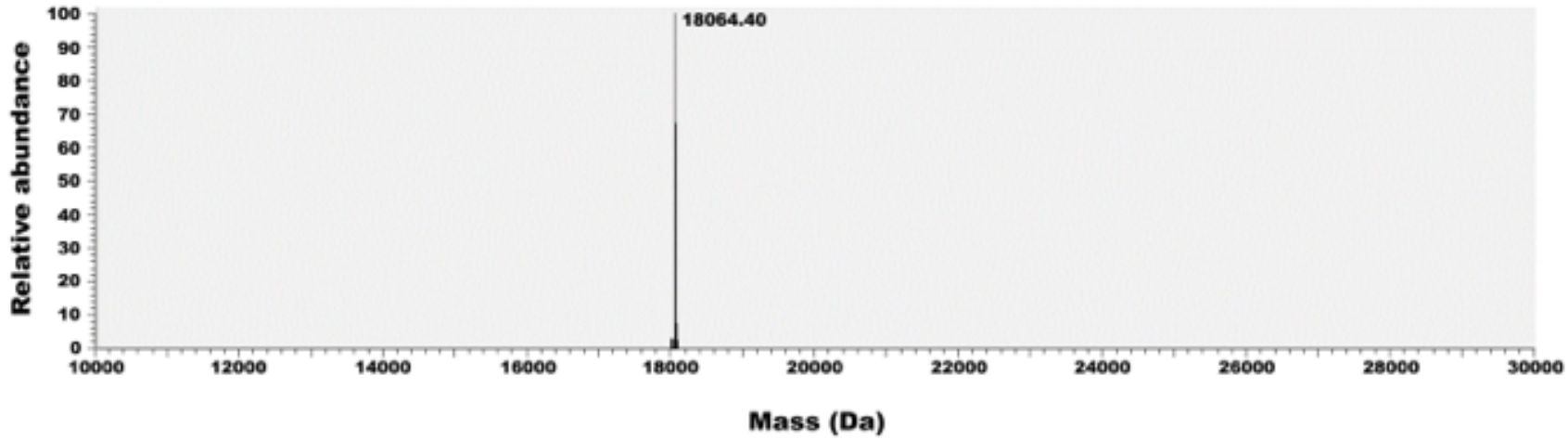
18064.40
Relative abundance
100
90
80
70
60
50
40
30
20
10
0
10000
12000
14000
16000
18000
20000
22000
24000
26000
28000
30000
Mass (Da)

Figure 6.3. Electrospray-ionization mass-spectrometry

The mass peak of the purified recombinant *Cj*Fur was observed with a molecular weight of 18064.40 Da, which was similar to the calculated mass of *Cj*Fur (18066.02 Da).

molecular weight of 18064.4 Da. Interestingly, no other protein contaminants were detected by the mass-spectrometer.

6.2.2 Untagged *Cj*Fur binds metal more efficiently

After confirming that a combination of three ion-chromatography steps followed by size exclusion chromatography yields homogeneous *Cj*Fur, we sought to measure the ability of the metalloregulator to bind the regulatory metal. Three different constructs of this metalloregulator namely *Cj*Fur (untagged Fur), s-*Cj*Fur (*Cj*FurZn) and ss-*Cj*Fur (*Cj*FurZn$_2$) (see sections 2.1.1-2.1.3 and sections 2.3.1-2.3.3 for details regarding the construction of the plasmids and the purification protocol, respectively) were incubated with equimolar amount of $MnCl_2$ and the metal content of the protein preparations was assessed by ICP-MS. As shown in **Figure 6.4A**, the untagged *Cj*Fur protein was able to incorporate manganese in a stoichiometric ratio of 1 atom of manganese per protomer. Given that the ability to incorporate manganese was two-folds less in the case of tagged proteins when compared to the untagged *Cj*Fur protein, our results suggest that adding a tag on the N-terminus of *Cj*Fur protein reduces its ability to incorporate the regulatory metal ions and consequently may impact its DNA binding activity.

6.2.3 Untagged *Cj*Fur binds DNA with more affinity

After determining the effect of the tag remnant on the ability of *Cj*Fur to incorporate regulatory metal ions, we sought to determine its effect on the DNA binding activity of *Cj*Fur. We performed gel shift assays with increasing concentration of *Cj*Fur (untagged Fur),

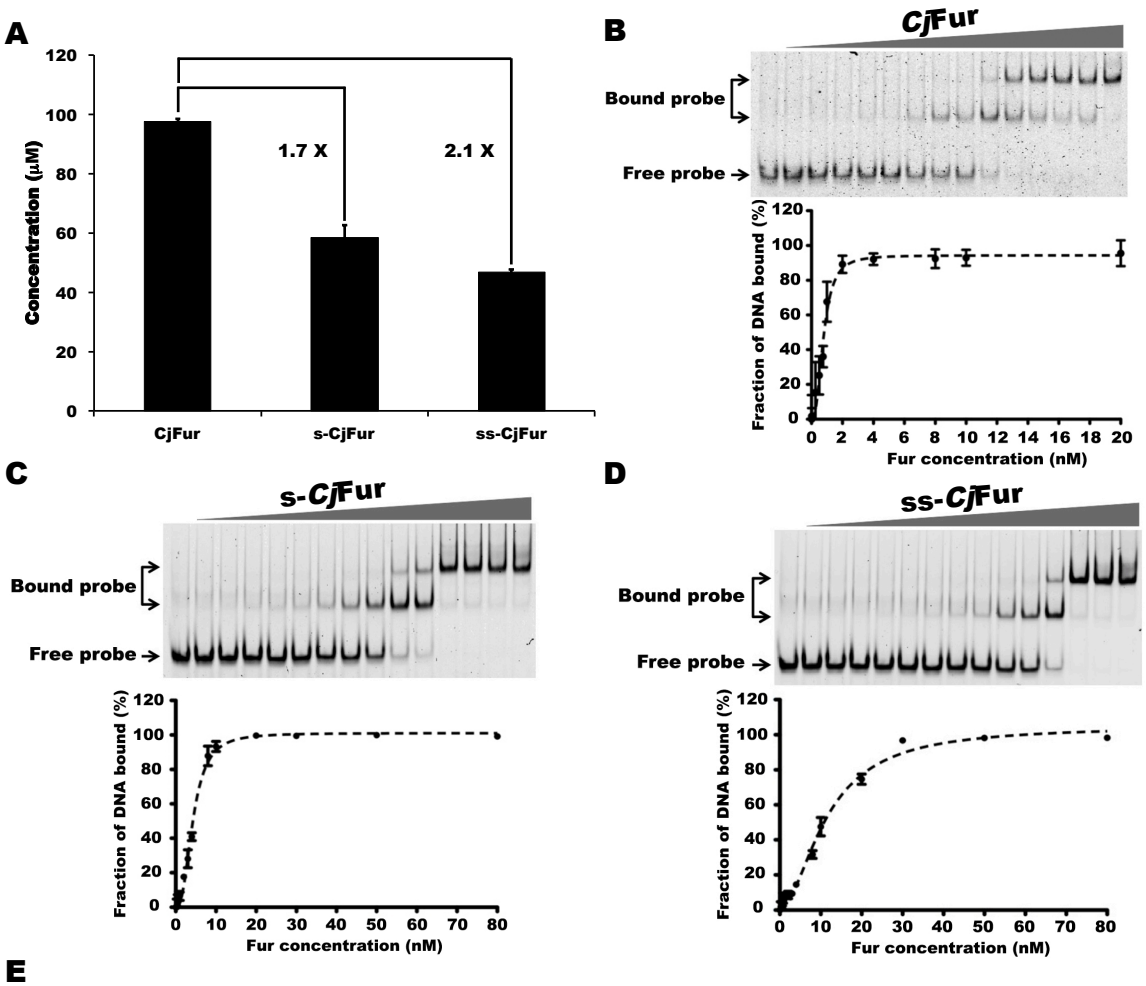

E

	Tag's remnant	Kd app (nM)
*Cj*Fur	N/A	0.78 ± 0.08
s-*Cj*Fur	GAMG	4.29 ± 0.11
ss-*Cj*Fur	ATYAMGS	11.39 ± 0.62

Figure 6.4. Untagged *Cj*Fur binds the regulatory metal and DNA more efficiently than ss-*Cj*Fur and s-*Cj*Fur

(A) Graph bar showing the concentration of Mn^{2+} in 100 μM of *Cj*Fur, s-*Cj*Fur and ss-*Cj*Fur.

(B) Electrophoretic mobility shift assay showing the separation of a Cy5 labeled *katA* promoter region with increasing concentrations of metallated untagged *Cj*Fur (0-20 nM) with the corresponding linear regression (GraphPad Prism). Lane 1: 0nM, lane 2: 0.01 nM, lane 3: 0.025 nM, lane 4: 0.05 nM, lane 5: 0.075 nM, lane 6: 0.1 nM, lane 7: 0.25 nM, lane 8: 0.5 nM, lane 9: 0.75 nM, lane 10: 1 nM, lane 11: 2 nM, lane 12: 4 nM, lane 13: 8 nM, lane 14: 10 nM and lane 15: 20 nM.

(C) Electrophoretic mobility shift assay showing the separation of a Cy5 labeled *katA* promoter region titrated with increasing concentrations of metallated s-*Cj*Fur (0-80 nM) with the corresponding linear regression. Lane 1: 0nM, lane 2: 0.1 nM, lane 3: 0.25 nM, lane 4: 0.5 nM, lane 5: 0.75 nM, lane 6: 1 nM, lane 7: 2 nM, lane 8: 3 nM, lane 9: 4 nM, lane 10: 8 nM, lane 11: 10 nM, lane 12: 20 nM, lane 13: 30 nM, lane 14: 50 nM and lane 15: 80 nM.

(D) Electrophoretic mobility shift assay showing the separation of a Cy5 labeled *katA* promoter region titrated with increasing concentrations of metallated and ss-*Cj*Fur (0-80 nM) with the corresponding linear regression. Lane 1: 0nM, lane 2: 0.1 nM, lane 3: 0.25 nM, lane 4: 0.5 nM, lane 5: 0.75 nM, lane 6: 1 nM, lane 7: 2 nM, lane 8: 3 nM, lane 9: 4 nM, lane 10: 8 nM, lane 11: 10 nM, lane 12: 20 nM, lane 13: 30 nM, lane 14: 50 nM and lane 15: 80 nM.

(E) Mean K_d^{app} values are given for each construct in which the remnant of the tag is also indicated for each construct.

s-*Cj*Fur (*Cj*FurZn) and ss-*Cj*Fur (*Cj*FurZn$_2$) and *katA* promoter regions as DNA probe. The three proteins are able to bind *katA* promoter region and generate a similar binding pattern highlighted by the presence of two shifted species (**Figure 6.4**). At low *Cj*Fur concentrations, a single band is detected by EMSA while a larger *Cj*Fur-DNA complex is obtained at higher concentration of *Cj*Fur suggesting that two dimers of the metalloregulator bind the same DNA element. We then sought to determine the apparent equilibrium dissociation constant (K_d^{app}) by quantifying the disappearance of the free Cy5 labeled probe and determining the bound fraction *vs* protein concentration. As shown in **Figure 6.4E**, the K_d^{app} of s-*Cj*Fur (*Cj*FurZn) and ss-*Cj*Fur for DNA is 5.5-fold and 14.6-fold higher when compared to *Cj*Fur, strongly suggesting that adding a tag at the N-terminal end of *Cj*Fur protein reduces its ability to bind DNA.

CHAPTER 7. DISCUSSION

Members of the Fur family of transcription factors have been characterized in diverse bacterial species and shown to play a crucial role in iron homeostasis as well as several other biological pathways including flagellar biogenesis, energy metabolism and oxidative stress defense (Butcher et al., 2012; Seo et al., 2015). Since the initial findings that Fe^{2+} acts as a corepressor of Fur protein to negatively regulate the expression of the operon controlling iron transport (Bagg and Neilands, 1987), the accepted dogma at the time was that Fur protein represses gene expression only when bound to iron. However, in the early 2000s, several pioneering studies expanded the gene regulatory mode employed by Fur to include models wherein Fur positively and negatively regulates gene expression and so in presence and absence of regulatory metals (Bsat and Helmann, 1999; Delany et al., 2001; Palyada et al., 2004). When I started my PhD, these additional regulatory mechanisms were confirmed only in *Helicobacter pylori.* However, the laboratory of Dr. Alain Stintzi had obtained evidence that *Campylobacter jejuni* Fur recognized divergent DNA consensus sequences and regulated gene expression independently of iron. These findings strongly suggested the presence of several regulatory mechanisms that include the repression and activation in holo and apo conditions. In order to better understand the structural determinants underlying *Cj*Fur ability to regulate gene expression via four general mechanisms, we undertook structural and functional studies of *Cj*Fur protein to characterize its interaction with DNA.

During my PhD, I have solved the first crystal structure of apo-Fur protein harboring the closed V-shaped conformation suitable for the interaction with DNA. I have shown that *Cj*Fur protein binds DNA in presence as well as in the absence of the regulatory metal ion. Moreover, despite the major conformational changes generated by the binding of the

regulatory metal ion, my studies demonstrated that *Cj*Fur employs the same evolutionary conserved positively charged region to regulate gene expression. I have also demonstrated the importance of the *Cj*Fur metal binding sites in maximizing *Cj*Fur binding affinity for a DNA element, the regulation of gene expression and colonization of chick colon. Finally, I have shown that the addition of a tag at the N-terminus of *Cj*Fur protein affects its ability to bind metal ions and DNA.

7.1 Unique set of interactions underlying apo-Fur conformation: an emerging paradigm?

Our structural studies of *Cj*Fur have uncovered the first structure of an active apo-Fur protein. Comparative analysis of *Cj*FurZn_2 with other Fur and Fur-like proteins revealed several structural similarities and differences. Similar to other Fur members, *Cj*FurZn_2 is a homodimer and each protomer folds in two domains including the N-terminal DNA binding and the C-terminal dimerization domains. Close inspection of metal binding sites revealed the presence of a zinc ion in the structural S1 site. This Zn^{2+} ion is tetracoordinated by two pairs of cysteine residues, forming a C4 zinc-finger motif, an important structural determinant for dimerization in *Ec*Fur, *Bs*PerR, *Hp*Fur, *Sc*Zur and *Ec*Zur (Gilston et al., 2014; Pecqueur et al., 2006; Shin et al., 2011; Traoré et al., 2006; Vitale et al., 2009). The S3 site also contains a zinc ion hexacoordinated by Glu120, Asp101, and His137 and two water molecules. Although the residues involved in the coordination of the zinc ion in the S3 site are well conserved in Fur proteins, the coordination number and geometry of this site differ greatly within this family. Similar to *Cj*Fur, the zinc ion in *Pa*Fur S3 site is also hexacoordinated while the same metal binding site in *Hp*Fur and *Vc*Fur harbors a

tetracoordinated zinc ion (Dian et al., 2011; Pohl et al., 2003; Sheikh and Taylor, 2009). The third metal binding site S2, known as the regulatory metal binding site in several members of the Fur family of proteins including *Pa*Fur, *Vc*Fur and *Hp*Fur (An et al., 2009; Deng et al., 2015; Dian et al., 2011; Gilston et al., 2014; Jacquamet et al., 2009; Sheikh and Taylor, 2009; Shin et al., 2011), is unoccupied in *Cj*Fur suggesting that the *Cj*FurZn$_2$ structure embodies the apo-form of the protein.

When compared to previously characterized Fur and Fur like proteins, *Cj*FurZn$_2$ adopts an atypical conformation resulting from a rotation of its DBD domain. Despite this conformational change, *Cj*FurZn$_2$ adopts a caliper like conformation important for the interaction with DNA. Two additional apo structures of *Mg*Fur and *Bs*PerZn were solved, however neither of these apo-proteins is amenable to bind DNA. While the apo-*Bs*PerRZn structure adopts a quasi-planar conformation which positions the DNA interacting helices in a non-permissive orientation for its interaction with DNA (Traoré et al., 2006), apo-*Mg*Fur adopts a more closed conformation but the asymmetric orientation of the DNA binding domains in this structure is not suitable for binding DNA (Deng et al., 2015). *Cj*FurZn$_2$ however preserves the canonical V-shaped conformation similar to other holo-Fur proteins, a conformation maintained by several interdomain contacts between the *Cj*Fur DBD and DD. Notably, the N-terminal end of α1 engages in several hydrophobic contacts and hydrogen bonds with the three stranded β-sheet of the DD. The residues Glu4, Val6, and Glu7, make several hydrogen bonds with Gln140, Tyr142 and Lys106 while the Ile3 side chain participates in hydrophobic interactions with Ile104 and Ile111 found in the β3-β4 sheet **(Figure 7.1)**. Moreover, residues found in the C-terminal end of α2, which include Tyr38 and Asp41, engage in hydrogen bonds with residues encompassing the β3−β4 hairpin and the

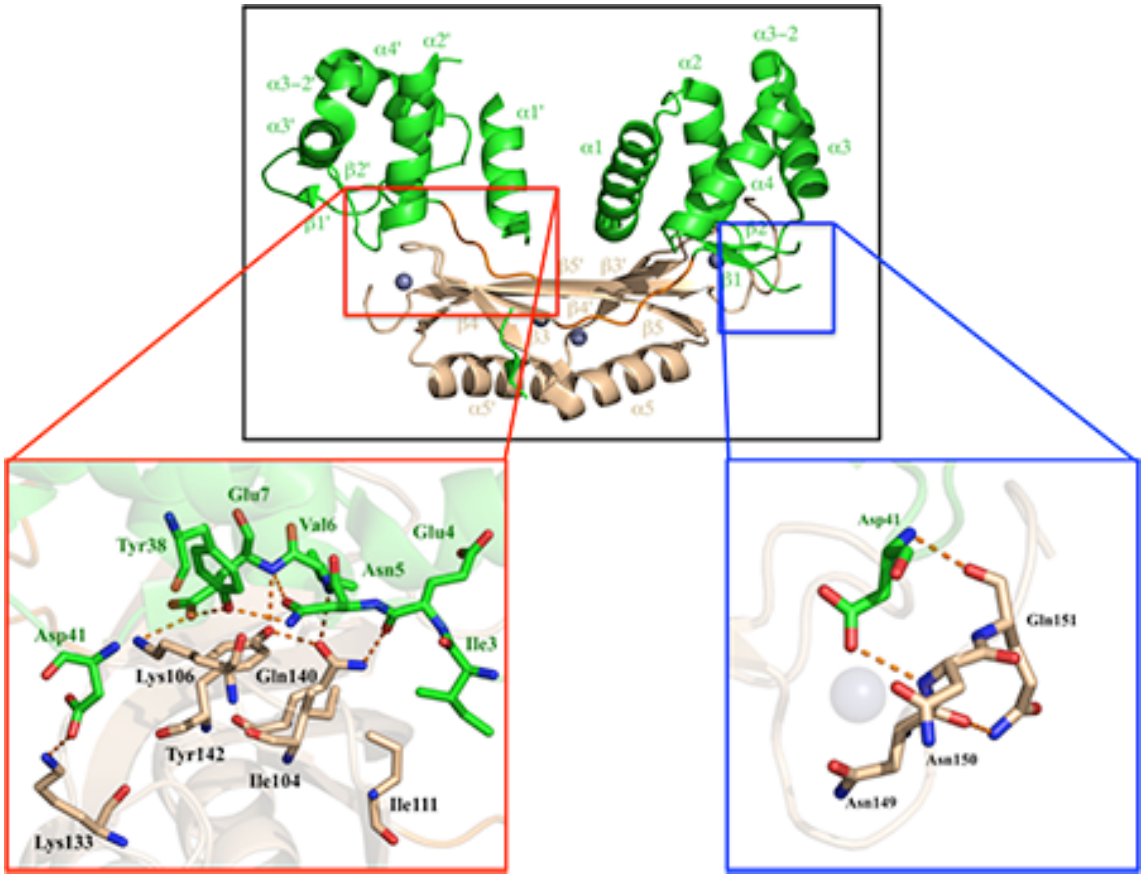
α4'
α2'
α3-2'
α3'
α1'
β2'
β1'
α3-2
α2
α1
α3
α4
β2
β1
β5'
β3'
β4'
β4
β3
β5
α5'
α5
Glu7
Val6
Tyr38
Glu4
Asn5
Asp41
Ile3
Lys106
Gln140
Tyr142
Ile104
Ile111
Lys133
Asp41
Gln151
Asn150
Asn149

Figure 7.1 Interactions stabilizing the apo-*Cj*Fur structure

Zoomed view on interactions between the *Cj*FurZn_2 DBD (green) and DD (wheat). The zinc ions and key hydrogen bonds are rendered as grey spheres and orange dashed lines, respectively.

N-terminal end of β5 of the *Cj*Fur DD. Finally, the residues succeeding the C4 zinc finger of the DD fold back onto the DBD and make hydrogen bonds with a loop connecting α2 and α3 of the DBD. Overall, this network of hydrogen bonds and hydrophobic contacts appears to stabilize the formation of apo-*Cj*Fur's V-shaped conformation.

Structural (**Figure 1.5** and **Figure 3.3**) and sequence (**Figure 7.2**) alignments of crystallized Fur family members showed that *Cj*Fur and *Hp*Fur are the only two proteins that have the additional ten residues at their N-terminus which results in an elongated N-terminal α1 helix. As mentioned above, residues forming this N-terminal extension engage in several hydrophobic contacts and hydrogen bonds in order to maintain the V-shaped conformation of the apo-*Cj*Fur protein. Since, among all of the crystallized Fur family members, *Cj*Fur and *Hp*Fur are the only two proteins that possess all four regulatory mechanisms, it is tempting to speculate that this unique N-terminal extension plays an important role in apo-Fur regulation by stabilizing the V-shaped conformation of Fur proteins in the absence of regulatory metal ion. To confirm this hypothesis, we could engineer a new Fur protein by attaching the *Cj*Fur's N-terminal extension to a Fur protein that does not possess apo-regulation function, *Mg*Fur for example, since it has been shown that this protein does not bind DNA in absence of regulatory metal ion (Deng et al., 2015). Thus, if the N-terminal extension is important for the stabilization of the apo-conformation and plays an important role in gene regulation in the absence of the regulatory metal ion, we would anticipate that the newly engineered protein would develop apo-regulatory function.

7.2 Holo and apo Fur regulation, two modes of gene regulation: two different binding modes with DNA

A recent study showed that *Cj*Fur protein recognizes several DNA-binding motifs depending on the regulatory mode. Consequently, novel consensus sequences controlling the holo-Fur activated and holo-Fur repressed gene regulatory programs were identified (Butcher et al., 2012). However, the biochemical basis underlying this expanded repertoire of DNA sequences remains unknown. In order to better understand the mechanistic basis underlying the binding of *Cj*Fur to different target promoters, we performed DNA binding assays in holo and apo conditions. To perform our binding studies, we used a DNA element corresponding to the promoter region of *Cj*1345c as this gene was found to be apo-regulated using microarray and Chi-Chip analysis (Butcher et al., 2012; Palyada et al., 2004). Moreover, this gene was shown to be differentially expressed in a *Δfur* mutant under iron-limited conditions. DNA binding assays performed in manganese-limited conditions with increasing amount of apo-*Cj*Fur showed the presence of one main shifted species migrating at a Rf of 0.07. However, upon substitution of Arg30 to a glutamic acid, an intermediary shifted species migrating at a Rf of 0.31 was observed. While the stoichiometry of binding of apo-*Cj*Fur to DNA is still unknown, our data suggest that wild type *Cj*Fur, in apo conditions, form oligomers on DNA and that Arg30 is important for the multimerization of the transcriptional regulator. Interestingly, the Protein Interfaces, Surfaces and Assemblies (PISA) analysis revealed that the homologous arginine residue in *Pa*Fur, Arg18, is important for the tetramerization of the transcription factor (Pérard et al., 2016) suggesting that this residues could also be involved in the multimerization of *Cj*Fur. Similarly, recent structural studies

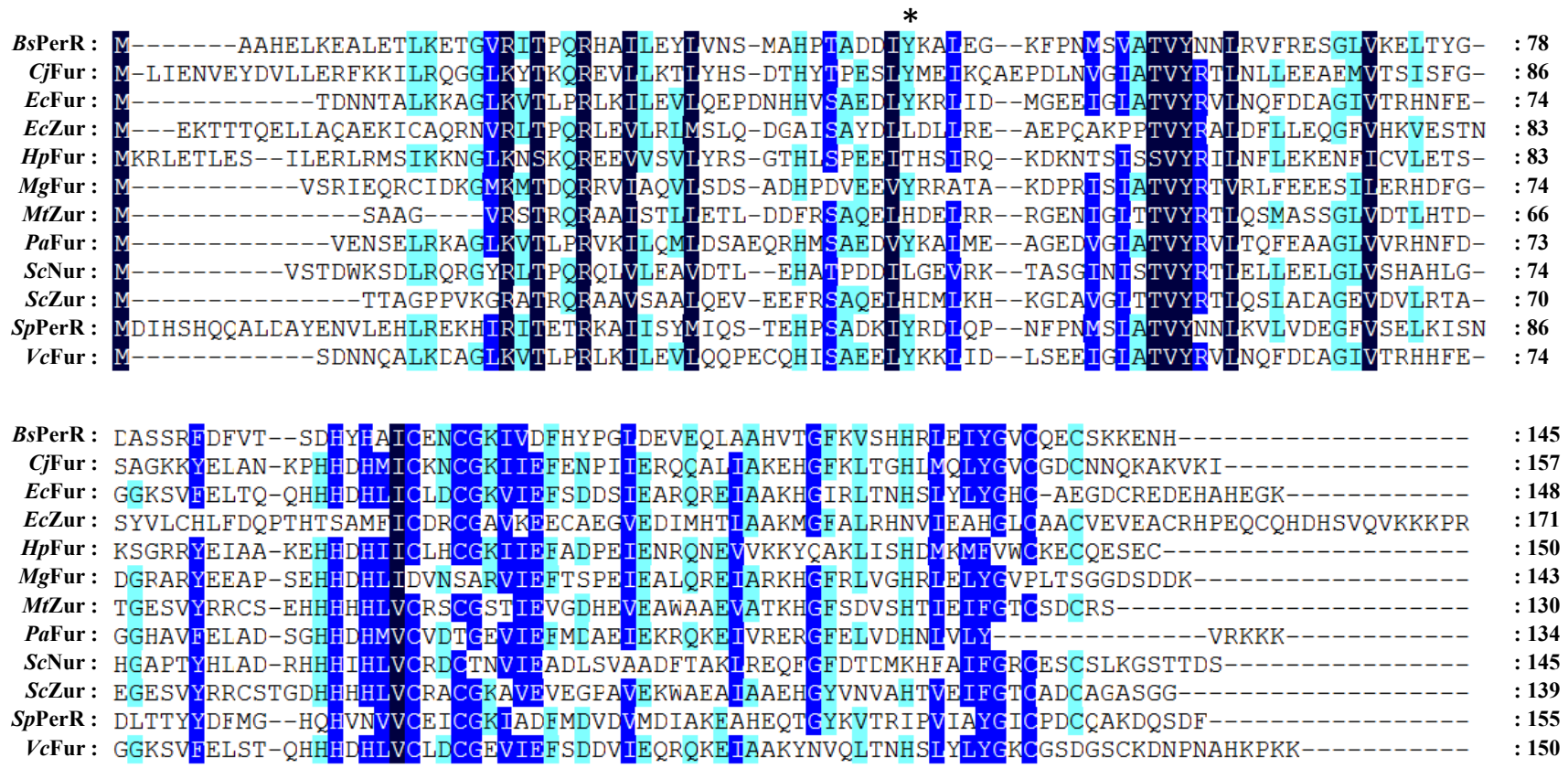
*
BsPerR : M-------AAHELKEALETLKETGVRITPQRHAILEYLVNS-MAHPTADDIYKALEG--KFPNMSVATVYNNLRVFRESGLVKELTYG- : 78
CjFur : M-LIENVEYDVLLERFKKILRQGGLKYTKQREVLLKTLYHS-DTHYTPESIYMEIKQAEPDLNVGIATVYRTLNLLEEAEMVTSISFG- : 86
EcFur : M------------TDNNTALKKAGLKVTLPRLKILEVLQEPDNHHVSAEDLYKRLID--MGEEIGLATVYRVLNQFDDAGIVTRHNFE- : 74
EcZur : M---EKTTTQELLAQAEKICAQRNVRLTPQRLEVLRLMSLQ-DGAISAYDLLDLIRE--AEPQAKPPTVYRALDFLLEQGFVHKVESTN : 83
HpFur : MKRLETLES--ILERLRMSIKKNGLKNSKQREEVVSVLYRS-GTHLSPEEITHSIRQ--KDKNTSISSVYRILNFLEKENFICVLETS- : 83
MgFur : M-----------VSRIEQRCIDKGMKMTDQRRVIAQVLSDS-ADHPDVEEVYRRATA--KDPRISIATVYRTVRLFEEESILERHDFG- : 74
MtZur : M---------------SAAG----VRSTRQRAAISTLLETL-DDFRSAQELHDELRR--RGENIGLTTVYRTLQSMASSGLVDTLHTD- : 66
PaFur : M-------------VENSELRKAGLKVTLPRVKILQMLDSAEQRHMSAEDVYKAIME--AGEDVGIATVYRVLTQFEAAGLVVRHNFD- : 73
ScNur : M----------VSTDWKSDLRQRGYRLTPQRQLVLEAVDTL--EHATPDDILGEVRK--TASGINISTVYRTLELLEELGLVSHAHLG- : 74
ScZur : M---------------TTAGPPVKGFATRQRAAVSAALQEV-EEFRSAQELHDMLKH--KGDAVGLTTVYRTLQSLADAGEVDVLRTA- : 70
SpPerR : MDIHSHQQALLAYENVLEHLREKHIRITETRKAIISYMIQS-TEHPSADKIYRDLQP--NFPNMSIATVYNNLKVLVDEGFVSELKISN : 86
VcFur : M------------SDNNQALKDAGLKVTLPRLKILEVLQQPECQHISAEELYKKLID--LSEEIGLATVYRVLNQFDDAGIVTRHHFE- : 74
BsPerR : DASSREDFVT--SDHYFAICENCGKIVDFHYPGLDEVEQLAAHVTGFKVSHHRLEIYGVCQECSKKENH------------------ : 145
CjFur : SAGKKYELAN-KPHHDHMICKNCGKIIEFENPIIERQQALIAKEHGFKLTGHLMQLYGVCGDCNNQKAKVKI---------------- : 157
EcFur : GGKSVFELTQ-QHHHDHLICLDCGKVIEFSDDSIEARQREIAAKHGIRLTNHSLYLYGHC-AEGDCREDEHAHEGK------------ : 148
EcZur : SYVLCHLFDQPTHTSAMFICDRCGAVKEECAEGVEDIMHTLAAKMGFALRHNVIEAHGLCAACVEVEACRHPEQCQHDHSVQVKKKPR : 171
HpFur : KSGRRYEIAA-KEHHDHIICLHCGKIIEFADPEIENRQNEVVKKYQAKLISHDMKMFVWCKECQESEC-------------------- : 150
MgFur : DGRARYEEAP-SEHHDHLIDVNSARVIEFTSPEIEALQREIARKHGFRLVGHRLELYGVPLTSGGDSDDK------------------ : 143
MtZur : TGESVYRRCS-EHHHHHLVCRSCGSTIEVGDHEVEAWAAEVATKHGFSDVSHTIEIFGTCSDCRS----------------------- : 130
PaFur : GGHAVFELAD-SGHHDHMVCVDTGEVIEFMLAEIEKRQKEIVRERGFELVDHNLVLY--------------VRKKK------------ : 134
ScNur : HGAPTYHLAD-RHHHIHLVCRDCTNVIEADLSVAADFTAKLREQFGFDTDMKHFAIFGRCESCSLKGSTTDS---------------- : 145
ScZur : EGESVYRRCSTGDHHHHLVCRACGKAVEVEGPAVEKWAEAIAAEHGYVNVAHTVEIFGTCADCAGASGG------------------ : 139
SpPerR : DLTTYYDFMG--HQHVNVVCEICGKIADFMDVDVMDIAKEAHEQTGYKVTRIPVIAYGICPDCQAKDQSDF---------------- : 155
VcFur : GGKSVFELST-QHHHDHLVCLDCGEVIEFSDDVIEQRQKEIAAKYNVQLTNHSLYLYGKCGSDGSCKDNPNAHKPKK---------- : 150

Figure 7.2. Sequence alignment of Fur and Fur-like proteins.

Sequence alignment of Fur proteins *C. jejuni* (*Cj*Fur), *E. coli* (*Ec*Fur) *H. pylori* (*Hp*Fur), *M. gryphiswaldense* MSR-1 (*Mg*Fur), *P. aeruginosa* (*Pa*Fur) and *V. cholerae* (*Vc*Fur), and of the Fur-like Zur from E.coli (*Ec*Zur), *M. tuberculosis* (*Mt*Zur), *S. coelicolor* (*Sc*Zur), Nur from *S. coelicolor* (*Sc*Nur), and PerR from *B. subtilis* (*Bs*PerR) and *S. pyogenes* (SpPerR). Sequences were aligned using the ClustalW option in MEGA6 (Tamura et al., 2013). Asterisks indicate the conserved Tyr residue in Fur proteins possibly equivalent to *Ec*Zur Tyr45. Positions with 100% amino acid conservation are indicated by dark blue, 100–80% by medium blue, and 80–60% by light blue.

revealed that the binding of *Ec*Zur to DNA is achieved by cooperative binding of two adjacent *Ec*Zur dimers. Such cooperativity arises from two salt bridges between Asp49 and Arg52 residues that connect two adjacent independent dimers (Gilston et al., 2014). Akin to *Ec*Zur Asp49 and Arg51, apo-*Cj*Fur Arg30 and Glu31 could possibly play a role in the interaction of adjacent *Cj*Fur dimers when bound to DNA. Intriguingly, while our initial studies were performed with a 200 bp fragment, EMSAs performed with DNA elements spanning this region of the promoter revealed that apo-*Cj*Fur predominantly binds to a region between -175 and -155 bp. Given the absence of similar sequences in *Cj1345c* promoter region, we conclude that the presence of a high molecular weight protein-DNA complex in apo conditions is not due to the presence of several apo-*Cj*Fur boxes but presumably originate from a single binding event that would therefore serve as a nucleation event triggering the oligomerization of apo-*Cj*Fur on *Cj1345c* promoter region. Thus, to discriminate between a single event binding leading to *Cj*Fur oligomerization and the presence of several apo-*Cj*Fur boxes on *Cj1345c* promoter region, additional experimental procedures namely DNase I footprinting assay, EMSA of apo-*Cj*Fur and 200 bp *Cj1345c* promoter region with mutated -175 to -155 bp region and analysis of apo-*Cj*Fur-DNA complex by electron microscopy combined with atomic force microscopy should be performed.

In manganese replete conditions, small increment of protein concentration enabled us to observe two shifted species in EMSA. Concentrations ranging from 0.1 to 4.0 nM yielded *Cj*Fur-DNA complex migrating at a Rf of 0.37 while increasing the protein concentration from 8 to 100 nM generated a nucleo-protein complex with a larger apparent molecular weight migrating at a Rf of 0.24; a binding profile reminiscent to previous binding studies of

*Ec*Zur with DNA (Gilston et al., 2014). In these studies, an intermediary species was observed and assigned as an *Ec*Zur-DNA complex with 1:1 stoichiometry while the higher molecular weight species was coined as being composed of two Zur dimers and one DNA molecule. These binding studies are in agreement with the binding model, proposed by Baichoo and Helmann, in which the Fur box contains recognition sites for two Fur dimers bound to opposite faces of the DNA helix, (Baichoo and Helmann, 2002). Moreover, the presence of two shifted species is consistent with the crystal structures of *Mg*Fur and *Ec*Zur in complex with DNA. Both studies revealed the presence of two dimers on the promoter region with one protomer of each dimer binding one half of the Fur-box (Deng et al., 2015; Gilston et al., 2014). In line with these findings, we conclude that the intermediary shifted species in our EMSA represents one holo-*Cj*Fur dimer in complex with the 60 bp *katA* promoter fragment while the higher molecular weight species represents two holo-Fur dimers bound to the Fur box on 60 bp *katA* promoter. However, DNA binding assays do not always result in the presence of two shifted species. A recent study tested the ability of *Pa*Fur and *Francisella tularensis* Fur to bind 25 bp DNA duplex containing 19 bp DNA Fur box and the results show one single shifted band suggesting a binding of a single Fur dimer to this DNA fragment (Pérard et al., 2016). Moreover, the ability of Fur protein to form higher molecular weight complexes depends on the DNA target. Deng *et al* tested the binding of holo-*Mg*Fur to *feoAB1* operator, a known *Mg*Fur target, and the *P. aeruginosa* Fur box and they showed that *Mg*Fur binds specifically to both DNA fragments however the binding mode is different for these DNA probes (Deng et al., 2015). While they observed only one shifted species for both DNA fragments, the *Mg*Fur- *feoAB1* operator complex had a higher mobility compared to the *Mg*Fur-*Pa*Fur box complex, suggesting that the stoichiometry of the binding is different for these two promoter regions. These results are further supported by the crystal

structures of the *Mg*Fur-*feoAB1* operator and *Mg*Fur-*Pa*Fur box complexes which showed that one Fur dimer binds to double stranded DNA in holo-*Mg*Fur - *feoAB1* operator structure while the structure of holo-*Mg*Fur- *P. aeruginosa* Fur box complex contained two Fur dimers bound to one dsDNA probe (Deng et al., 2015). Altogether, these studies suggest that the DNA binding mechanism of Fur proteins is complex and does not only depend on presence of the regulatory metal ion, it also depends on the DNA target.

7.3 An emerging consensus motif for apo-Fur regulation?

The consensus motifs for holo-*Cj*Fur-activated and holo-*Cj*Fur-repressed genes have been recently identified (Butcher et al., 2012) but the equivalent for apo-*Cj*Fur regulated genes remain unknown. In order to shed new lights on apo-*Cj*Fur-DNA interaction, we decided to map the minimal DNA region required for the binding of *Cj*Fur on *Cj1345c* promoter region. Using fragments spanning the first 200 bp upstream of *Cj1345c* gene as well as mutants of the *Cj1345c* promoter region, we determined the minimal DNA fragment required for the interaction with apo-*Cj*Fur. The apo-*Cj*Fur binding region is located between -175 and -155 bp upstream of the *Cj*1345c gene and contains a palindromic sequence (underlined) TTTAAA-TCATACT-AAAAA. This DNA element differs in several aspects from the established holo-Fur repressed motif. First, while holo-*Cj*Fur repressed element is inverted palindromic sequence (TGATAATTATTATCA), the apo-*Cj*Fur element is simply palindromic sequence with a gap (-) in the middle of the sequence. Second, the nucleotide sequence is significantly different with three consecutive adenosines forming the tip of the apo-*Cj*Fur element while the holo-*Cj*Fur box starts with TGA and ends with TCA. Moreover, the apo-*Cj*Fur motif differs significantly from the holo-*Cj*Fur activated element, which

contrary to apo-*C*jFur and holo-*Cj*Fur repressed element is not palindromic and consists of two repeats of TTTGG separated by seven nucleotides. Analogously, the element identified in our studies differs significantly from the apo-*Hp*Fur element ($TCATT_{n10}TT$) which may explain why *Cj*Fur is not able to complement the apo-regulation within the context of *H. pylori* fur mutant (Miles et al., 2010) while the iron-bound regulation is rescued by *Cj*Fur in *HpΔfur*. These results suggest that despite the high degree of sequence homology between *Hp*Fur and *Cj*Fur proteins, the apo-regulation is not conserved in these two bacterial species and is unique to each protein.

In order to fully understand the apo-*Cj*Fur-DNA interaction, characterization of apo-*Cj*Fur binding on different apo-regulated targets is greatly needed. Moreover, it is not known if *Cj*Fur recognizes a unique apo-consensus motif or if two distinct, the apo-repressed and apo-activated, consensus sequences are present. Systematic evolution of ligands by exponential enrichment (SELEX) method could be performed in order to identify DNA sequences that specifically bind to apo-*Cj*Fur, which could lead to the identification of the consensus motif(s) for apo-*Cj*Fur regulated genes. In conclusion, this confirms that the apo-Fur regulation is poorly understood and additional structural and functional characterization of apo-Fur-DNA interactions is required.

7.4 *Cj*Fur employs the same evolutionary conserved positively charged region to bind DNA in absence and presence of regulatory metal ion

Until recently, the structural basis for the DNA binding activity of all members of the Fur family of metalloregulators had remained ambiguous with most models relying on computational approaches to characterize the Fur-DNA complex (Dian et al., 2011; Pohl et

al., 2003; Tiss et al., 2005). Using an extensive library of mutants and electrophoretic mobility shift assay as well as RT-qPCR analysis, we mapped *Cj*Fur residues important for DNA binding.

In our study, we purposely mutated residues that cover different regions of the DNA binding domain. In apo conditions, we mutated residues Arg14, Lys17 and Arg20 in order to assess the role of the inside of the V-shape form of the protein in DNA binding activity. We also mutated residues located at the tip of the DBD namely Lys25, Lys28, Arg30 and Arg69 as well as Tyr68 which has been shown to play an important role in the *Ec*Fur interaction with DNA (Tiss et al., 2005). In apo conditions, substitution of either Arg20, Lys25, Lys28 or Arg69 for an acidic residue yield an inactive *Cj*Fur while mutation of other residues forming the positively charged region on *Cj*Fur impaired, to different extent, the activity of the transcriptional regulator. For example, replacement of Lys17 and Tyr68 moderately affected the activity of *Cj*Fur while the substitution of Arg30 maintained some DNA binding activity but the migration characteristics of the *Cj*Fur-DNA complex differed. Finally, expression analysis revealed that all these substitutions were equally affecting the apo-repression and activation of genes. These observations suggest that in apo conditions, a similar set of residues interacts with DNA regardless whether *Cj*Fur acts as an activator or repressor. In order to test the function of the same regions of the modeled holo-*Cj*Fur, a similar set of mutants, with the exception of Arg14 and Lys17, were tested in the holo conditions. Similar to binding reactions performed in absence of regulatory metals, substitution of Lys25, Arg30, Tyr68 and Arg69 was detrimental for holo-*Cj*Fur interaction with DNA, while the replacement of Arg20 and Lys28 moderately affected the binding activity. Complementation assays in iron rich conditions revealed that the residues forming the positively charged patch on Fur protein are important for gene expression regulation in *C.*

jejuni and that the regulation mode is conserved for the holo-repressed genes since these mutations equally affected the expression of *katA* and *cfrA* genes. Seemingly, the effect of *Cj*Fur mutations is more important *in vivo* than *in vitro*. Indeed, while some mutations namely Arg30Glu and Tyr68Ala, and Arg20Glu in apo and holo conditions, respectively, only moderately affect the DNA binding activity of *Cj*Fur *in vitro*, the impact of these mutations is comparable to other more severe mutations *in vivo.* Our results are in line with recently published structures of *Ec*Zur-DNA and *Mg*Fur-DNA complexes. Residues equivalent to those identified to be essential for *Cj*Fur-DNA interaction, namely Lys25, Arg30, Tyr68 and Arg69, interact with DNA in *Mg*Fur and *Ec*Zur. These residues participate in base readout through direct contacts in the major groove and shape readout of the narrow minor-groove. The crystal structure of *Ec*Zur in complex with DNA was the first structure to shed new lights onto the molecular underpinnings controlling the interaction between a member of the Fur family and DNA (Gilston et al., 2014). In the structure, *Ec*Zur DBD inserts itself in the DNA major and minor grooves enabling interactions between one of the helix-turn-helix (HTH) motif and the nitrogenous bases and the phosphate backbone of the DNA molecule. There are 2 hydrogen bonds between the Tyr45 and Arg65 of each monomer with N7 nitrogen of bases, resulting in a total of eight direct interactions, which correspond to a base readout mechanism of recognition. Arg65 (Arg69 in *Cj*Fur) is well conserved in Zur and Fur proteins and is crucial for the interaction with DNA as shown by previous mutational analysis (Patzer and Hantke, 2000). However, Tyr45 is only conserved in gram-negative Zur proteins (Gilston et al., 2014) and could play a role in discrimination between Zur and Fur operators. Fur proteins possess a glutamate residue at this position but there is a tyrosine residue further downstream (+3 residues) in the protein sequence and this Tyr residue is conserved in all Fur proteins (**Figure 7.2**), however its involvement in Fur-DNA

interaction has not been shown. The second mechanism of recognition observed in *Ec*Zur-DNA structure is the shape readout mechanisms and it involves highly conserved residues including Arg23 (Lys25 in *Cj*Fur), Thr25, Gln27, Arg28 (Arg30 in *Cj*Fur) and Tyr64 (Tyr68 in *Cj*Fur), which contact sugar and phosphate backbone of DNA. In addition to the crystal structure of *Ec*Zur-DNA complex, two crystal structures of *Mg*Fur in complex with DNA are available (Deng et al., 2015) which include the crystal structure of a single dimer of *Mg*Fur in complex with a 25 bp long oligonucleotide corresponding to the *feoAB1* operator and the structure of two *Mg*Fur dimers bound to one double stranded DNA corresponding to *P. aeruginosa* Fur box (PaFur box) (Deng et al., 2015). These observations suggest that Fur can bind DNA targets at different ratios. The binding of Fur protein to DNA induces moderate conformational changes in the DBDs that result in the decreased distance between the α4 helices of the two monomers allowing an optimal insertion of the α4 recognition helices in consecutive major grooves (Deng et al., 2015). Several direct interactions with bases are observed and they involved three main residues that recognize DNA through three different interaction modes. First, van der Waals interactions between the phenyl ring of Tyr56 (Tyr68 in *Cj*Fur) and methyl groups on T12' (' denotes the non-coding strand) or two consecutive thymine, T15' and T16', in the major groove of the *P. aeruginos*a Fur box and the *feoAB1* operator, respectively. Second, Arg57 (Arg69 in *Cj*Fur) forms bidentate hydrogen bonds with G7 in the *feoAB1* operator and the G10 in the *P. aeruginosa* Fur box, two nucleotides found in the major groove of DNA. Finally, the third mode of interaction involves the shape readout of a minor groove with enhanced negative electrostatic potential by a lysine residue. Lys15 (Lys25 in *Cj*Fur) forms hydrogen bonds with A24' of the *feoAB1* operator and with T6 and T21' of the *P. aeruginosa* Fur box. These DNA interacting residues are highly

conserved in other Fur proteins suggesting that the DNA-interaction modes observed in these studies are conserved in holo proteins. Altogether, these studies demonstrate that the residues forming the evolutionary conserved positively charged region on Fur proteins are important for the DNA binding in presence as well as in the absence of the regulatory metal ion.

Our mapping analysis revealed that a similar set of residues found on the surface of *Cj*Fur DBD are important for the function of the transcription factor in both apo and holo regulation. However, despite these similarities, the mode of interactions may not be necessarily the same. Structural study of *Mg*Fur-DNA complexes showed that in *Mg*Fur, the side chain of Lys15 (corresponding to Lys25 in *Cj*Fur) recognizes the target through shape readout while Tyr56 and Arg57 (corresponding to Tyr68 and Arg69 in *Cj*Fur) recognize DNA through base readout. It is conceivable that these interactions are conserved in holo-*Cj*Fur-DNA interaction. However, in the apo-conformation, the shape readout could be mediated by a different set of residues. For example, previous study revealed that arginine residues are most frequently involved in recognizing the narrow minor groove (Rohs et al., 2009). Interestingly, in the apo-*Cj*Fur structure, Arg69 is positioned on the tip of the structure and could potentially participate in shape readout. Moreover, the base readout, which in the holo structure is mediated by residues lining the α4 helix located inside the V-shaped dimer could be also done by residues found on the inner part of the apo-*Cj*Fur V-shaped dimer corresponding to the residues lining the α1 and α2 helices. Thus, solving the crystal structure of apo-Fur protein in complex with DNA would provide additional insights into DNA recognition by apo-Fur proteins and the ability of Fur proteins to discriminate different target operators.

7.5 Metal binding at *Cj*Fur's sites S2 and S3 is interdependent and both sites are important for DNA binding, gene regulation and chick colonization

In order to determine the role of *Cj*Fur metal binding sites, *Cj*Fur mutants with amino acid substitutions of metal coordinating residues at S2 site (His43Ala and His102Ala) and site S3 (His99Ala and His137Ala) were purified and characterized. First, we showed that upon mutation of residues forming the S2 or the S3 site, *Cj*Fur protein loses its ability to incorporate Mn^{2+} as well as the Zn^{2+} in the S3 site. Our results suggest that mutations of residues in one metal binding site not only affect the incorporation of the metal ion in their respective metal binding site, but also affect the incorporation of metal ion in the adjacent metal binding site. Similar phenomenon showing the interplay between the S2 and S3 metal binding sites has been reported in *Bs*Fur and *Hp*Fur (Gilbreath et al., 2013; Ma et al., 2012). For example, in *Bacillus subtilis* Fur, mutations of His96 and His97 impact the incorporation of metals in both metal binding sites. Analogously, in *Helicobacter pylori*, mutation of Ala92 and His134 impacts the metallation of the S2 and S3 sites. Based on these observations, we surmised that the DNA binding activity of *Cj*FurΔS2 and *Cj*FurΔS3 would be similarly affected for the same binding elements. Intriguingly, the binding profiles of both mutants differ quite significantly. Indeed, while the DNA binding mode of ΔS3 mutant resembles that of WT *Cj*Fur, DNA binding assay with the ΔS2 in apo conditions yields a "track ladder" pattern. This unusual binding pattern was observed only in apo conditions and the phenotype is restored, to some extent, when the binding reactions are performed in holo conditions. The mutation of S3 site results in a protein unable to bind DNA with the same affinity than wild type but is less affected than ΔS2. Interestingly, the impact of these mutations is more important in binding reactions performed in absence of metals. Since we are using excess of

$MnCl_2$ in our binding reactions (50 μM in the binding buffer and 100 μM in the gel and migration buffer), it is possible that the mutants incorporate Mn^{2+} to some extent, which results in milder effects when the binding reactions are performed in holo conditions. In agreement with our results, a recent study showed that both S2 and S3 sites are important for apo and holo-regulation in *Hp*Fur (Carpenter et al., 2010). Specifically, this study showed that mutation of His96 and Glu117, two residues forming the S3 site in *Hp*Fur as well as the mutation of Glu110 found in the S2 site, affected the expression of *Hp*Fur holo-target, *amiE*. Moreover, the expression of the apo-*Hp*Fur regulated *pfr* gene was affected when residues forming the S2 site (Glu90 and Glu110) as well as the residues forming the S3 site (His96 and His134) were mutated. These data suggest that there is an interplay between the two metal binding sites and that they are both important for Fur function.

Furthermore, mutation of S2 and S3 metal binding sites impairs *Cj*Fur ability to form higher molecular weight complexes with DNA in holo conditions, since this complex can't be detected (ΔS2) or higher concentration of protein is need to detect the appearance of the second shifted Fur/DNA species (ΔS3) (**Figure 5.1B**). Our results suggest that these mutations induce conformational changes that position residues important for the interaction of different *Cj*Fur dimers on DNA element in one or multiple orientations non-conducive for protein oligomerization. The importance of these metal binding sites for the oligomerization of Fur protein was demonstrated in *H. pylori*. As shown in *H. pylori*, the decreased ability to bind iron impacts the ability of Fur to form higher-order structures (Carpenter et al., 2010). Mutation of residues involved in the coordination of metal ions in S2 and S3 sites in *Helicobacter pylori* namely residues His96 (S3 site) and Glu110 (S2 site) resulted in the reduced ability to form higher-order structures (Carpenter et al., 2010). Similarly, both S2

and S3 sites in *Mg*Fur have been shown to play regulatory roles in modulating Fur activity (Deng et al., 2015). One possibility is that the S2 site serves as the main regulatory high affinity iron binding site but the S3 site could also bind iron but with lower affinity. One potential model is that, as a global regulator, some genes regulated by Fur are responsive to different iron concentrations and thus binding of iron to the regulatory site S2 is not sufficient to regulate the expression of all of the genes and the binding of an additional iron ion in the S3 site is necessary to repress/activate genes that are less sensitive to iron (Deng et al., 2015).

To assess the biological significance of *Cj*Fur metal binding sites, *C. jejuni* strains expressing *Cj*FurΔS2 and *Cj*FurΔS3 in *Δfur* mutant background were constructed and tested for hydrogen peroxide sensitivity using disc inhibition assay. Growth inhibition diameters of strains expressing *Cj*FurS2 and *Cj*FurS3 mutants are comparable to the diameter observed in *Δfur* mutant strains and significantly different from the wild type *C. jejuni* NCTC strain as well as the strain expressing WT Fur in *Δfur* background, suggesting that these mutants affect the regulation of *Cj*Fur target genes *in vivo* as well. Decreased sensitivity to hydrogen peroxide in *Δfur*, *Δfur* + *Cj*FurΔS2 and *Δfur* + *Cj*FurΔS3 indicates that the catalase (KatA) is no longer repressed by *Cj*Fur and is able to catalyze the dismutation of H_2O_2 in H_2O and O_2. This is in accordance with previous study, which showed that S2 and S3 sites are important for regulation of *pfr* and *amiE* expression in *Hp*Fur (Gilbreath et al., 2013). In S2 mutant strain, *amiE* transcript levels were increased when compared to WT strain and *pfr* gene was repressed to a higher degree when compared to WT. In S3 mutant strain, the *pfr* transcript levels were comparable to WT strain however, the S3 mutant had the ΔFur-like phenotype for *amiE* regulation since the transcript level of *amiE* was higher than the wild type. Similar

to *Cj*Fur and *Hp*Fur, the importance of metal binding sites for gene regulation was showed in *Mg*Fur. Strains containing mutations in metal binding sites showed reduced size of magnetosomes which were dispersed in cells and arranged in irregular chains (Deng et al., 2015). Moreover, we showed for the first time the importance of the metal binding sites for the colonization of animal model. *Cj*FurΔS2 and *Cj*FurΔS3 expressing strains had a significant reduction in their ability to colonize chick ceca relative to the wild type *C. jejuni* NCTC and the *Δfur* + *Cj*Fur strains further supporting the important role these metal binding sites play in *Cj*Fur function.

In conclusion, our results have demonstrated that the S2 and S3 binding sites are important for the binding of both regulatory metal ions and DNA by *Cj*Fur *in vitro* and *in vivo*.

CHAPTER 8. CONCLUSIONS

In conclusion, we have solved the first crystal structure of apo-Fur protein and identified a set of unique interactions stabilizing this protein conformation. I have shown that *Cj*Fur employs the same evolutionary conserved positively charged region to regulate gene expression in presence as well as in the absence of the regulatory metal ion. I have also demonstrated the interplay between the *Cj*Fur metal binding sites and their importance in maximizing DNA binding activity, the regulation of gene expression and colonization of chick colon. Finally, I have shown that the addition of a tag at the N-terminus of *Cj*Fur protein affects its ability to bind metal ions and DNA. Altogether, the research presented here increased our understanding on the mechanistic basis underlying the Fur regulation of gene expression in *C. jejuni* and further research into *Cj*Fur function could lead to a development of therapeutic molecules for the treatment of *Campylobacter jejuni* enteric infections.

REFERENCES

Abergel, R.J., Zawadzka, A.M., Hoette, T.M., and Raymond, K.N. (2009). Enzymatic hydrolysis of trilactone siderophores: where chiral recognition occurs in enterobactin and bacillibactin iron transport. J. Am. Chem. Soc. *131*, 12682–12692.

Agarwal, S., King, C.A., Klein, E.K., Soper, D.E., Rice, P.A., Wetzler, L.M., and Genco, C.A. (2005). The gonococcal Fur-regulated tbpA and tbpB genes are expressed during natural mucosal gonococcal infection. Infect. Immun. *73*, 4281–4287.

Ahn, B.E., Cha, J., Lee, E.J., Han, A.R., Thompson, C.J., and Roe, J.H. (2006). Nur, a nickel-responsive regulator of the Fur family, regulates superoxide dismutases and nickel transport in Streptomyces coelicolor. Mol. Microbiol. *59*, 1848–1858.

Alamuri, P., Mehta, N., Burk, A., and Maier, R.J. (2006). Regulation of the Helicobacter pylori Fe-S cluster synthesis protein NifS by iron, oxidative stress conditions, and Fur. J. Bacteriol. *188*, 5325–5330.

Allard, K.A., Viswanathan, V.K., Cianciotto, N.P., and Al, A.E.T. (2006). lbtA and lbtB Are Required for Production of the Legionella pneumophila Siderophore Legiobactin. *188*, 1351–1363.

An, Y.J., Ahn, B.E., Han, A.R., Kim, H.M., Chung, K.M., Shin, J.H., Cho, Y.B., Roe, J.H., and Cha, S.S. (2009). Structural basis for the specialization of Nur, a nickel-specific Fur homolog, in metal sensing and DNA recognition. Nucleic Acids Res. *37*, 3442–3451.

Andrews, S.C., Robinson, A.K., and RodrÃ-guez-QuiÃ±ones, F. (2003). Bacterial iron homeostasis. FEMS Microbiol. Rev. *27*, 215–237.

Arnold, K., Bordoli, L., Kopp, J., and Schwede, T. (2006). The SWISS-MODEL workspace: A web-based environment for protein structure homology modelling. Bioinformatics *22*, 195–201.

Askoura, M., Sarvan, S., Couture, J.F., and Stintzi, A. (2016). The Campylobacter jejuni ferric uptake regulator promotes acid survival and cross-protection against oxidative stress. Infect. Immun. *84*, 1287–1300.

Bagg, A., and Neilands, J.B. (1985). Mapping of a mutation affecting regulation of iron uptake systems in Escherichia coli K-12. J. Bacteriol. *161*, 450–453.

Bagg, A., and Neilands, J.B. (1987). Ferric uptake regulation protein acts as a repressor, employing iron(II) as a cofactor to bind the operator of an iron transport operon in Escherichia coli. Biochemistry *26*, 5471–5477.

Baichoo, N., and Helmann, J.D. (2002). Recognition of DNA by Fur : a Reinterpretation of the Fur Box Consensus Sequence. Society *184*.

Ball, J.C., Straccia, a M., Young, W.C., and Aust, a E. (2000). The formation of reactive oxygen species catalyzed by neutral, aqueous extracts of NIST ambient particulate matter and diesel engine particles. J. Air Waste Manag. Assoc. *50*, 1897–1903.

Bender, K.S., Yen, H.C.B., Hemme, C.L., Yang, Z., He, Z., He, Q., Zhou, J., Huang, K.H., Alm, E.J., Hazen, T.C., et al. (2007). Analysis of a ferric uptake regulator (Fur) mutant of Desulfovibrio vulgaris Hildenborough. Appl. Environ. Microbiol. *73*, 5389–5400.

Bereswill, S., Lichte, F., Vey, T., Fassbinder, F., and Kist, M. (1998). Cloning and characterization of the fur gene from Helicobacter pylori. FEMS Microbiol. Lett.

159, 193–200.
Berish, S.A., Subbarao, S., Chen, C.Y., Trees, D.L., and Morse, S.A. (1993). Identification and cloning of a fur homolog from Neisseria gonorrhoeae. Infect. Immun. *61*, 4599–4606.
Bes, M.T., Hernández, J.A., Peleato, M.L., and Fillat, M.F. (2001). Cloning, overexpression and interaction of recombinant Fur from the cyanobacterium Anabaena PCC 7119 with isiB and its own promoter. FEMS Microbiol. Lett. *194*, 187–192.
Biegel Carson, S.D., Thomas, C.E., and Elkins, C. (1996). Cloning and sequencing of a Haemophilus ducreyi fur homolog. Gene *176*, 125–129.
Bijlsma, J.J.E., Waidner, B., Van Vliet, A.H.M., Hughes, N.J., Häg, S., Bereswill, S., Kelly, D.J., Vandenbroucke-Grauls, C.M.J.E., Kist, M., and Kusters, J.G. (2002). The Helicobacter pylori homologue of the ferric uptake regulator is involved in acid resistance. Infect. Immun. *70*, 606–611.
Bindereif, A., and Neilands, J.B. (1985). Promoter mapping and transcriptional regulation of the iron assimilation system of plasmid ColV-K30 in Escherichia coli K-12. J. Bacteriol. *162*, 1039–1046.
Black, R.E., Levine, M.M., Clements, M. Lou, Hughes, T.P., Blaser, M.J., and Black, R.E. (1988). Experimental campylobacter jejuni infection in humans. J. Infect. Dis. *157*, 472–479.
Bolton, D.J. (2015). Campylobacter virulence and survival factors. Food Microbiol. *48*, 99–108.
Bozym, R.A., Chimienti, F., Giblin, L.J., Gross, G.W., Korichneva, I., Li, Y., Libert, S., Maret, W., Parviz, M., Frederickson, C.J., et al. (2010). Free zinc ions outside a narrow concentration range are toxic to a variety of cells in vitro. Exp. Biol. Med. (Maywood). *235*, 741–750.
Braun, V. (2001). Iron uptake mechanisms and their regulation in pathogenic bacteria. Int. J. Med. Microbiol. *291*, 67–79.
Brickman, T.J., and Armstrong, S.K. (1995). Bordetella pertussis fur gene restores iron repressibility of siderophore and protein expression to deregulated Bordetella Bronchiseptica mutants. J. Bacteriol. *177*, 268–270.
Bricogne, G., Blanc, E., Brandl, M., Flensburg, C., Keller, P., Paciorek, W., Roversi, P., Sharff, A., Smart, O.S., Vonrhein, C., et al. (2011). BUSTER version 2.10.1.
Bsat, N., and Helmann, J.D. (1999). Interaction of Bacillus subtilis Fur (Ferric Uptake Repressor) with the dhb Operator In Vitro and In Vivo. J. Bacteriol. *181*, 4299–4307.
Bsat, N., Herbig, A., Casillas-Martinez, L., Setlow, P., and Helmann, J.D. (1998). Bacillus subtilis contains multiple Fur homologues: Identification of the iron uptake (Fur) and peroxide regulon (PerR) repressors. Mol. Microbiol. *29*, 189–198.
Bury-Moné, S., Thiberge, J.-M., Contreras, M., Maitournam, A., Labigne, A., and De Reuse, H. (2004). Responsiveness to acidity via metal ion regulators mediates virulence in the gastric pathogen Helicobacter pylori. Mol. Microbiol. *53*, 623–638.
Butcher, J., Flint, A., Stahl, M., and Stintzi, A. (2010). Campylobacter Fur and PerR Regulons. Iron Uptake Homeost. Microorg. 167–202.
Butcher, J., Sarvan, S., Brunzelle, J.S., Couture, J.-F., and Stintzi, A. (2012). Structure and regulon of Campylobacter jejuni ferric uptake regulator Fur define apo-Fur regulation. Proc. Natl. Acad. Sci. U. S. A. *109*, 1–6.
Carpenter, B.M., Whitmire, J.M., and Merrell, D.S. (2009a). This is not your mother's

repressor: the complex role of fur in pathogenesis. Infect. Immun. *77*, 2590–2601.
Carpenter, B.M., Gancz, H., Gonzalez-Nieves, R.P., West, A.L., Whitmire, J.M., Michel, S.L.J., and Merrell, D.S. (2009b). A single nucleotide change affects fur-dependent regulation of sodB in H. pylori. PLoS One *4*, e5369.
Carpenter, B.M., Gancz, H., Benoit, S.L., Evans, S., Olsen, C.H., Michel, S.L.J., Maier, R.J., and Merrell, D.S. (2010). Mutagenesis of conserved amino acids of Helicobacter pylori fur reveals residues important for function. J. Bacteriol. *192*, 5037–5052.
Carpenter, B.M., Gilbreath, J.J., Pich, O.Q., McKelvey, A.M., Maynard, E.L., Li, Z.Z., and Scott Merrell, D. (2013). Identification and characterization of novel helicobacter pylori apo-Fur-Regulated target genes. J. Bacteriol. *195*, 5526–5539.
Carson, S.D., Thomas, C.E., and Elkins, C. (1996). Cloning and sequencing of a Haemophilus ducreyi fur homolog. Gene *176*, 125–129.
Cha, J.Y., Lee, J.S., Oh, J. Il, Choi, J.W., and Baik, H.S. (2008). Functional analysis of the role of Fur in the virulence of Pseudomonas syringae pv. tabaci 11528: Fur controls expression of genes involved in quorum-sensing. Biochem. Biophys. Res. Commun. *366*, 281–287.
Chen, V.B., Arendall, W.B., Headd, J.J., Keedy, D. a., Immormino, R.M., Kapral, G.J., Murray, L.W., Richardson, J.S., and Richardson, D.C. (2010). MolProbity: All-atom structure validation for macromolecular crystallography. Acta Crystallogr. Sect. D Biol. Crystallogr. *66*, 12–21.
Coker, A.O., Isokpehi, R.D., Thomas, B.N., Amisu, K.O., and Obi, C.L. (2002). Human campylobacteriosis in developing countries. Emerg. Infect. Dis. *8*, 237–244.
Craig, S.A., Carpenter, C.D., Mey, A.R., Wyckoff, E.E., and Payne, S.M. (2011). Positive regulation of the Vibrio cholerae porin OmpT by Iron and Fur. J. Bacteriol. *193*, 6505–6511.
Daniel, C., Haentjens, S., Bissinger, M.C., and Courcol, R.J. (1999). Characterization of the Acinetobacter baumannii Fur regulator: Cloning and sequencing of the fur homolog gene. FEMS Microbiol. Lett. *170*, 199–209.
Danielli, A., Roncarati, D., Delany, I., Chiarini, V., Rappuoli, R., and Scarlato, V. (2006). In vivo dissection of the Helicobacter pylori fur regulatory circuit by genome-wide location analysis. J. Bacteriol. *188*, 4654–4662.
Dash, S., R Pai, A., Kamath, U., and Rao, P. (2014). Pathophysiology and diagnosis of Guillain-Barré syndrome -challenges and needs. Int. J. Neurosci. *2014 May 2*, [Epub ahead of print].
Dasti, J.I., Tareen, A.M., Lugert, R., Zautner, A.E., and Groß, U. (2010). Campylobacter jejuni: A brief overview on pathogenicity-associated factors and disease-mediating mechanisms. Int. J. Med. Microbiol. *300*, 205–211.
Davis, I.W., Leaver-Fay, A., Chen, V.B., Block, J.N., Kapral, G.J., Wang, X., Murray, L.W., Arendall, W.B., Snoeyink, J., Richardson, J.S., et al. (2007). MolProbity: All-atom contacts and structure validation for proteins and nucleic acids. Nucleic Acids Res. *35*.
Delany, I., Spohn, G., Rappuoli, R., and Scarlato, V. (2001). The Fur repressor controls transcription of iron-activated and -repressed genes in Helicobacter pylori. Mol. Microbiol. *42*, 1297–1309.
Delany, I., Grifantini, R., Bartolini, E., Rappuoli, R., and Scarlato, V. (2006). Effect of Neisseria meningitidis Fur Mutations on Global Control of Gene Transcription Effect of Neisseria meningitidis Fur Mutations on Global Control of Gene

Transcription †. *188*, 2483–2492.
Deng, X., Sun, F., Ji, Q., Liang, H., Missiakas, D., Lan, L., and He, C. (2012). Expression of multidrug resistance efflux pump gene norA Is iron responsive in Staphylococcus aureus. J. Bacteriol. *194*, 1753–1762.
Deng, Z., Wang, Q., Liu, Z., Zhang, M., Machado, A.C.D., Chiu, T.-P., Feng, C., Zhang, Q., Yu, L., Qi, L., et al. (2015). Mechanistic insights into metal ion activation and operator recognition by the ferric uptake regulator. Nat. Commun. *6*, 7642.
Dian, C., Vitale, S., Leonard, G.A., Bahlawane, C., Fauquant, C., Leduc, D., Muller, C., de Reuse, H., Michaud-Soret, I., and Terradot, L. (2011). The structure of the Helicobacter pylori ferric uptake regulator Fur reveals three functional metal binding sites. Mol. Microbiol. *79*, 1260–1275.
Díaz-Mireles, E., Wexler, M., Sawers, G., Bellini, D., Todd, J.D., and Johnston, A.W.B. (2004). The Fur-like protein Mur of Rhizobium leguminosarum is a Mn2+ - responsive transcriptional regulator. Microbiology *150*, 1447–1456.
Dowd, G.C., Casey, P.G., Begley, M., Hill, C., and Gahan, C.G.M. (2012). Investigation of the role of ZurR in the physiology and pathogenesis of Listeria monocytogenes. FEMS Microbiol. Lett. *327*, 118–125.
Dubbs, J.M., and Mongkolsuk, S. (2012). Peroxide-sensing transcriptional regulators in bacteria. J. Bacteriol. *194*, 5495–5503.
Ducey, T.F., Jackson, L., Orvis, J., and Dyer, D.W. (2009). Transcript analysis of nrrF, a Fur repressed sRNA of Neisseria gonorrhoeae. Microb. Pathog. *46*, 166–170.
Emsley, P., and Cowtan, K. (2004). Coot: Model-building tools for molecular graphics. Acta Crystallogr. Sect. D Biol. Crystallogr. *60*, 2126–2132.
Engberg, J., Aarestrup, F.M., Taylor, D.E., Gerner-Smidt, P., and Nachamkin, I. (2001). Quinolone and macrolide resistance in Campylobacter jejuni and C-coli: Resistance mechanisms and trends in human isolates. Emerg. Infect. Dis. *7*, 24–34.
Ernst, F.D., Homuth, G., Stoof, J., Mäder, U., Waidner, B., Kuipers, E.J., Kist, M., Kusters, J.G., Bereswill, S., and van Vliet, A.H.M. (2005). Iron-responsive regulation of the Helicobacter pylori iron-cofactored superoxide dismutase SodB is mediated by Fur. J. Bacteriol. *187*, 3687–3692.
Ernst, J.F., Bennett, R.L., and Rothfield, L.I. (1978). Constitutive expression of the iron-enterochelin and ferrichrome uptake systems in a mutant strain of Salmonella typhimurium. J. Bacteriol. *135*, 928–934.
Escolar, L., Pérez-Martín, J., and de Lorenzo, V. (1998). Binding of the fur (ferric uptake regulator) repressor of Escherichia coli to arrays of the GATAAT sequence. J. Mol. Biol. *283*, 537–547.
Evans, P.R., and Murshudov, G.N. (2013). How good are my data and what is the resolution? Acta Crystallogr. Sect. D Biol. Crystallogr. *69*, 1204–1214.
Fillat, M.F. (2014). The fur (ferric uptake regulator) superfamily: Diversity and versatility of key transcriptional regulators. Arch. Biochem. Biophys. *546*, 41–52.
Fiorini, F., Stefanini, S., Valenti, P., Chiancone, E., and De Biase, D. (2008). Transcription of the Listeria monocytogenes fri gene is growth-phase dependent and is repressed directly by Fur, the ferric uptake regulator. Gene *410*, 113–121.
Foster, J.W. (1991). Salmonella acid shock proteins are required for the adaptive acid tolerance response. J. Bacteriol. *173*, 6896–6902.
Foster, J.W., and Hall, H.K. (1992). Effect of Salmonella-Typhimurium Ferric Uptake Regulator (Fur) Mutations on Iron-Regulated and Ph-Regulated Protein-Synthesis. J.

Bacteriol. *174*, 4317–4323.
Gaballa, A., and Helmann, J.D. (1998). Identification of a zinc-specific metalloregulatory protein, Zur, controlling zinc transport operons in Bacillus subtilis. J. Bacteriol. *180*, 5815–5821.
Gaballa, A., Antelmann, H., Aguilar, C., Khakh, S.K., Song, K.-B., Smaldone, G.T., and Helmann, J.D. (2008). The *Bacillus subtilis* iron-sparing response is mediated by a Fur-regulated small RNA and three small, basic proteins. Proc. Natl. Acad. Sci. U. S. A. *105*, 11927–11932.
Gancz, H., Censini, S., and Merrell, D.S. (2006). Iron and pH homeostasis intersect at the level of fur regulation in the gastric pathogen Helicobacter pylori. Infect. Immun. *74*, 602–614.
Gao, H., Zhou, D., Li, Y., Guo, Z., Han, Y., Song, Y., Zhai, J., Du, Z., Wang, X., Lu, J., et al. (2008). The iron-responsive fur regulon in Yersinia pestis. J. Bacteriol. *190*, 3063–3075.
Ghassemian, M., and Straus, N.A. (1996). Fur regulates the expression of iron-stress genes in the cyanobacterium Synechococcus sp. strain PCC 7942. Microbiology *142 (Pt 6*, 1469–1476.
Gibney, K.B., O'Toole, J., Sinclair, M., and Leder, K. (2014). Disease burden of selected gastrointestinal pathogens in Australia, 2010. Int. J. Infect. Dis. *28*, 176–185.
Gibreel, A., and Taylor, D.E. (2006). Macrolide resistance in Campylobacter jejuni and Campylobacter coli. J. Antimicrob. Chemother. *58*, 243–255.
Giedroc, D.P., and Arunkumar, A.I. (2007). Metal sensor proteins: nature's metalloregulated allosteric switches. Dalton Trans. 3107–3120.
Gilbreath, J.J., Pich, O.Q., Benoit, S.L., Besold, A.N., Cha, J.H., Maier, R.J., Michel, S.L.J., Maynard, E.L., and Merrell, D.S. (2013). Random and site-specific mutagenesis of the Helicobacter pylori ferric uptake regulator provides insight into Fur structure-function relationships. Mol. Microbiol. *89*, 304–323.
Gilston, B. a, Wang, S., Marcus, M.D., Canalizo-Hernández, M. a, Swindell, E.P., Xue, Y., Mondragón, A., and O'Halloran, T. V (2014). Structural and Mechanistic Basis of Zinc Regulation Across the E. coli Zur Regulon. PLoS Biol. *12*, e1001987.
Godschalk, P.C.R., Heikema, A.P., Gilbert, M., Komagamine, T., Ang, C.W., Glerum, J., Brochu, D., Li, J., Yuki, N., Jacobs, B.C., et al. (2004). The crucial role of Campylobacter jejuni genes in anti-ganglioside antibody induction in Guillain-Barré syndrome. J. Clin. Invest. *114*, 1659–1665.
Gölz, G., Rosner, B., Hofreuter, D., Josenhans, C., Kreienbrock, L., Löwenstein, A., Schielke, A., Stark, K., Suerbaum, S., Wieler, L.H., et al. (2014). Relevance of Campylobacter to public health-The need for a One Health approach. Int. J. Med. Microbiol. *304*, 817–823.
González, A., Bes, M.T., Valladares, A., Peleato, M.L., and Fillat, M.F. (2012). FurA is the master regulator of iron homeostasis and modulates the expression of tetrapyrrole biosynthesis genes in Anabaena sp. PCC 7120. Environ. Microbiol. *14*, 3175–3187.
Grifantini, R., Sebastian, S., Frigimelica, E., Draghi, M., Bartolini, E., Muzzi, A., Rappuoli, R., Grandi, G., and Genco, C.A. (2003). Identification of iron-activated and -repressed Fur-dependent genes by transcriptome analysis of Neisseria meningitidis group B. Proc. Natl. Acad. Sci. U. S. A. *100*, 9542–9547.
Guex, N., and Peitsch, M.C. (1997). SWISS-MODEL and the Swiss-PdbViewer: An environment for comparative protein modeling. Electrophoresis *18*, 2714–2723.

Hall, H.K., and Foster, J.W. (1996). The role of Fur in the acid tolerance response of Salmonella typhimurium is physiologically and genetically separable from its role in iron acquisition. J. Bacteriol. *178*, 5683–5691.

Hamza, I., Chauhan, S., Hassett, R., and O'Brian, M.R. (1998). The bacterial irr protein is required for coordination of heme biosynthesis with iron availability. J. Biol. Chem. *273*, 21669–21674.

Hantke, K. (1981). Regulation of ferric iron transport in Escherichia coli K12: isolation of a constitutive mutant. Mol. Gen. Genet. *182*, 288–292.

Hantke, K. (1982). Negative control of iron uptake systems in Escherichia coli. FEMS Microbiol. Lett. *15*, 83–86.

Hantke, K. (1984). Cloning of the repressor protein gene of iron-regulated systems in Escherichia coli K12. Mol. Gen. Genet. *197*, 337–341.

Hassett, D.J., Sokol, P.A., Howell, M.L., Ma, J.U.F., Schweizer, H.T., Ochsner, U., and Vasil, M.L. (1996). Ferric uptake regulator (Fur) mutants of Pseudomonas aeruginosa demonstrate defective siderophore-mediated iron uptake, altered aerobic growth, and decreased superoxide dismutase and catalase activities. J. Bacteriol. *178*, 3996–4003.

Heidrich, C., Hantke, K., Bierbaum, G., and Sahl, H.G. (1996). Identification and analysis of a gene encoding a Fur-like protein of Staphylococcus epidermidis. FEMS Microbiol. Lett. *140*, 253–259.

Hickey, E.K., and Cianciotto, N.P. (1994). Cloning and sequencing of the Legionella pneumophila fur gene. Gene *143*, 117–121.

Holmes, K., Mulholland, F., Pearson, B.M., Pin, C., McNicholl-Kennedy, J., Ketley, J.M., and Wells, J.M. (2005). Campylobacter jejuni gene expression in response to iron limitation and the role of Fur. Microbiology *151*, 243–257.

Horsburgh, M.J., Ingham, E., and Foster, S.J. (2001). In Staphylococcus aureus, Fur is an interactive regulator with PerR, contributes to virulence, and is necessary for oxidative stress resistance through positive regulation of catalase and iron homeostasis. J. Bacteriol. *183*, 468–475.

Imlay, J.A. (2003). Pathways of oxidative damage. Annu. Rev. Microbiol. *57*, 395–418.

Imlay, J.A., Chin, S.M., and Linn, S. (1988). Toxic DNA damage by hydrogen peroxide through the Fenton reaction in vivo and in vitro. Science (80-.). *240*, 640–642.

Isabella, V., Wright, L.F., Barth, K., Spence, J.M., Grogan, S., Genco, C.A., and Clark, V.L. (2008). cis- and trans-acting elements involved in regulation of norB (norZ), the gene encoding nitric oxide reductase in Neisseria gonorrhoeae. Microbiology *154*, 226–239.

Jackson, L.A., Ducey, T.F., Day, M.W., Zaitshik, J.B., Orvis, J., and Dyer, D.W. (2010). Transcriptional and functional analysis of the Neisseria gonorrhoeae fur regulon. J. Bacteriol. *192*, 77–85.

Jacoby, G.A. (2005). Mechanisms of resistance to quinolones. Clin. Infect. Dis. *41 Suppl 2*, S120-6.

Jacquamet, L., Traoré, D. a K., Ferrer, J.-L., Proux, O., Testemale, D., Hazemann, J.-L., Nazarenko, E., El Ghazouani, a, Caux-Thang, C., Duarte, V., et al. (2009). Structural characterization of the active form of PerR: insights into the metal-induced activation of PerR and Fur proteins for DNA binding. Mol. Microbiol. *73*, 20–31.

Jung, Y.-S., and Kwon, Y.-M. (2008). Small RNA ArrF Regulates the Expression of sodB

and feSII Genes in Azotobacter vinelandii. Curr. Microbiol. *57*, 593–597.
Kaakoush, N.O., Mitchell, H.M., and Man, S.M. (2015). Campylobacter (Elsevier Ltd).
Kabsch, W. (2010a). Integration, scaling, space-group assignment and post-refinement. Acta Crystallogr. Sect. D Biol. Crystallogr. *66*, 133–144.
Kabsch, W. (2010b). Xds. Acta Crystallogr. Sect. D Biol. Crystallogr. *66*, 125–132.
Kaneko, T., Sato, S., Kotani, H., Tanaka, A., Asamizu, E., Nakamura, Y., Miyajima, N., Hirosawa, M., Sugiura, M., Sasamoto, S., et al. (1996). Sequence analysis of the genome of the unicellular cyanobacterium Synechocystis sp. strain PCC6803. II. Sequence determination of the entire genome and assignment of potential protein-coding regions (supplement). DNA Res. *3*, 185–209.
Kim, I.H., Wen, Y., Son, J., Lee, K., and Kim, K. (2013). The Fur-Iron Complex Modulates Expression of the Quorum-Sensing Master Regulator , SmcR , To Control Expression of Virulence Factors in Vibrio vulnificus. *81*, 2888–2898.
Langer, G., Cohen, S.X., Lamzin, V.S., and Perrakis, A. (2008). Automated macromolecular model building for X-ray crystallography using ARP/wARP version 7. Nat. Protoc. *3*, 1171–1179.
Lavrrar, J.L., Christoffersen, C.A., and McIntosh, M.A. (2002). Fur–DNA Interactions at the Bidirectional fepDGC-entS Promoter Region in Escherichia coli. J. Mol. Biol. *322*, 983–995.
Lee, J.-W., and Helmann, J.D. (2007). Functional specialization within the Fur family of metalloregulators. Biometals *20*, 485–499.
Lee, M.D., and Newell, D.G. (2006). Campylobacter in poultry: filling an ecological niche. Avian Dis. *50*, 1–9.
Lee, H.-J., Bang, S.H., Lee, K.-H., and Park, S.-J. (2007). Positive Regulation of fur Gene Expression via Direct Interaction of Fur in a Pathogenic Bacterium, Vibrio vulnificus. J. Bacteriol. *189*, 2629–2636.
Lin, C.S.H., Chao, S.Y., Hammel, M., Nix, J.C., Tseng, H.L., Tsou, C.C., Fei, C.H., Chiou, H.S., Jeng, U.S., Lin, Y.S., et al. (2014). Distinct structural features of the peroxide response regulator from group A streptococcus drive DNA binding. PLoS One *9*.
Litwin, C.M., Boyko, S.A., and Calderwood, S.B. (1992). Cloning, sequencing, and transcriptional regulation of the Vibrio cholerae fur gene. J. Bacteriol. *174*, 1897–1903.
Lucarelli, D., Russo, S., Garman, E., Milano, A., Meyer-Klaucke, W., and Pohl, E. (2007). Crystal structure and function of the zinc uptake regulator FurB from Mycobacterium tuberculosis. J. Biol. Chem. *282*, 9914–9922.
Ma, Z., Faulkner, M.J., and Helmann, J.D. (2012). Origins of specificity and cross-talk in metal ion sensing by Bacillus subtilis Fur. Mol. Microbiol. *86*, 1144–1155.
Makthal, N., Rastegari, S., Sanson, M., Ma, Z., Olsen, R.J., Helmann, J.D., Musser, J.M., and Kumaraswami, M. (2013). Crystal structure of peroxide stress regulator from streptococcus pyogenes provides functional insights into the mechanism of oxidative stress sensing. J. Biol. Chem. *288*, 18311–18324.
Massé, E., and Gottesman, S. (2002). A small RNA regulates the expression of genes involved in iron metabolism in Escherichia coli. Proc. Natl. Acad. Sci. U. S. A. *99*, 4620–4625.
McCoy, A.J., Grosse-Kunstleve, R.W., Adams, P.D., Winn, M.D., Storoni, L.C., and Read, R.J. (2007). Phaser crystallographic software. J. Appl. Crystallogr. *40*, 658–674.
Mellin, J.R., Goswami, S., Grogan, S., Tjaden, B., and Genco, C.A. (2007). A novel fur- and

iron-regulated small RNA, NrrF, is required for indirect fur-mediated regulation of the sdhA and sdhC genes in Neisseria meningitidis. J. Bacteriol. *189*, 3686–3694.

Metruccio, M.M.E., Fantappiè, L., Serruto, D., Muzzi, A., Roncarati, D., Donati, C., Scarlato, V., and Delany, I. (2009). The Hfq-dependent small noncoding RNA NrrF directly mediates fur-dependent positive regulation of succinate dehydrogenase in Neisseria meningitidis. J. Bacteriol. *191*, 1330–1342.

Mey, A.R., Wyckoff, E.E., Kanukurthy, V., Fisher, C.R., and Payne, S.M. (2005). Iron and Fur Regulation in Vibrio cholerae and the Role of Fur in Virulence. *73*, 8167–8178.

Miles, S., Carpenter, B.M., Gancz, H., and Merrell, D.S. (2010). Helicobacter pylori apo-Fur regulation appears unconserved across species. J. Microbiol. *48*, 378–386.

Miller, C.E., Rock, J.D., Ridley, K.A., Williams, P.H., and Ketley, J.M. (2008). Utilization of lactoferrin-bound and transferrin-bound iron by Campylobacter jejuni. J. Bacteriol. *190*, 1900–1911.

Miller, C.E., Williams, P.H., and Ketley, J.M. (2009). Pumping iron: mechanisms for iron uptake by Campylobacter. Microbiology *155*, 3157–3165.

Mills, S.A., and Marletta, M.A. (2005). Metal binding characteristics and role of iron oxidation in the ferric uptake regulator from Escherichia coli. Biochemistry *44*, 13553–13559.

Mishu, B., Ilyas, a a, Koski, C.L., Vriesendorp, F., Cook, S.D., Mithen, F. a, and Blaser, M.J. (1993). Serologic evidence of previous Campylobacter jejuni infection in patients with the Guillain-Barré syndrome. Ann. Intern. Med. *118*, 947–953.

Nachamkin, I., Allos, B.M., and Ho, T. (1998). Campylobacter species and Guillain-Barré syndrome. Clin. Microbiol. Rev. *11*, 555–567.

Nandal, A., Huggins, C.C.O., Woodhall, M.R., McHugh, J., Rodríguez-Quiñones, F., Quail, M.A., Guest, J.R., and Andrews, S.C. (2010). Induction of the ferritin gene (ftnA) of Escherichia coli by Fe 2+-Fur is mediated by reversal of H-NS silencing and is RyhB independent. Mol. Microbiol. *75*, 637–657.

Ochsner, U.R.S.A., Vasil, A.I., and Vasil, M.L. (1995). Role of the Ferric Uptake Regulator of Pseudomonas aeruginosa in the Regulation of Siderophores and Exotoxin A Expression : Purification and Activity on Iron-Regulated Promoters. *177*, 7194–7201.

Otwinowski, Z., and Minor, W. (1997). Processing of X-ray diffraction data collected in oscillation mode. Methods Enzymol. *276*, 307–326.

Palyada, K., Threadgill, D., and Stintzi, A. (2004). Iron Acquisition and Regulation in Campylobacter jejuni. Society *186*.

Parrow, N.L., Fleming, R.E., and Minnick, M.F. (2013). Sequestration and scavenging of iron in infection. Infect. Immun. *81*, 3503–3514.

Patzer, S.I., and Hantke, K. (1998). The ZnuABC high-affinity zinc uptake system and its regulator Zur in Escherichia coli. Mol. Microbiol. *28*, 1199–1210.

Patzer, S.I., and Hantke, K. (2000). The zinc-responsive regulator Zur and its control of the znu gene cluster encoding the ZnuABC zinc uptake system in Escherichia coli. J. Biol. Chem. *275*, 24321–24332.

Pecqueur, L., D'Autréaux, B., Dupuy, J., Nicolet, Y., Jacquamet, L., Brutscher, B., Michaud-Soret, I., and Bersch, B. (2006). Structural changes of Escherichia coli ferric uptake regulator during metal-dependent dimerization and activation explored by NMR and X-ray crystallography. J. Biol. Chem. *281*, 21286–21295.

Pérard, J., Cove, S, J., Castellan, M., Solard, C., Savard, M., Miras, R., Galop, S., Signor, L.,

Crouzy, S., et al. (2016). Quaternary Structure of fur Proteins, a New Subfamily of Tetrameric Proteins. Biochemistry *55*, 1503–1515.

Percival, S.L., and Williams, D.W. (2014). Chapter Four - Campylobacter. In Microbiology of Waterborne Diseases, pp. 65–78.

Platero, R., De Lorenzo, V., Garat, B., and Fabiano, E. (2007). Sinorhizobium meliloti fur-like (Mur) protein binds a fur box-like sequence present in the mntA promoter in a manganese-responsive manner. Appl. Environ. Microbiol. *73*, 4832–4838.

Platts-Mills, J. a., and Kosek, M. (2014). Update on the burden of Campylobacter in developing countries. Curr. Opin. Infect. Dis. *27*, 444–450.

Pohl, E., Haller, J.C., Mijovilovich, A., Meyer-Klaucke, W., Garman, E., and Vasil, M.L. (2003). Architecture of a protein central to iron homeostasis: Crystal structure and spectroscopic analysis of the ferric uptake regulator. Mol. Microbiol. *47*, 903–915.

Pope, J.E., Krizova, A., Garg, A.X., Thiessen-Philbrook, H., and Ouimet, J.M. (2007). Campylobacter Reactive Arthritis: A Systematic Review. Semin. Arthritis Rheum. *37*, 48–55.

Prince, R.W., Cox, C.D., and Vasil, M.L. (1993). Coordinate regulation of siderophore and exotoxin A production: Molecular cloning and sequencing of the Pseudomonas aeruginosa fur gene. J. Bacteriol. *175*, 2589–2598.

Pym, A.S., Domenech, P., Honoré, N., Song, J., Deretic, V., and Cole, S.T. (2001). Regulation of catalase-peroxidase (KatG) expression, isoniazid sensitivity and virulence by furA of Mycobacterium tuberculosis. Mol. Microbiol. *40*, 879–889.

Qin, H.-Y., Wu, J.C.Y., Tong, X.-D., Sung, J.J.Y., Xu, H.-X., and Bian, Z.-X. (2011). Systematic review of animal models of post-infectious/post-inflammatory irritable bowel syndrome. J. Gastroenterol. *46*, 164–174.

Rea, R.B., Gahan, C.G.M., and Hill, C. (2004). Disruption of Putative Regulatory Loci in Listeria monocytogenes Demonstrates a Significant Role for Fur and PerR in Virulence. Society *72*, 717–727.

Rees, J.H., Soudain, S.E., Gregson, N.A., and Hughes, R.A.. (1995). Campylobacter jejuni infection and Guillain-Barre Syndrome. N. Engl. J. Med. *333*, 1374–1379.

Reid, A.N., Pandey, R., Palyada, K., Naikare, H., and Stintzi, A. (2008). Identification of Campylobacter jejuni genes involved in the response to acidic pH and stomach transit. Appl. Environ. Microbiol. *74*, 1583–1597.

Ridley, K. a, Rock, J.D., Li, Y., and Ketley, J.M. (2006). Heme utilization in Campylobacter jejuni. J. Bacteriol. *188*, 7862–7875.

Rimsky, S. (2004). Structure of the histone-like protein H-NS and its role in regulation and genome superstructure. Curr. Opin. Microbiol. *7*, 109–114.

Robinson, D.A. (1981). Infective dose of Campylobacter jejuni in milk. Br. Med. J. *282*, 1584.

Rohs, R., West, S.M., Sosinsky, A., Liu, P., Mann, R.S., and Honig, B. (2009). The role of DNA shape in protein – DNA recognition. Nature *461*, 1248–1253.

Sahin, O., Morishita, T.Y., and Zhang, Q. (2002). Campylobacter colonization in poultry: sources of infection and modes of transmission. Anim. Heal. Res. Rev. *3*, 95–105.

Sahin, O., Kassem, I.I., Shen, Z., Lin, J., Rajashekara, G., Zhang, Q., Kassem, a I.I., Shen, B.Z., Lin, a J., Rajashekara, C.G., et al. (2015). Campylobacter in Poultry: Ecology and Potential Interventions. Avian Dis. *59*, 185–200.

Salloway, S., Mermel, L., Seamans, M., Aspinall, G., Nam Shin, J., Kurjanczyk, L., and Penner, J. (1996). Miller-Fisher syndrome associated with Campylobacter jejuni

bearing lipopolysaccharide molecules that mimic human ganglioside GD3. Infect. Immun. *64*, 2945–2949.
Schäffer, S., Hantke, K., and Braun, V. (1985). Nucleotide sequence of the iron regulatory gene fur. Mol. Gen. Genet. MGG *200*, 110–113.
Schwede, T., Kopp, J., Guex, N., and Peitsch, M.C. (2003). SWISS-MODEL: An automated protein homology-modeling server. Nucleic Acids Res. *31*, 3381–3385.
Seo, S.W., Kim, D., Latif, H., O'Brien, E.J., Szubin, R., and Palsson, B.O.Ø. (2015). Deciphering Fur transcriptional regulatory network highlights its complex role beyond iron metabolism in Escherichia coli. Nat. Commun. *5*, 4910.
Sevilla, E., Martin-luna, B., Vela, L., Bes, M.T., Fillat, M.F., and Peleato, M.L. (2008). Iron availability affects mcyD expression and microcystin-LR synthesis in Microcystis aeruginosa PCC7806. *10*, 2476–2483.
Shane, S.M. (1992). The significance of Campylobacter jejuni infection in poultry: a review. Avian Pathol. *21*, 189–213.
Sheffield, P., Garrard, S., and Derewenda, Z. (1999). Overcoming expression and purification problems of RhoGDI using a family of "parallel" expression vectors. Protein Expr. Purif. *15*, 34–39.
Sheikh, M.A., and Taylor, G.L. (2009). Crystal structure of the Vibrio cholerae ferric uptake regulator (Fur) reveals insights into metal co-ordination. Mol. Microbiol. *72*, 1208–1220.
Sheldrick, G.M. (2010). Experimental phasing with SHELXC/D/E: Combining chain tracing with density modification. Acta Crystallogr. Sect. D Biol. Crystallogr. *66*, 479–485.
Shin, J.-H., Jung, H.J., An, Y.J., Cho, Y.-B., Cha, S.-S., and Roe, J.-H. (2011). Graded expression of zinc-responsive genes through two regulatory zinc-binding sites in Zur. Proc. Natl. Acad. Sci. U. S. A. *108*, 5045–5050.
Skirrow, M.B. (2006). John McFadyean and the centenary of the first isolation of Campylobacter species. Clin. Infect. Dis. *43*, 1213–1217.
Smith, T. (1918). SPIRILLA ASSOCIATED WITH DISEASE OF THE FETAL MEMBRANES IN CATTLE (INFECTIOUS ABORTION). J. Exp. Med. *28*, 701–719.
Staggs, T.M., and Perry, R.D. (1991). Identification and cloning of a fur regulatory gene in Yersinia pestis. J. Bacteriol. *173*, 417–425.
Summers, A.O. (2009). Damage control: regulating defenses against toxic metals and metalloids. Curr. Opin. Microbiol. *12*, 138–144.
Tamura, K., Peterson, D., Peterson, N., Stecher, G., Nei, M., and Kumar, S. (2011). MEGA5: Molecular evolutionary genetics analysis using maximum likelihood, evolutionary distance, and maximum parsimony methods. Mol. Biol. Evol. *28*, 2731–2739.
Tamura, K., Stecher, G., Peterson, D., Filipski, A., and Kumar, S. (2013). MEGA6: Molecular evolutionary genetics analysis version 6.0. Mol. Biol. Evol. *30*, 2725–2729.
Teixidó, L., Carrasco, B., Alonso, J.C., Barbé, J., and Campoy, S. (2011). Fur activates the expression of Salmonella enterica pathogenicity island 1 by directly interacting with the hilD operator in vivo and in vitro. PLoS One *6*, e19711.
Thomas, C.E., and Sparling, P.F. (1994). Identification and cloning of a fur homologue from Neisseria meningitidis. Mol. Microbiol. *11*, 725–737.
Thomas, C.E., Sparling, P.F., and Thomas, C.E. (1996). Isolation and analysis of a fur mutant of Neisseria gonorrhoeae. *178*, 4224–4232.

Tiss, A., Barre, O., Michaud-Soret, I., and Forest, E. (2005). Characterization of the DNA-binding site in the ferric uptake regulator protein from Escherichia coli by UV crosslinking and mass spectrometry. FEBS Lett. *579*, 5454–5460.

Tong, S., Porco, A., Isturiz, T., and Conway, T. (1996). Cloning and molecular genetic characterization of the Escherichia coli gntR, gntK, and gntU genes of GntI, the main system for gluconate metabolism. J. Bacteriol. *178*, 3260–3269.

Traoré, D. a K., El Ghazouani, A., Ilango, S., Dupuy, J., Jacquamet, L., Ferrer, J.-L., Caux-Thang, C., Duarte, V., and Latour, J.-M. (2006). Crystal structure of the apo-PerR-Zn protein from Bacillus subtilis. Mol. Microbiol. *61*, 1211–1219.

Traoré, D. a K., El Ghazouani, A., Jacquamet, L., Borel, F., Ferrer, J.-L., Lascoux, D., Ravanat, J.-L., Jaquinod, M., Blondin, G., Caux-Thang, C., et al. (2009). Structural and functional characterization of 2-oxo-histidine in oxidized PerR protein. Nat. Chem. Biol. *5*, 53–59.

Troxell, B., and Hassan, H.M. (2013). Transcriptional regulation by Ferric Uptake Regulator (Fur) in pathogenic bacteria. Front. Cell. Infect. Microbiol. *3*, 59.

Venturi, V., Ottevanger, C., Bracke, M., and Weisbeek, P. (1995). Iron regulation of siderophore biosynthesis and transport in Pseudomonas putida WCS358: involvement of a transcriptional activator and of the Fur protein. Mol. Microbiol. *15*, 1081–1093.

Vitale, S., Fauquant, C., Lascoux, D., Schauer, K., Saint-Pierre, C., and Michaud-Soret, I. (2009). A ZnS4 structural zinc site in the Helicobacter pylori ferric uptake regulator. Biochemistry *48*, 5582–5591.

Vliet, A.H.M. Van, Wooldridge, K.G., and Julian, M. (1998). Iron-Responsive Gene Regulation in a Campylobacter jejuni fur Mutant. Society *180*.

van Vliet, a H., and Ketley, J.M. (2001). Pathogenesis of enteric Campylobacter infection. Symp. Ser. Soc. Appl. Microbiol. 45S–56S.

Van Vliet, A.H.M., Ketley, J.M., Park, S.F., and Penn, C.W. (2002). The role of iron in Campylobacter gene regulation, metabolism and oxidative stress defense. FEMS Microbiol. Rev. *26*, 173–186.

Wang, F., Cheng, S., Sun, K., and Sun, L. (2008). Molecular analysis of the fur (ferric uptake regulator) gene of a pathogenic Edwardsiella tarda strain. J. Microbiol. *46*, 350–355.

Wen, Y.-T., Tsou, C.-C., Kuo, H.-T., Wang, J.-S., Wu, J.-J., and Liao, P.-C. (2011). Differential Secretomics of Streptococcus pyogenes Reveals a Novel Peroxide Regulator (PerR)-regulated Extracellular Virulence Factor Mitogen Factor3 (MF3). Mol. Cell. Proteomics *10*, M110.007013.

Wilderman, P.J., Sowa, N.A., FitzGerald, D.J., FitzGerald, P.C., Gottesman, S., Ochsner, U.A., and Vasil, M.L. (2004). Identification of tandem duplicate regulatory small RNAs in Pseudomonas aeruginosa involved in iron homeostasis. Proc. Natl. Acad. Sci. U. S. A. *101*, 9792–9797.

Winn, M.D. (2003). An overview of the CCP4 project in protein crystallography: An example of a collaborative project. J. Synchrotron Radiat. *10*, 23–25.

Wooldridge, K., and Vliet, A. Van (2005). Iron transport and regulation. In Campylobacter Molecular and Cellular Biology, (Wymondham, UK: Horizon Bioscience), pp. 293–310.

Wooldridge, K.G., Williams, P.H., and Ketley, J.M. (1994). Iron-Responsive Genetic Regulation in Campylobacter jejuni: Clining and Characterization of a fur Homolog. J. Bacteriol. *176*, 5852–5856.

Xiong, A., Singh, V.K., Cabrera, G., and Jayaswal, R.K. (2000). Molecular characterization of the ferric-uptake regulator. Fur, from Staphylococcus aureus. Microbiology *146*, 659–668.

Yu, C., and Genco, C.A. (2012). Fur-mediated global regulatory circuits in pathogenic Neisseria species. J. Bacteriol. *194*, 6372–6381.

Zilbauer, M., Dorrell, N., Wren, B.W., and Bajaj-Elliott, M. (2008). Campylobacter jejuni-mediated disease pathogenesis: an update. Trans. R. Soc. Trop. Med. Hyg. *102*, 123–129.

CONTRIBUTIONS OF COLLABORATORS

1. Dr. Jean-François Couture (University of Ottawa)

My supervisor solved the crystal structure of *Cj*FurZn$_2$ (chapter 3). He also contributed to the critical reading and editing of my thesis.

2. Dr. Joseph S. Brunzelle (professor at Northwestern University)

Dr. Brunzelle collected full diffraction data sets for *Cj*FurZn2 and *Cj*FurZn crystal structured and greatly contributed to solving these structures.

3. Dr. James Butcher (University of Ottawa)

James performed the chick colonization assays using the *C. jejuni* NCTC 11168 and *C. jejuni* Δfur + furWT strains and provided several strains.

4. Dr. Momen Askoura (University of Ottawa)

Momen performed the chick colonization assays using *C. jejuni* Δfur + furΔS2 strains and finalized the **Figure 5.2B**.

5. Karim François Charih (My honour's student, University of Ottawa)

Karim crystallized s-*Cj*Fur protein.

6. Allison Yeung (My honour's student, University of Ottawa)

Allison cloned the *Cjfur* gene in pET3d vector and helped me purify untagged *Cj*Fur.

APPENDICES

Appendix 1

Table 1. List of primers used for cloning in this study

Name	Description	Primer sequence	Target Vector
Primer 1	*Cj*Fur_Nter_BamHI	AGCAGGATGGATCCATGCTGATAGAAAATGTG	pSS
Primer 2	*Cj*Fur_Cter_XhoI	CTATCTCGCTCGAGTTATATTTTTACCTTTGCTTTTTGA	pSS
Primer 3	SUMO_Nter_NdeI	GGATTAGCATATGTGGAGCCACCCGCAGTTCGAAAAGG GTTCGGACTCAGAAGTCAATCAAGAAGC	pSS
Primer 4	SUMO_Cter_NcoI	ATCCTATCTCCATGGCATACGTAGCACCACCAAT	pSS
Primer 5	*Cj*Fur_Nter_NcoI	AGCAGGATCCATGGGGATGCTGATAGAAAATGTG	pStrep
Primer 6	*Cj*Fur_Cter_XhoI	CTATCTCGCTCGAGTTATATTTTTACCTTTGCTTTTTGA	pStrep
Primer 7	*Cj*Fur_Nter_NdeI	AGCAGGATCATATGCTGATAGAAAATGTGGAATA	pET3d
Primer 8	*Cj*Fur_Cter_XhoI	CTATCTCGCTCGAGTTATATTTTTACCTTTGCTTTTTGA	pET3d
Primer 9	*Cj*Fur_Nter	GATTTAGATGTCTAGCATGCTAGTGAAAAGTTGCAAGA	pRRK
Primer 10	*Cj*Fur_Cter	GGGGAAGCTTTCTAGGCTTTTTCTATTCTTTGCTGCTC	pRRK

Figure 1. Nucleotide and amino acid sequence of *Cj*Fur

***Cj*Fur nucleotide sequence**

ATGCTGATAGAAAATGTGGAATATGATGTTTTACTTGAGAGATTTAAAAAAATA
TTAAGACAAGGCGGACTTAAATATACCAAGCAAAGAGAAGTACTTTTAAAAACT
CTTTATCACAGTGATATTCATTACACACCCGAAAGTTTATATATGGAAATCAAAC
AAGCTGAACCTGATTTAAATGTAGGAATTGCAACTGTTTATCGTACTTTAAATTT
ACTTGAAGAAGCAGAAATGGTAACTTCCATTTCTTTTGGTTCAGCAGGTAAAAA
ATATGAGCTTGCTAATAAACCTCACCATGATCATATGATATGTAAAAATTGCGG
AAAAATTATAGAGTTTGAAAATCCTATTATAGAAAGACAGCAAGCCTTGATTGC
AAAAGAACATGGTTTTAAACTTACAGGGCATTTGATGCAGCTTTATGGTGTTTGT
GGTGATTGTAATAATCAAAAAGCAAAGGTAAAAATATAA

***Cj*Fur amino acid sequence**

MLIENVEYDVLLERFKKILRQGGLKYTKQREVLLKTLYHSDIHYTPESLYMEIKQAE
PDLNVGIATVYRTLNLLEEAEMVTSISFGSAGKKYELANKPHHDHMICKNCGKIIEFE
NPIIERQQALIAKEHGFKLTGHLMQLYGVCGDCNNQKAKVKI

pSS Vector

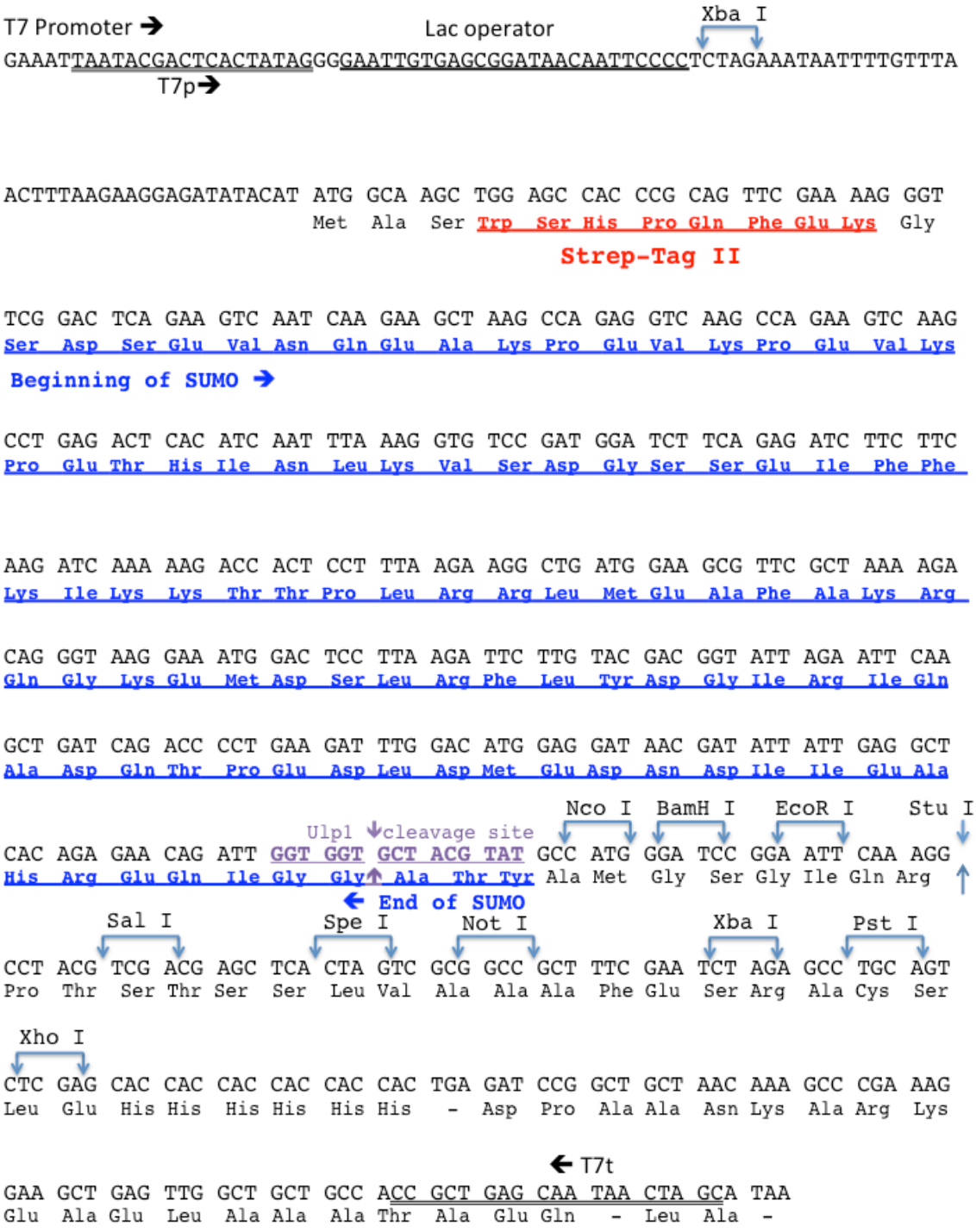
T7 Promoter
Lac operator
Xba I
GAAATTAATACGACTCACTATAGGGGAATTGTGAGCGGATAACAATTCCCCTCTAGAAATAATTTTGTTTA
T7p
ACTTTAAGAAGGAGATATACAT ATG GCA AGC TGG AGC CAC CCG CAG TTC GAA AAG GGT
Met Ala Ser Trp Ser His Pro Gln Phe Glu Lys Gly
Strep-Tag II
TCG GAC TCA GAA GTC AAT CAA GAA GCT AAG CCA GAG GTC AAG CCA GAA GTC AAG
Ser Asp Ser Glu Val Asn Gln Glu Ala Lys Pro Glu Val Lys Pro Glu Val Lys
Beginning of SUMO
CCT GAG ACT CAC ATC AAT TTA AAG GTG TCC GAT GGA TCT TCA GAG ATC TTC TTC
Pro Glu Thr His Ile Asn Leu Lys Val Ser Asp Gly Ser Ser Glu Ile Phe Phe
AAG ATC AAA AAG ACC ACT CCT TTA AGA AGG CTG ATG GAA GCG TTC GCT AAA AGA
Lys Ile Lys Lys Thr Thr Pro Leu Arg Arg Leu Met Glu Ala Phe Ala Lys Arg
CAG GGT AAG GAA ATG GAC TCC TTA AGA TTC TTG TAC GAC GGT ATT AGA ATT CAA
Gln Gly Lys Glu Met Asp Ser Leu Arg Phe Leu Tyr Asp Gly Ile Arg Ile Gln
GCT GAT CAG ACC CCT GAA GAT TTG GAC ATG GAG GAT AAC GAT ATT ATT GAG GCT
Ala Asp Gln Thr Pro Glu Asp Leu Asp Met Glu Asp Asn Asp Ile Ile Glu Ala
Nco I
BamH I
EcoR I
Stu I
Ulp1 cleavage site
CAC AGA GAA CAG ATT GGT GGT GCT ACG TAT GCC ATG GGA TCC GGA ATT CAA AGG
His Arg Glu Gln Ile Gly Gly Ala Thr Tyr Ala Met Gly Ser Gly Ile Gln Arg
End of SUMO
Sal I
Spe I
Not I
Xba I
Pst I
CCT ACG TCG ACG AGC TCA CTA GTC GCG GCC GCT TTC GAA TCT AGA GCC TGC AGT
Pro Thr Ser Thr Ser Ser Leu Val Ala Ala Ala Phe Glu Ser Arg Ala Cys Ser
Xho I
CTC GAG CAC CAC CAC CAC CAC CAC TGA GAT CCG GCT GCT AAC AAA GCC CGA AAG
Leu Glu His His His His His His - Asp Pro Ala Ala Asn Lys Ala Arg Lys
T7t
GAA GCT GAG TTG GCT GCT GCC ACC GCT GAG CAA TAA CTA GCA TAA
Glu Ala Glu Leu Ala Ala Ala Thr Ala Glu Gln - Leu Ala -

Figure 2. Multi-Cloning site of the pStrepSumo (pSS) vector. The T7 promoter (T7p), T7 terminator (T7t) and the lac operator are underlined. The Strep-Tag II coding sequence is coloured in red. The sequence corresponding the *SMT3* gene is represented in blue. The Ulp1 cleavage site as well as key restriction sites are indicated.

pStrep

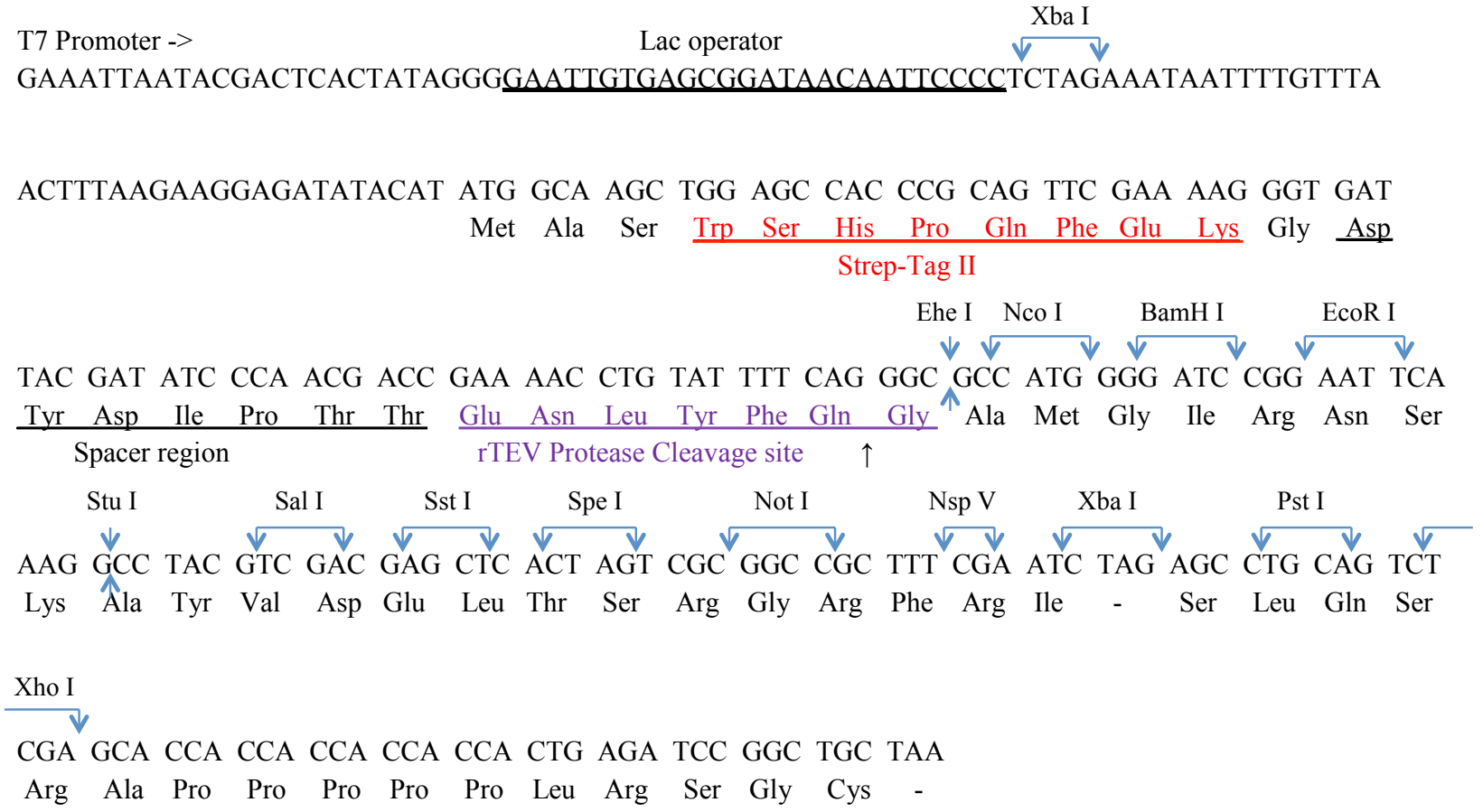
Xba I
T7 Promoter ->
Lac operator
GAAATTAATACGACTCACTATAGGGGAATTGTGAGCGGATAACAATTCCCCTCTAGAAATAATTTTGTTTA
ACTTTAAGAAGGAGATATACAT ATG GCA AGC TGG AGC CAC CCG CAG TTC GAA AAG GGT GAT
Met Ala Ser Trp Ser His Pro Gln Phe Glu Lys Gly Asp
Strep-Tag II
Ehe I
Nco I
BamH I
EcoR I
TAC GAT ATC CCA ACG ACC GAA AAC CTG TAT TTT CAG GGC GCC ATG GGG ATC CGG AAT TCA
Tyr Asp Ile Pro Thr Thr Glu Asn Leu Tyr Phe Gln Gly Ala Met Gly Ile Arg Asn Ser
Spacer region
rTEV Protease Cleavage site
Stu I
Sal I
Sst I
Spe I
Not I
Nsp V
Xba I
Pst I
AAG GCC TAC GTC GAC GAG CTC ACT AGT CGC GGC CGC TTT CGA ATC TAG AGC CTG CAG TCT
Lys Ala Tyr Val Asp Glu Leu Thr Ser Arg Gly Arg Phe Arg Ile - Ser Leu Gln Ser
Xho I
CGA GCA CCA CCA CCA CCA CCA CTG AGA TCC GGC TGC TAA
Arg Ala Pro Pro Pro Pro Pro Leu Arg Ser Gly Cys -

Figure 3. Multi-Cloning site of the pStrep (pS) vector. The T7 promoter (T7p) and the lac operator are underlined. The Strep-Tag II coding sequence is identified. The horizontal arrows indicate the 5' and 3' regions of the sequence corresponding the *SMT3* gene. The Ulp1 cleavage site as well as key restriction sites are indicated.

Table 2. List of buffers used for the purification of different *Cj*Fur constructs in this study

	Protein construct		
	ss-*Cj*Fur	**s-*Cj*Fur**	**untagged *Cj*Fur**
Lysis buffer	PBS 1X	50 mM Tris pH7.0 100 mM NaCl 5 mM Bme	50 mM Tris pH7.0 100 mM NaCl 5 mM Bme
Strep-Tactin elution buffer	PBS 1X 2.5 mM d-desthiobiotin	50 mM Tris pH7.0 100 mM NaCl 5 mM Bme 2.5 mM d-desthiobiotin	
Protease cleavage buffer*	PBS 1X	50 mM Tris pH7.0 250 mM NaCl 5 mM Bme	
Ion exchange chromatography (Q sepharose)			20 mM Citrate pH 6.0 5 mM BMe
Ion exchange chromatography (SP sepharose) Buffer A	20 mM Citrate pH 6.0 5 mM BMe		20 mM Citrate pH 6.0 5 mM BMe
Ion exchange chromatography (SP sepharose) Buffer B	20 mM Citrate pH 6.0 1M NaCl 5 mM BMe		20 mM Citrate pH 6.0 500 mM NaCl 5 mM BMe
Ion exchange chromatography (Heparin) Buffer A			20 mM Citrate pH 6.0 5 mM BMe
Ion exchange chromatography (Heparin) Buffer B			20 mM Citrate pH 6.0 1M NaCl 5 mM BMe
Size exclusion chromatography (Superdex S75)	20 mM Tris pH7.0 250 mM NaCl 5 mM Bme	20 mM Tris pH7.0 250 mM NaCl 5 mM Bme	20 mM Tris pH7.0 250 mM NaCl 5 mM Bme

* ULP1 protease used for ss-*Cj*Fur and Tev protease used for s-*Cj*Fur

Table 3. List of primers used for EMSA in this study

Name	Description	Primer sequence
Primer 1	katA_60bp_Forward (Cy5 5')	ACTGAATAATTGCATTTTATTGATAATAAATTTCAAAATAAATTTAGTTTTTTTATATTA
Primer 2	katA_60bp_Reverse (Cy5 5')	TAATATAAAAAAACTAAATTTATTTTGAAATTTATTATCAATAAAATGCAATTATTCAGT
Primer 3	*Cj*1345c_200bp_Forward (Cy5 5')	GGGAAAAGAGCCAAATTTAGGTGTTATCATCAA
Primer 4	*Cj*1345c_200bp_Reverse	TTTAACTCCTTAAATACTCTCTTGTTTTAA
Primer 5	hddA_200bp_Forward (Cy5 5')	GGGTGAAGGAATGGAGTTTGAGATAATGAAAAA
Primer 6	hddA_200bp_Reverse	AAATCTCCTAATTTATTTATCATATCCAAT
Primer 7	rrc_200bp_Forward (Cy5 5')	GGGGGTGCTCTTAAATGTCCTTTTTTTATCGCA
Primer 8	rrc_200bp_Reverse	TTTGACTCCTTTTTTGATTATCAAAAAGTA
Primer 9	*Cj*0415_200bp_Forward (Cy5 5')	GGGATCTTCTTATTTTTTCACACTTTTAAGAGA
Primer 10	*Cj*0415c_200bp_Reverse	TTTAACTCTCCATATCTGCTAAACCCATAG
Primer 11	*Cj*1345c_1-50_Forward (Cy5 5')	TTTAACTCCTTAAATACTCTCTTGTTTTAAAATCATACTCAAAAACTTCT
Primer 12	*Cj*1345c_1-50_Reverse	AGAAGTTTTTGAGTATGATTTTAAAACAAGAGAGTATTTAAGGAGTTAAA
Primer 13	*Cj*1345c_51-100_Forward (Cy5 5')	TCTATGCTTGAAATTTTAGGTACTCCAAAATGATCAAGGGCTTTAAAAAT
Primer 14	*Cj*1345c_51-100_Reverse	ATTTTTAAAGCCCTTGATCATTTTGGAGTACCTAAAATTTCAAGCATAGA
Primer 15	*Cj*1345c_101-150_Forward (Cy5 5')	GCATTTAGCAATGTCTAAAAATCCACTTTTATTTTCTAAAAAATTATAAA
Primer 16	*Cj*1345c_101-150_Reverse	TTTATAATTTTTTAGAAAATAAAAGTGGATTTTTAGACATTGCTAAATGC
Primer 17	*Cj*1345c_151-200_Forward (Cy5 5')	CACCAACTTCATTAGCAGCATTGATGATAACACCTAAATTTGGCTCTTTT
Primer 18	*Cj*1345c_151-200_Reverse	AAAAGAGCCAAATTTAGGTGTTATCATCAATGCTGCTAATGAAGTTGGTG
Primer 19	*Cj*1345c_1-60_Forward (Cy5 5')	TTTAACTCCTTAAATACTCTCTTGTTTTAAAATCATACTCAAAAACTTCTTCTATGCTTG
Primer 20	*Cj*1345c_1-60_Reverse	CAAGCATAGAAGAAGTTTTTGAGTATGATTTTAAAACAAGAGAGTATTTAAGGAGTTAAA
Primer 21	*Cj*1345c_11-60_Forward (Cy5 5')	TAAATACTCTCTTGTTTTAAAATCATACTCAAAAACTTCTTCTATGCTTG
Primer 22	*Cj*1345c_11-60_Reverse	CAAGCATAGAAGAAGTTTTTGAGTATGATTTTAAAACAAGAGAGTATTTA
Primer 23	*Cj*1345c_21-60_Forward (Cy5 5')	CTTGTTTTAAAATCATACTCAAAAACTTCTTCTATGCTTG
Primer 24	*Cj*1345c_21-60_Reverse	CAAGCATAGAAGAAGTTTTTGAGTATGATTTTAAAACAAG
Primer 25	*Cj*1345c_31-60_Forward (Cy5 5')	AATCATACTCAAAAACTTCTTCTATGCTTG
Primer 26	*Cj*1345c_31-60_Reverse	CAAGCATAGAAGAAGTTTTTGAGTATGATT
Primer 27	*Cj*1345c_1-40_Forward (Cy5 5')	TTTAACTCCTTAAATACTCTCTTGTTTTAAAATCATACTC
Primer 28	*Cj*1345c_1-40_Reverse	GAGTATGATTTTAAAACAAGAGAGTATTTAAGGAGTTAAA
Primer 29	*Cj*1345c_1-30_Forward (Cy5 5')	TTTAACTCCTTAAATACTCTCTTGTTTTAA
Primer 30	*Cj*1345c_1-30_Reverse	TTAAAACAAGAGAGTATTTAAGGAGTTAAA
Primer 31	*Cj*1345c_11-40_Forward (Cy5 5')	TAAATACTCTCTTGTTTTAAAATCATACTC
Primer 32	*Cj*1345c_11-40_Reverse	GAGTATGATTTTAAAACAAGAGAGTATTTA
Primer 33	*Cj*1345c_21-50_Forward (Cy5 5')	CTTGTTTTAAAATCATACTCAAAAACTTCT
Primer 34	*Cj*1345c_21-50_Reverse	AGAAGTTTTTGAGTATGATTTTAAAACAAG
Primer 35	*Cj*1345c_Mut21-25_Forward (Cy5 5')	CGGGCTTTAAAATCATACTCAAAAACTTCTTCTATGCTTG
Primer 36	*Cj*1345c_Mut21-25_Reverse	CAAGCATAGAAGAAGTTTTTGAGTATGATTTTAAAGCCCG
Primer 37	*Cj*1345c_Mut26-30_Forward (Cy5 5')	CTTGTCGGGCAATCATACTCAAAAACTTCTTCTATGCTTG
Primer 38	*Cj*1345c_Mut26-30_Reverse	CAAGCATAGAAGAAGTTTTTGAGTATGATTGCCCGACAAG
Primer 39	*Cj*1345c_Mut31-35_Forward (Cy5 5')	CTTGTTTTAACGGGCTACTCAAAAACTTCTTCTATGCTTG
Primer 40	*Cj*1345c_Mut31-35_Reverse	CAAGCATAGAAGAAGTTTTTGAGTAGCCCGTTAAAACAAG
Primer 41	*Cj*1345c_Mut36-40_Forward (Cy5 5')	CTTGTTTTAAAATCACGGGCAAAAACTTCTTCTATGCTTG
Primer 42	*Cj*1345c_Mut36-40_Reverse	CAAGCATAGAAGAAGTTTTTGCCCGTGATTTTAAAACAAG
Primer 43	*Cj*1345c_Mut41-45_Forward (Cy5 5')	CTTGTTTTAAAATCATACTCCGGGCCTTCTTCTATGCTTG
Primer 44	*Cj*1345c_Mut41-45_Reverse	CAAGCATAGAAGAAGGCCCGGAGTATGATTTTAAAACAAG
Primer 45	*Cj*1345c_Mut46-50_Forward (Cy5 5')	CTTGTTTTAAAATCATACTCAAAAACGGGCTCTATGCTTG
Primer 46	*Cj*1345c_Mut46-50_Reverse	CAAGCATAGAGCCCGTTTTTGAGTATGATTTTAAAACAAG
Primer 47	*Cj*1345c_Mut51-55_Forward (Cy5 5')	CTTGTTTTAAAATCATACTCAAAAACTTCTCGGGCGCTTG
Primer 48	*Cj*1345c_Mut51-55_Reverse	CAAGCGCCCGAGAAGTTTTTGAGTATGATTTTAAAACAAG
Primer 49	*Cj*1345c_Mut56-60_Forward (Cy5 5')	CTTGTTTTAAAATCATACTCAAAAACTTCTTCTATCGGGC
Primer 50	*Cj*1345c_Mut56-60_Reverse	GCCCGATAGAAGAAGTTTTTGAGTATGATTTTAAAACAAG

Table 4. List of primers used for site-directed mutagenesis in this study

Mutant	Name	Sequence (5'➔3')
Arg14Glu	*Cj*FurR14E-Forward	GTGGAATATGATGTTTTACTTGAGGAATTTAAAAAAATATTAAGACAAGGC
	*Cj*FurR14E-Reverse	GCCTTGTCTTAATATTTTTTTAAATTCCTCAAGTAAAACATCATATTCCAC
Lys17Glu	*Cj*FurK17E-Forward	GATGTTTTACTTGAGAGATTTAAAGAAATATTAAGACAAGGCGGACTTAAA
	*Cj*FurK17E-Reverse	TTTAAGTCCGCCTTGTCTTAATATTTCTTTAAATCTCTCAAGTAAAACATC
Arg20Glu	*Cj*FurR20E-Forward	CTTGAGAGATTTAAAAAAATATTAGAACAAGGCGGACTTAAATATACTAAG
	*Cj*FurR20E-Reverse	CTTAGTATATTTAAGTCCGCCTTGTTCTAATATTTTTTTAAATCTCTCAAG
Lys25Glu	*Cj*FurK25E-Forward	AAAATATTAAGACAAGGCGGACTTGAATATACTAAGCAAAGAGAAGTGCTT
	*Cj*FurK25E-Reverse	AAGCACTTCTCTTTGCTTAGTATATTCAAGTCCGCCTTGTCTTAATATTTT
Lys28Glu	*Cj*FurK28E-Forward	AGACAAGGCGGACTTAAATATACTGAACAAAGAGAAGTGCTTTTAAAAACT
	*Cj*FurK28E-Reverse	AGTTTTTAAAAGCACTTCTCTTTGTTCAGTATATTTAAGTCCGCCTTGTCT
Arg30Glu	*Cj*FurR30E-Forward	GGCGGACTTAAATATACTAAGCAAGAAGAAGTGCTTTTAAAAACTCTTTAT
	*Cj*FurR30E-Reverse	ATAAAGAGTTTTTAAAAGCACTTCTTCTTGCTTAGTATATTTAAGTCCGCC
Tyr68Ala	*Cj*FurY68A-Forward	TTAAATGTAGGAATTGCAACTGTTGCGCGTACTTTAAATTTGCTTGAAG
	*Cj*FurY68A-Reverse	TTCTTCAAGCAAATTTAAAGTACGCGCAACAGTTGCAATTCCTACATTTAA
Arg69Glu	*Cj*FurR69E-Forward	AATGTAGGAATTGCAACTGTTTATGAAACTTTAAATTTACTTGAAGAAGCA
	*Cj*FurR69E-Reverse	TGCTTCTTCAAGTAAATTTAAAGTTTCATAAACAGTTGCAATTCCTACATT
ΔS2	*Cj*FurΔS2-H43A-Forward	AAAACTCTTTATCACAGTGATACTGCCTACACACCCGAAAGTTTATATATG
	*Cj*FurΔS2-H43A-Reverse	CATATATAAACTTTCGGGTGTGTAGGCAGTATCACTGTGATAAAGAGTTTT
	*Cj*FurΔS2-H102A-Forward	CTTGCCAATAAACCTCACCATGATGCCATGATATGTAAAAATTGCGGAAAA
	*Cj*FurΔS2-H102A-Reverse	TTTTCCGCAATTTTTACATATCATGGCATCATGGTGAGGTTTATTGGCAAG
ΔS3	*Cj*FurΔS2-H99A-Forward	AAATACGAGCTTGCCAATAAACCTGCCCATGATCATATGATATGTAAAAAT
	*Cj*FurΔS2-H99A-Reverse	ATTTTTACATATCATATGATCATGGGCAGGTTTATTGGCAAGCTCGTATTT
	*Cj*FurΔS2-H137A-Forward	GAACATGGTTTTAAACTTACAGGGGCCTTGATGCAGCTTTATGGTGTTTGT
	*Cj*FurΔS2-H137A-Reverse	ACAAACACCATAAAGCTGCATCAAGGCCCCTGTAAGTTTAAAACCATGTTC

Table 5. List of primers used for RT-qPCR analysis in this study

Gene	Primer Name	Sequence
cfrA	cfrA_Forward	TCTATCAGTTTGCGCCATTG
	cfrA_Reverse	ATCAACGCCTGGGATATCTG
Cj0948c	Cj0948c_Forward	ACAAGTGGTTCTGTTGCAGT
	Cj0948c_Reverse	TTCATTCGCCTTTTGTGAGC
Cj1345c	Cj1345c_Forward	GCGTAGGAGAAAATGGAAAAA
	Cj1345c_Reverse	AAAAGCTAAATTTGGAGCCACT
fur	fur_Forward	CATTTCTTTTGGTTCAGCAGGT
	fur_Reverse	AAGCTGCATCAAATGCCCT
katA	katA_Forward	CTTTAGTCCAAGCAATATCGTTCC
	katA_Reverse	CAGCGACATTGTAAGTATTCACTTC
slyD	slyD_Forward	TACGATGAAAATGCCGTTCA
	slyD_Reverse	TTCGCCAAAAAGCTCCATAC

Appendix 2

Table 1. Data collection, phasing and refinement statistics for the crystal structure of *Cj*FurZn$_2$.

Data collection	Zn SAD	Native
Space group	$P2_12_12_1$	$P2_12_12_1$
Cell dimensions		
a, b, c (Å)	35.8, 84.5, 128.2	35.9, 85.3, 128.4
Resolution	30-2.1 (2.2-2.1)!	30-2.1 (2.2-2.1)
Rsym	6.0 (50.8)	4.5 (47.2)
I /σI	22.3 (3.0)	22.3 (3.1)
Completeness	99.9 (99.0)	99.9 (99.9)
Redundancy	4.7 (4.5)	4.7 (4.5)
Phasing		
atom found	4	
CC_{all} (%)	45.3	
CC_{weak} (%)	28.4	
PATFOM	49.8	
Refinement		
Resolution		27.8 – 2.1
Reflections		22655
R_{work}/R_{free}		23.7 / 26.7
No. atoms		
Protein		2353
Ligands		4
Water		61
B-factors (Å^2)		
Protein		38.0
Ligands		32.7
Water		41.1
R.m.s. deviations		
Bond lengths (Å)		0.019
Bond angles (°)		1.783
Molprobity score		1.82
Ramachandran favored (%)*		97.78

! Highest resolution shell.
*There are no Ramachandran outliers

Table 2. Data collection, phasing and refinement statistics for the crystal structure of *Cj*FurZn

Data collection			Zn SAD
	Space group		$P2_12_12_1$
	Cell dimensions		
		a, b, c (Å)	35.74, 84.36,123.63
	Resolution		34.8 – 1.81
	Rsym		6.3 (48.3)
	I /σI		5.3 (2.9)
	Completeness (%)		100 (100)
	Redundancy		3.4 (2.1)
Refinement			
	Resolution		34.65-1.81
	Reflections		34629
	R_{work}/R_{free}		18.6/23.1
	No. atoms		
		Protein	2369
		Ligands	
		Water	398
	B-factors (Å^2)		
		Protein	25.7
		Ligands	13.7
		Water	37.6
	R.m.s. deviations		
		Bond lengths (Å)	0.016
		Bond angles (°)	1.33
	Molprobity score		1.59
		Ramachandran favored (%)*	98.9

! Highest resolution shell.
*There are no Ramachandran outliers

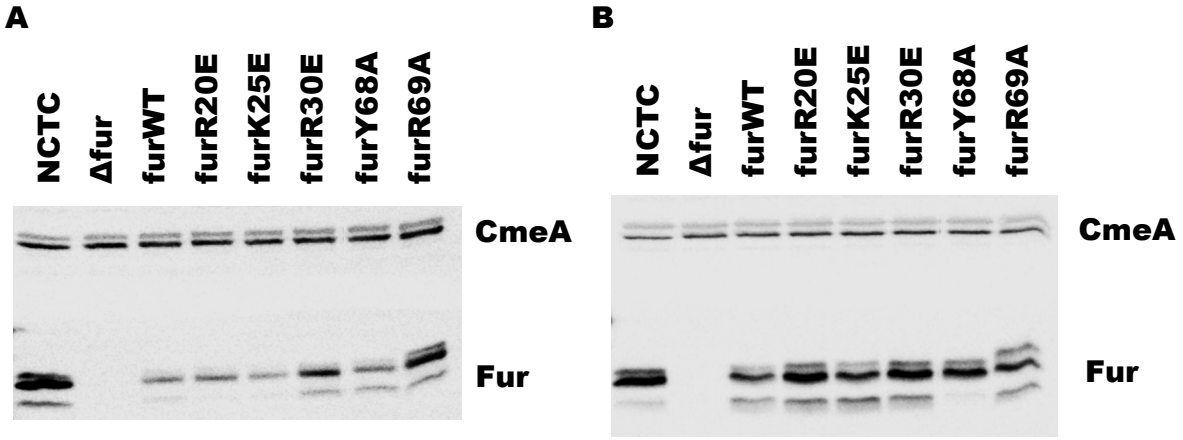
A
NCTC
Δfur
furWT
furR20E
furK25E
furR30E
furY68A
furR69A
CmeA
Fur
B
NCTC
Δfur
furWT
furR20E
furK25E
furR30E
furY68A
furR69A
CmeA
Fur

Figure 1. Expression of complemented *Campylobacter jejuni* Fur mutants in MEM-α medium in iron poor (A) and iron rich (B) conditions. CmeA was used as loading control.

CURRICULUM VITAE

EDUCATION

PhD Degree - Biochemistry **2010-2017**
Structural and Functional Characterization of Campylobacter jejuni Ferric Uptake regulator
Supervisor: Jean-François Couture, Ph.D.
Faculty of Medicine
University of Ottawa, Ontario, Canada

Bachelor Degree **2006-2010**
Honours Bachelor of Science with Specialization in Biochemistry (Co-op)
Faculty of Sciences
University of Ottawa, Ontario, Canada

College Degree **2004-2006**
Diploma of collegiate studies in Natural Sciences
CÉGEP de l'Outaouais, Gatineau, Québec, Canada

PUBLICATIONS

1. **Sarvan**., Lam W., & Couture J-F., *Structural and functional characterization of Campylobacter jejuni Peroxide stress regulator (CjPerR).* (in preparation, to be submitted to *Journal of Bacteriology*)

2. **Sarvan S**., Charih F., Askoura M., Butcher J., Brunzelle J.S., Stintzi A., & Couture J-F. *Biochemical insights into the interplay between Campylobacter jejuni Ferric uptake regulator metal binding sites.* (in preparation, to be submitted to *Molecular Microbiology* Journal)

3. **Sarvan S**., Yeung A., Charih F., Stintzi A., & Couture J-F. *Purification and Characterization of Campylobacter jejuni Ferric Uptake Regulator.* (in preparation, to be submitted to *Protein Expression and Purification* Journal)

4. Bergamin E., **Sarvan S**., Malette J., Eram M. S., Yeung S., Mongeon V., Joshi M., Brunzelle J. S., Michaels S. D., Blais A., Vedadi M., & Couture J-F. *Molecular basis for the methylation specificity of ATXR5 for histone H3.* Nucleic Acids Res. (2017)

5. **Sarvan S**., & Couture J-F., *Method for Successful Crystallization of the Ferric Uptake Regulator from Campylobacter jejuni.* Methods Mol Biol. (2017) 1512 : 78-89

6. Askoura M., **Sarvan S**., Couture J-F., & Stintzi A., *The Campylobacter jejuni Ferric Uptake Regulator Promotes Acid Survival and Cross-Protection against Oxidative Stress.* Infect Immun. (2016), 84(5) :1287-1300

7. Pandelieva A. T., Baran M. J., Calderini G.F., McCann J. L., Tremblay V., **Sarvan S**., Davey J. A., Couture J-F., & Chica R. A., *Brighter Red Fluorescent Proteins by Rational Design of Triple-Decker Motif.* ACS Chem Biol (2016), 11(2) :508-517

8. Butcher J., **Sarvan S**., Brunzelle J.S., Couture J-F., & Stintzi A., *Structure and regulon of Campylobacter jejuni ferric uptake regulator Fur define apo-Fur regulation.* PNAS (2012), 109(25) :10047-10052

9. **Sarvan S**., Avdic V., Tremblay V, Chaturvedi C. P., Zhang P., Lanouette S., Blais A., Brunzelle J. S., Brand M., & Couture J-F.*Crystal structure of the trithorax group protein ASH2L reveals a Forkhead-like DNA binding domain*. Nat Struct Mol Biol. (2011), 18(7) : 857-859

ORAL PRESENTATIONS

1. **Sabina Sarvan,** Jean-François Couture. *From the structural and functional studies of Ferric uptake regulator (Fur) to new treatment of Campylobacteriosis* (June 2016) 4th China Canada Systems Biology conference, Ottawa, ON, (PhD work) (International)

POSTER PRESENTATIONS

1. **Sabina Sarvan** et al. *Molecular insights into the interplay between metal coordination and DNA binding by the Campylobacter jejuni Ferric Uptake Regulator (CjFur)* (May 2017) Poster presented at the CSMB2017 "Celebrating Canadian Molecular Biosciences – from organelles to systems biology", Ottawa, ON (National)

2. **Sabina Sarvan** et al. *Molecular insights into the interplay between metal coordination and DNA binding by the Campylobacter jejuni Ferric Uptake Regulator (CjFur)* (June 2016) Poster presented at the 2nd Protein Engineering Canada Conference, Ottawa, ON (National)

3. **Sabina Sarvan** et al. *Molecular insights into the interplay between metal coordination and DNA binding by the Campylobacter jejuni Ferric Uptake Regulator (CjFur)* (May 2016) Poster presented at 16e symposium annuel de PROTEO, Québec, QC (National)

4. **Sabina Sarvan** et al. *Molecular insights into the interplay between metal coordination and DNA binding by the Campylobacter jejuni Ferric Uptake*

Regulator (CjFur) (November 2015) Poster presented at the Annual GRASP/MSBM Symposium, Montreal, QC (National)

5. **Sabina Sarvan** et al. *Structural insights into the interaction between the Fur family of metalloregulators and DNA* (May 2015) Poster presented at 15e symposium annuel de PROTEO, Québec, QC (National)

6. **Sabina Sarvan** et al. *Structural insights into the interaction between the Fur family of metalloregulators and DNA* (June 2014) Poster presented at the Protein Engineering Canada Conference, Ottawa, ON (National)

7. **Sabina Sarvan** *et al., Structural insights into an atypical Ferric uptake regulator*. (July 2013). Poster presented at the American Crystallographic Association Annual Meeting, Honolulu, Hawaii (International)

8. **Sabina Sarvan** *et al., Structural insights into an atypical Ferric uptake regulator*. (June 2012). Poster presented at the 19th Methods in Protein Structure Analysis (MPSA 2012) conference, Ottawa, ON (International)

9. **Sabina Sarvan** *et al.*, *An atypical helix-wing-helix domain mediates ASH2L binding to the β-globin locus control region.* (December 2011) Poster presented at the Chromatin: Structure & Function, Aruba (International)

10. **Sabina Sarvan** *et al., Structural insights into an atypical Ferric uptake regulator.* (November 2011) Poster presented at the Annual GRASP/MSBM Symposium, Montreal, QC (National)

11. **Sabina Sarvan** *et al., Structural insights into an atypical Ferric uptake regulator.* (August 2011) Poster presented at the 16th International Workshop on Campylobacter, Helicobacter and Related organisms, Vancouver, BC (International)

12. **Sabina Sarvan** *et al.*, *An atypical helix-wing-helix domain mediates ASH2L binding to the β-globin locus control region.* (September 2011) Poster presented at the Ottawa Institute for Systems Biology Symposium, Montebello, QC (Regional)

13. **Sabina Sarvan** *et al., Structural and functional insights into a DNA binding domain of the trithorax protein ASH2L.* (May 2011) Poster presented at the Epigenetics Eh! conference, London, ON (International)

14. **Sabina Sarvan** *et al.*, *An atypical helix-wing-helix domain mediates ASH2L binding to the beta-globin gene.* (November 2010) Poster presented at the Annual GRASP/MSBM Symposium, Montreal, QC (National)

WORK EXPERIENCE

Trainee Co-op **May 2009-August 2009**
Natural Resources Canada, Ottawa (Ontario)
Production of naphtha-range additive from depolymerized lignin in 70 mL autoclave A : Investigation with model compounds

Trainee Co-op **September 2008 - December 2008**
Natural Resources Canada, Ottawa (Ontario)
Production of high octane fuel additive from depolymerized lignin

Trainee Co-op **May 2008 - August 2008**
University of Ottawa, Ottawa (Ontario)
Purification and crystallization of Ferric uptake regulator

Trainee Co-op **January 2008 - April 2008**
Natural Resources Canada, Ottawa (Ontario)
Isomerization of normal Hexadecane

TEACHING EXPERIENCE

Lab demonstrator/Teaching assistant **Winter 2017**
University of Ottawa
TMM3009 Laboratoire de recherche biomédicale / Biomedical Research Laboratory

Lab demonstrator/Teaching assistant **Fall 2017**
University of Ottawa
TMM3009 Laboratoire de recherche biomédicale / Biomedical Research Laboratory

AWARDS AND SCHOLARSHIPS

1. CanmetENERGY-Ottawa Aileen Proudfoot Award, January 2009
2. Mitacs Travel Award for the 16th International Workshop on Campylobacter, Helicobacter and Related organisms, August 2011, 250$
3. Biochemistry Travel award for the ABCAM: Chromatin Structure and Function 2011 Conference, December 2011, 1000$
4. Faculty of Graduate and Postdoctoral Studies (FGPS) Travel Grant for the ABCAM: Chromatin Structure and Function 2011 Conference, December 2011, 550$
5. PhD Admission scholarship, University of Ottawa, 3000$ May 2012 to August 2012

6. Queen Elizabeth II graduate scholarship in science and technology (QEII - GSST), 15000$ per year, September 2012 to August 2013
7. Excellence scholarship, University of Ottawa, 2380 $ per semester, September 2012 to August 2016
8. Bourse de formation en recherche en santé– Doctorat par le Fonds de recherché du Québec-Santé (FRQS), 20000$ per year, September 2013 to August 2016
9. Biochemistry Travel award for the American Crystallographic Associationa Conference, July 2013, 1000$
10. Faculty of Graduate and Postdoctoral Studies (FGPS) Travel Grant for the American Crystallographic Association Cenference, July 2013, 550$
11. Graduate Students' Association (GSAÉD) Academic Project Fund, University of Ottawa, for the American Crystallographic Association Conference, July 2013, 400$
12. American Crystallographic Association Travel Grant for the American Crystallographic Association Meeting, July 2013, 600$
13. Louis Delbaere Pauling Poster Prize at the American Crystallographic Association Conference, July 2013, 250$
14. Graduate student poster award at the GRIP poster Symposium, University of Ottawa, August 2014, 50$
15. PhD Biochemistry 2nd place at the BMI Poster Day, University of Ottawa, May 2015, 75$

RIGHTS AND PERMISSIONS

For Butcher J*, Sarvan S*, Brunzelle J, Couture JF, Stintzi A. (2012) "The structure and regulon of *Campylobacter jejuni* ferric uptake regulator Fur define apo-Fur regulation" PNAS 109(25):10047-52 PMID:22665794:

For Sarvan S., Couture JF. (2017) "Method for the Successful Crystallization of the Ferric Uptake Regulator from *Campylobacter jejuni*." In: Butcher J., Stintzi A. (eds) Campylobacter jejuni. Methods in Molecular Biology, vol 1512. Humana Press, New York, NY

SPRINGER LICENSE
TERMS AND CONDITIONS

Mar 30, 2017

This Agreement between Sabina Sarvan ("You") and Springer ("Springer") consists of your license details and the terms and conditions provided by Springer and Copyright Clearance Center.

License Number	4078931364655
License date	Mar 30, 2017
Licensed Content Publisher	Springer
Licensed Content Publication	Springer eBook
Licensed Content Title	Method for the Successful Crystallization of the Ferric Uptake Regulator from Campylobacter jejuni
Licensed Content Author	Sabina Sarvan
Licensed Content Date	Jan 1, 2017
Type of Use	Thesis/Dissertation
Portion	Figures/tables/illustrations
Number of figures/tables/illustrations	2
Author of this Springer article	Yes and you are the sole author of the new work
Order reference number	
Original figure numbers	Figures 2 and 3
Title of your thesis / dissertation	Structural and functional characterization of Campylobacter jejuni Ferric uptake regulator (CjFur) and Peroxide stress regulator (CjPerR)
Expected completion date	Sep 2017
Estimated size(pages)	200
Requestor Location	Sabina Sarvan 451 Smyth Road Ottawa, ON K1H 8M5 Canada Attn: Sabina Sarvan
Billing Type	Invoice
Billing Address	Sabina Sarvan 451 Smyth Road Ottawa, ON K1H 8M5 Canada Attn: Sabina Sarvan
Total	0.00 CAD
Terms and Conditions	

Introduction

The publisher for this copyrighted material is Springer. By clicking "accept" in connection with completing this licensing transaction, you agree that the following terms and conditions apply to this transaction (along with the Billing and Payment terms and conditions established by Copyright Clearance Center, Inc. ("CCC"), at the time that you opened your Rightslink account and that are available at any time at http://myaccount.copyright.com).

Limited License

With reference to your request to reuse material on which Springer controls the copyright, permission is granted for the use indicated in your enquiry under the following conditions:

- Licenses are for one-time use only with a maximum distribution equal to the number stated in your request.
- Springer material represents original material which does not carry references to other sources. If the material in question appears with a credit to another source, this permission is not valid and authorization has to be obtained from the original copyright holder.
- This permission
• is non-exclusive
• is only valid if no personal rights, trademarks, or competitive products are infringed.
• explicitly excludes the right for derivatives.
- Springer does not supply original artwork or content.
- According to the format which you have selected, the following conditions apply accordingly:
• **Print and Electronic:** This License include use in electronic form provided it is password protected, on intranet, or CD-Rom/DVD or E-book/E-journal. It may not be republished in electronic open access.
• **Print:** This License excludes use in electronic form.
• **Electronic:** This License only pertains to use in electronic form provided it is password protected, on intranet, or CD-Rom/DVD or E-book/E-journal. It may not be republished in electronic open access.

For any electronic use not mentioned, please contact Springer at permissions.springer@spi-global.com.

- Although Springer controls the copyright to the material and is entitled to negotiate on rights, this license is only valid subject to courtesy information to the author (address is given in the article/chapter).
- If you are an STM Signatory or your work will be published by an STM Signatory and you are requesting to reuse figures/tables/illustrations or single text extracts, permission is granted according to STM Permissions Guidelines: http://www.stm-assoc.org/permissions-guidelines/

For any electronic use not mentioned in the Guidelines, please contact Springer at permissions.springer@spi-global.com. If you request to reuse more content than stipulated in the STM Permissions Guidelines, you will be charged a permission fee for the excess content.

Permission is valid upon payment of the fee as indicated in the licensing process. If permission is granted free of charge on this occasion, that does not prejudice any rights we might have to charge for reproduction of our copyrighted material in the future.

-If your request is for reuse in a Thesis, permission is granted free of charge under the following conditions:

This license is valid for one-time use only for the purpose of defending your thesis and with a maximum of 100 extra copies in paper. If the thesis is going to be published, permission needs to be reobtained.

- includes use in an electronic form, provided it is an author-created version of the thesis on his/her own website and his/her university's repository, including UMI (according to the definition on the Sherpa website: http://www.sherpa.ac.uk/romeo/);
- is subject to courtesy information to the co-author or corresponding author.

Geographic Rights: Scope
Licenses may be exercised anywhere in the world.
Altering/Modifying Material: Not Permitted
Figures, tables, and illustrations may be altered minimally to serve your work. You may not alter or modify text in any manner. Abbreviations, additions, deletions and/or any other alterations shall be made only with prior written authorization of the author(s).
Reservation of Rights
Springer reserves all rights not specifically granted in the combination of (i) the license details provided by you and accepted in the course of this licensing transaction and (ii) these terms and conditions and (iii) CCC's Billing and Payment terms and conditions.
License Contingent on Payment
While you may exercise the rights licensed immediately upon issuance of the license at the end of the licensing process for the transaction, provided that you have disclosed complete and accurate details of your proposed use, no license is finally effective unless and until full payment is received from you (either by Springer or by CCC) as provided in CCC's Billing and Payment terms and conditions. If full payment is not received by the date due, then any license preliminarily granted shall be deemed automatically revoked and shall be void as if never granted. Further, in the event that you breach any of these terms and conditions or any of CCC's Billing and Payment terms and conditions, the license is automatically revoked and shall be void as if never granted. Use of materials as described in a revoked license, as well as any use of the materials beyond the scope of an unrevoked license, may constitute copyright infringement and Springer reserves the right to take any and all action to protect its copyright in the materials.
Copyright Notice: Disclaimer
You must include the following copyright and permission notice in connection with any reproduction of the licensed material:
"Springer book/journal title, chapter/article title, volume, year of publication, page, name(s) of author(s), (original copyright notice as given in the publication in which the material was originally published) "With permission of Springer"
In case of use of a graph or illustration, the caption of the graph or illustration must be included, as it is indicated in the original publication.
Warranties: None
Springer makes no representations or warranties with respect to the licensed material and adopts on its own behalf the limitations and disclaimers established by CCC on its behalf in its Billing and Payment terms and conditions for this licensing transaction.
Indemnity
You hereby indemnify and agree to hold harmless Springer and CCC, and their respective officers, directors, employees and agents, from and against any and all claims arising out of your use of the licensed material other than as specifically authorized pursuant to this license.
No Transfer of License
This license is personal to you and may not be sublicensed, assigned, or transferred by you without Springer's written permission.
No Amendment Except in Writing
This license may not be amended except in a writing signed by both parties (or, in the case of Springer, by CCC on Springer's behalf).
Objection to Contrary Terms
Springer hereby objects to any terms contained in any purchase order, acknowledgment, check endorsement or other writing prepared by you, which terms are inconsistent with these terms and conditions or CCC's Billing and Payment terms and conditions. These terms and conditions, together with CCC's Billing and Payment terms and conditions (which are incorporated herein), comprise the entire agreement between you and Springer (and CCC) concerning this licensing transaction. In the event of any conflict between your obligations

established by these terms and conditions and those established by CCC's Billing and Payment terms and conditions, these terms and conditions shall control.

Jurisdiction

All disputes that may arise in connection with this present License, or the breach thereof, shall be settled exclusively by arbitration, to be held in the Federal Republic of Germany, in accordance with German law.

Other conditions:

V 12AUG2015

Questions? customercare@copyright.com or +1-855-239-3415 (toll free in the US) or +1-978-646-2777.